University of Texas at El Paso
DigitalCommons@UTEP

Open Access Theses & Dissertations

2014-01-01

Characterizing Cryogenic Propellant Flow Behavior Through a Cavitating Venturi in Comparison to Alternative Flow Control Mechanisms

Marjorie Adele Ingle
University of Texas at El Paso, maingle@miners.utep.edu

Follow this and additional works at: https://digitalcommons.utep.edu/open_etd

 Part of the Aerospace Engineering Commons, and the Mechanical Engineering Commons

Recommended Citation
Ingle, Marjorie Adele, "Characterizing Cryogenic Propellant Flow Behavior Through a Cavitating Venturi in Comparison to Alternative Flow Control Mechanisms" (2014). *Open Access Theses & Dissertations*. 1262.
https://digitalcommons.utep.edu/open_etd/1262

This is brought to you for free and open access by DigitalCommons@UTEP. It has been accepted for inclusion in Open Access Theses & Dissertations by an authorized administrator of DigitalCommons@UTEP. For more information, please contact lweber@utep.edu.

CHARACTERIZING CRYOGENIC PROPELLANT FLOW BEHAVIOR THROUGH A CAVITATING VENTURI IN COMPARISON TO ALTERNATIVE FLOW CONTROL MECHANISMS

MARJORIE ADELE INGLE

Department of Mechanical Engineering

APPROVED:

Ahsan R. Choudhuri, Ph.D., Chair

Vinod Kumar, Ph.D.

Stephen Stafford, Ph.D.

Charles Ambler, Ph.D.
Dean of the Graduate School

Copyright ©

by

Marjorie Adele Ingle

2014

Dedication

I dedicate this work to my grandfather, World War II veteran S Sgt. Richard W. Maly, a military and self-educated rocket engineer at White Sands Missile Range. He spent his life serving his God, his country, and his family through his honest, tireless, and conscientious work. From his priorities, I mirror my own; and in his courageous footsteps, I will walk.

I also dedicate this work to my siblings, most especially eldest sister, who has never failed to pick me up one more time than I've fallen. My niece and nephews have shown me the kind of woman and professional that I aspire to be through their honesty, curiosity, and concern for others; and it is with their future in mind that I dedicate myself to the vocation of engineering.

I dedicate this work to the strong women who mothered me through life, such as my grandmothers, my Aunt "the astronaut-maker", and all of my most encouraging teachers. It was from them that I learned to do the things that were hard; not for glory or notoriety, but simply because it was my dream. And for this lesson, I especially thank my mom.

I dedicate this work to my sister, Laura Cristina Velarde, who passed on before achieving her goals. I hope that I honor her memory and spirit through the work I do for others and that my future successes bring comfort and solace to her family—reassurance that she lives on, because I know that I would not be here today without her love and guidance.

I must also thank through dedication, the truly uplifting support of my friends, sorors, and spiritual family members. They have adopted me into their families and loved me through all of the "hard stuff." From them I've learned that life must be lived with unapologetic humor—because finding the funny side of everything (including personal successes and failures) allows a person to be happy, confident, and humble all at the same time.

But I would most of all, I would like to dedicate this work to my dad, who believed in me even when I didn't believe in myself, and always encouraged me to pursue my dreams even when reason and harsh reality told me it was impossible. He has served as a living example of honorable and selfless leadership and has taught me through his strength of character, how to do the right thing no matter the resulting adversity.

Thanks to him, I'm here today, well on my way to doing the impossible.

CHARACTERIZING CRYOGENIC PROPELLANT FLOW BEHAVIOR THROUGH A CAVITATING VENTURI IN COMPARISON TO ALTERNATIVE FLOW CONTROL MECHANISMS

by

MARJORIE ADELE INGLE, B.S.M.E.

THESIS

Presented to the Faculty of the Graduate School of

The University of Texas at El Paso

in Partial Fulfillment

of the Requirements

for the Degree of

MASTER OF SCIENCE

Department of Mechanical Engineering

THE UNIVERSITY OF TEXAS AT EL PASO

August 2014

Acknowledgements

First, I would like to gratefully acknowledge the contributions of both my predecessors and my colleagues whose assistance made this work possible, specifically Mohammad Arif Hossain, Luz Bugarin, Christopher Bradly, Brenda Arellano, Alejandra Vargas, Javier Chaparro, Aaron Johnson, Gustavo A. Martinez, José L. Mena, and Arturo Acosta-Zamora. Special gratitude is extended to the "Quantum Quattro," whose membership includes Jesus Ortega, John Carey, and Daniel H. Hernandez.

I would specifically like to acknowledge the contributions and mentorship of Dr. Ahsan Choudhuri, Nathan V. Robinson, and Charles Scott Hill.

During my time at the cSETR, it was a privilege to have been mentored by Dr. Jesus Flores, Dr. Adrian Trejo, Dr. Chance Garcia, Francisco Pineda, Carlos Gomez, Jesus Betancourt-Roque, Dr. Bidhan Dam, and Dr. Sudipa Sarker.

Furthermore, I would like to acknowledge the technical advice and mentorship of Dr. Steve Stafford and Dr. Vinod Kumar.

I would like to extend special gratitude to Dr. Vivek Shirsat for his advice and review of my thesis work.

Lastly but certainly not least of all, I would like to thank the UTEP Principal Investigators, Dr. Benjamin Flores and Dr. Helmut Knaust, and staff of the National Science Foundation Bridge to the Doctorate Program/LS-AMP Program, Ariana Arciero-Pino and Sara E. Rodriguez for their seven years of guidance and support.

Abstract

The work detailed is an investigation of the use of a cavitating venturi as both a flow control and metering device. This was achieved through the combination of actual experimentation and numerical modeling of the fluid behavior of both liquid water and liquid methane as it passes through the test article designed, developed, and validated here within this study. The discharge coefficient of the cavitating venturi was determined through weigh flow calibration testing to determine an average mass flow rate. Turbine flow meter flow rate readings were used as a point of comparison and the discharge coefficient was computed. The discharge coefficient was then implemented into the Bernoulli Equation along with experimental pressure and temperature data to again calculate mass flow rate through the cavitating venturi. The agreement of the venturi flow rate data to that of the turbine flow meter effectively established its applicability as a passive flow control and metering feature. A preliminary CFD cavitation model was developed and validated for cavitating water flow regimes using ANSYS FLUENT. Agreement between mass flow rates obtained from the model to experimental data for cavitating water flow indicates that deviations in results for liquid methane analysis from experimental results could simply be the result of insufficiently defined fluid characteristics in the ANSYS FLUENT materials database. SEM surface roughness analysis of a secondary test article indicated that the default average surface roughness for steel in ANSYS FLUENT was reasonable. In addition, the methodology could be further applied to future duty life studies for the cavitating venturi flow meter.

Table of Contents

Acknowledgements v

Abstract vi

Table of Contents vii

List of Tables ix

List of Figures x

Chapter 1: Literature Review of Flow Control Features and Analysis Techniques 1

1.1 Applications for Passive Flow Control Features 3

1.2 Discussion of CFD Analysis Techniques 10

1.3 Discussion of Combustion Performance Analysis 11

Chapter 2: Research Question and Design Methodology 12

2.1 Research Question 12

2.2 Success Criteria 12

2.3 Cavitating Venturi Design and Characterization Process 13

Chapter 3: Experimental Parameters 19

3.1 Mass Flow Rate and Mixture Ratio Requirements 21

3.2 P ratio range (Required Inlet Pressure) 21

3.3 Operating Temperature Range 22

3.4 Testing Duration 22

Chapter 4: Experimental Setup and Procedure 23

4.1 Venturi Test Setup 23

Chapter 5: Experimental Results 38

5.1 Water Testing, determination of the steady cavitation flow regime C_d and $P_{critical}$ 38

5.2 Cavitation Transience and Pressure Dependency 42

Chapter 6: Surface Roughness Analysis and Determination 48

6.1 Scanning Electron Microscope Technology (SEM) and Sample Preparation Process 48

6.2 Image Processing and Surface Roughness Determination 54

Chapter 7: CFD Analysis 56

7.1 Description of CFD Model and Software Selection 56

7.2 Model Case Development....56
7.3 Results and Analysis....71
Chapter 8: Conclusions....73
8.1 Coefficient of Discharge....73
8.2 Experimental vs. CFD Results....73
8.3 SEM Roughness Analysis....74
Chapter 9: Proposed Legacy Work....75
9.1 Continued Repeatability Tests and Pulse-width Modifications....75
9.2 Increased inlet pressure testing....75
9.3 Life Cycle Studies....76
9.5 Alternative Materials and Manufacturing Techniques....77
9.6 Alternative CFD Techniques....78
References....79
Vita....82

List of Tables

Table 3.1: DAQ System....19
Table 3.2: Propellant Feed System....19
Table 3.3: Torsional Thrust Balance Specifications....20
Table 3.4: Pencil Thruster Engine....20
Table 4.1: Liquid Turbine Flow meter [14]....24
Table 4.2: Cryogenic Pressure Transducers [15]....24
Table 4.3: Thermocouples [15]....24
Table 4.4: Liquid Water Cavitating Venturi Flow meter Testing Parameters....26
Table 4.5: Liquid Methane Cavitating Venturi Flow meter Testing Parameters....36
Table 5.1: Venturi Dimensions....39
Table 5.2: Cavitating Venturi Discharge Coefficients....40
Table 6.1: Roughness Variation Chart....54
Table 7.1: Orthogonal Mesh Quality vs. Mesh Discretization Size....57

List of Figures

Figure 2.1: Cross sectional view of the Cavitating Venturi. *Flow runs from left to right, all inner geometries are uniform in design, and the dimensions are in inches.*.....17

Figure 2.2: Cavitating Venturi overall view. *Flow runs from left to right.*.....17

Figure 4.1: Water test setup (a) for Venturi. *Solenoid valve 1 is located upstream of the venturi. Figure is compliments of source [16].*.....25

Figure 4.2: Water test setup (b) for Venturi. *Solenoid valve 1 is located downstream of the venturi. Figure is compliments of source [16].*.....26

Figure 4.3: Water test ran at pressure ratio below the critical pressure ratio. *Mass flow rate versus time when solenoid valve 1 is upstream of the venturi. See figure 4.1. [16]*.....28

Figure 4.4: Water test ran at pressure ratio above the critical pressure ratio. *Mass flow rate versus time when solenoid valve 1 is upstream of the venturi. See figure 4.1. [16]*.....29

Figure 4.5: Water test ran at pressure ratio below the critical pressure ratio. *Mass flow rate versus time when solenoid valve 1 is downstream of the venturi. See figure 4.2.* 30

Figure 4.6: Water test ran at pressure ratio above the critical pressure ratio. *Mass flow rate versus time when solenoid valve 1 is downstream of the venturi. See figure 4.2.* 31

Figure 4.7: Discharge coefficient vs. Pressure Ratio. *Liquid Water at standard inlet conditions. [16]* 32

Figure 4.8: Liquid Methane Condensation Unit. *Photo was taken by Manuel Galvan.*.....34

Figure 4.9: Venturi setup for liquid methane tests. *Figure is compliments of source [15].* 35

Figure 5.1: Cavitating Venturi Reference Geometry. *See table below for reference identifiers.*.....39

Figure 5.2: VFM-001 Discharge Coefficient vs. Pressure Ratio. [18].....41

Figure 5.3: VFM-002 Discharge Coefficient vs. Pressure Ratio. [18].....41

Figure 5.4: Cavitating Venturi and turbine flow meter mass flow readings at varying pressure ratios. ***The C_d was not applied to the cavitating venturi mass flow rate readings.*** [16].....43

Figure 5.5: Cavitating Venturi and turbine flow meter mass flow readings at varying pressure ratios. ***The curve fitted C_d was applied to the cavitating venturi mass flow rate readings. [16]*** 44

Figure 5.6: Transient data for liquid methane (above) and water (below). [16] 45

Figure 5.7: Bubble radius versus ambient pressure for a cavitating water bubble. [16].....46

Figure 6.1: Cavitating Venturi Sectioning for SEM Analysis. ***The yellow arrows indicate along which diametral sections the venturi was prepared for analysis.*** 48

Figure 6.2: Light Refraction Example. *Cavitating Venturi converging section, digital DinoLite microscope, 55x magnification with overhead lighting (left) and side light (right).*.....49

Figure 6.3: Cavitating Venturi Sectioning for SEM Analysis. ***Samples 1-3 are shown from left to right respectively starting with the near throat sample, the converging cross-section and the inlet.***.....51

Figure 6.4: Surface Roughness Measurement Techniques. *Figure courtesy of source [20].*.....52

Figure 6.5: Sample Charging. *Image on the left is with copper tape and image on the right is of the same cross-section with gold coating.* 53

Figure 7.1: Mesh independence test with static pressure along the symmetry line. *Mesh independence achieved in range of 2.52-2.6 e-002 inch discretization sizing.* 58

Figure 7.2: Mesh of the fluid domain. *Discretization sizing is detailed in inches.*.....59

Figure 7.3: Discharge coefficient comparison. *All three of the water Cd values are within the 3.57% range of agreement.* 65

Figure 7.4: Static Pressure Profile of Water at P2/P1=0.69. *Contour of Static Pressure (mixture) in Pa, produced in ANSYS FLUENT.* 66

Figure 7.5: Velocity Magnitude Profile of Water at P2/P1=0.69. *Contour of Velocity Magnitude (mixture) in (m/s), produced in ANSYS FLUENT.*.....67

Figure 7.6: Liquid Phase Profile of Water at P2/P1=0.69. *Contour of Liquid Volume Fraction, produced in ANSYS FLUENT.*.....68

Figure 7.7: Static Pressure Profile of Liquid Methane at P2/P1=0.69. *Contour of Static Pressure (mixture) in Pa, produced in ANSYS FLUENT.* 69

Figure 7.8: Velocity Profile of Liquid Methane at P2/P1=0.69. *Contour of Velocity Magnitude (mixture) in (m/s), produced in ANSYS FLUENT.*.....70

Figure 7.9: Liquid Phase Profile of Liquid Methane at P2/P1=0.69. *Contour of Liquid Volume Fraction, produced in ANSYS FLUENT.*.....71

Chapter 1: Literature Review of Flow Control Features and Analysis Techniques

The scholarly work detailed herein this publication is the design, development, and performance evaluation of a cavitating venturi flow control feature utilized in the cryogenic propellant supply to a Liquid Oxygen (LOx)/Liquid Methane (LCH_4) reaction control engine. It was produced as a necessary component of the propellant feed system for a reaction control engine that was jointly developed by the NASA Johnson Space Center and the Center for Space Exploration Technology Research (cSETR), a NASA University Research Center (URC) based out of the University of Texas at El Paso's Department of Mechanical Engineering. The RCS engine itself, which will subsequently be referred to as the "Pencil Thruster," was originally developed as part of the NASA Project Morpheus but then also became a benchmark test article utilized to demonstrate the plausibility of a LOx/LCH_4 reaction control engine. The engine was designed and produced by previous students and it became clear through their preliminary testing that flow control features beyond the simple use of actuated solenoid valves and flow monitoring devices (such as pressure transducers, thermocouples, and turbine flow meters) would be necessary for ensuring proper flow rates to achieve the desired propellant mixture ratios. A cavitating venturi was designed to meet this specific need.

In current spacecraft technologies, reaction control system engines, commonly known as RCS thrusters, are typically fed from separate propellant tanks that are independent of those for the main engines. This tends to increase overall vehicle weight, complexity, power consumption and cost. In the effort to mitigate the previous design concerns, the propulsion industry is embracing the use of passive flow metering and regulation devices that allow for the low inlet pressure design requirements for RCS thrusters to be fulfilled while withstanding the technical demands imposed by feeding them from the high pressure main engine tanks. The performance of micro-scaled propulsion systems, particularly those that deal with cryogenic propellants, is heavily dependent upon the reliability and consistency of their fuel delivery systems. In general, the mass flow rate ranges in which these systems operate are so minimal that even seemingly minor disruptions in fuel supply can cause combustion instability that leads to a number of undesirable situations. The resulting behaviors span from poor performance of the engine to actual hardware damage. Such disruptions generally arise from physical characteristics of the

propellant delivery system that cause changes in pressure and temperature leading to at least a partial change in phase. Gases and cryogenic liquids combust at drastically different rates and when propellants consist of mixed qualities, it can be difficult to ensure that a proper mixture ratio is maintained to achieve stable, self-sustained combustion.

This study will endeavor to characterize the fluid behavior of the liquid methane/liquid oxygen propellant delivery system for the current benchmark reaction control system engine (2-15 lbf class). Most specifically, the cavitating venturi will be evaluated in its use as both a flow control device and flow metering feature. The literature review detailed in this chapter will explain why the cavitating venturi was chosen over other flow obstruction and control features. Its performance as a flow meter will be compared to other devices such as turbine flow meters and corialis flow meters in terms of comparable accuracy. In subsequent chapters it will be shown that the cavitating venturi's flow metering performance will be evaluated in part, by comparing it with the results obtained with a turbine flow meter. In this chapter however, an explanation for this preference over the corialis flow meter will be detailed.

Another method for evaluating the performance of the cavitating venturi will include the creation of a CFD model of the fluid flow through the cavitating flow regulation point. The goal is to provide a computationally obtained point of comparison for the observed test data in terms of pressure, temperature, and mass flow rate profiles. Sufficiently discretized models and accurate solution schemes could then be evaluated for their ability to characterize the tested flow regimes. This would be shown if they can corroborate the experimentally indicated level of cavitation, to the degree that the modeling techniques can be considered accurate. It is also hoped that these models, if run for longer time steps/iterations than the experimental test lengths, could provide insight regarding whether or not the experimentally observed flow behavior was a result of transient fluid responses or steady state, fully developed flow. This information, when combined with the observation of the combustion characteristics could provide a more complete understanding of the quality of the propellants as they enter the combustion chamber when the cavitating venturi is placed in-situ. Furthermore, it could indicate whether or not the quality remains fairly constant or changes during the span of a test. During

the course of typical RCS thruster maneuver operations, the pulse width of the burns can be so short that a passive flow control device with slow response such as a cavitating venturi may not have the opportunity to reach fully developed flow conditions, including a fully developed cavitation region. So it would be vital for the CFD model to capture transient response as well. The current chapter will include a review of various CFD modeling techniques that are used to capture cavitation in flow obstructions using commercially available software such as ANSYS FLUENT. Such knowledge will then be utilized in the CFD model detailed in this work to ensure that proper propellant mixing is achieved for the desired combustion process (fuel rich versus fuel lean) in the effort to optimize engine thrust/specific impulse generation. It will be shown in later chapters that this is also important for the prevention of detonation and/or deflagration conditions resulting from improperly mixed fuel that could pose serious safety hazards to both hardware and researchers.

1.1 Applications for Passive Flow Control Features

Passive flow control features have been vital components of propellant supply systems since the early days of the modern rocket era that began during World War II and the subsequent space race. In terms of weight and envelope optimization, they are preferable to pumps and active flow meters in that they minimize weight by likewise reducing power requirements and control system complexity. In many studies and industrial applications it has also been shown that they are capable of minimizing flow measurement error because their flow readings are derived from devices that have more reliability and sensitivity (such as upstream and downstream pressure transducers and temperature sensors) than the built-in piezoelectric sensors common to most turbine flow meters. This is a direct result of the often unknown performance degradation (from cavitation and thermal stresses, etc.) of the turbine and piezoelectric sensors experienced during the service life of the turbine flow meters. Furthermore, since most are either calibrated for liquid or gas use exclusively, they are impractical, and can even be damaged when utilized in situations where the phases of the propellants are not relatively constant. The sensitive nature of their components and the overall high cost of their production is another inhibitive factor when considering the use of turbine or corialis flow meters. In short, passive flow control features such as a cavitating venturi often prove to be more advantageous simply because they are

cheaper, lighter, less complex, less susceptible to damage, and have lower power consumption requirements. [1]

1.1.1 Common types of Passive Flow Control Features

Passive flow control features can be described in common terms, simply as geometric features placed within a flow field that are intended to disrupt the free flow patterns in a desired manner without the need for mechanically or electronically actuated components. In essence, passive flow control features rely on the physics of the fluid interaction with the stationary geometric features to influence the mechanics of the fluid flow into which they are introduced. Passive flow control features have a number of engineering applications that include, but are certainly not limited to normalization/steadying of fluid flow, obstruction of fluid flow, introduction of turbulence, and influencing fluid flow through the modification of heat transfer. For the purposes of this study, the focus is on the utilization of passive flow control features to obstruct the fluid flow, and in doing so, accurately control and meter the mass flow rate out of this device. As mentioned in the previous sections, the cavitating venturi flow feature was selected, but the following sections will also detail the alternatives and the reasons they were not chosen. For this portion of the literature review, both well-established devices as well as more newly developed flow control features will be detailed from sources that range from design text books, to scholarly articles, to U.S. Patents that are still pending. These sources were chosen specifically to show a progression in the advancements of available flow control technologies and how they specifically address problems that only became apparent as the knowledge of cavitation and cryogenic fluid behavior became more widely studied, often as a result of implementation.

Obstruction Flow meters

Obstruction flow meters are a type of passive flow control system that utilizes a geometric feature (or an array of such structures) placed downstream of the control volume inlet to limit or reduce the flow rate of the fluid exiting the control volume region. In this simple form, the flow obstructions simply alter the fluid flow in the control volume rather than an actuated device. It becomes a metering system when instrumentation such as pressure transducers and thermocouples are introduced upstream and downstream of the flow obstruction. This data allows for the mass flow rate to be computed when

input into the Bernoulli equation with a correlation factor known as the discharge coefficient (C_d). Simply stated, in an obstruction flow meter, a flow rate of a fluid through a pipe can be observed by through flow constriction. This is possible because one can measure the pressure drop from the inlet to the outlet caused by the velocity increase at the point of constriction. [2] For incompressible fluids such as water at room temperature in standard atmospheric conditions the pressure transducers or manometers in the aforementioned locations would alone, is enough to calculate the mass flow rate. However, for cryogens, particularly when they are near their critical point, the thermocouples are necessary additions to the instrumentation of the obstruction flow meter because they are used to in conjunction with the pressure transducers to indicate if the fluid is near the saturation and/or critical values. In terms of mass flow rate metering, this is particularly important when cavitating conditions are desired as the throat pressures must fall below the saturation pressure at the given throat temperature conditions for cavitation to actually occur. [3] It is important to note that it is primarily the venturi flow meter in which cavitation is desired. In most other obstruction flow meters, such as orifice flow meters, cavitation could cause damage to the orifice and does not serve to enhance the flow control capabilities of the device.

One type of obstruction that could be incorporated into a flow metering system is called a bluff body and is in essence, simply a flat front object with a trailing edge behind it. In terms of propellant supply, this is an impractical flow control approach because the production of such a feature within most standard propellant supply lines would be challenging in terms of manufacturing. Furthermore, the propellant mass flow would still be highly dependent upon the downstream conditions. This fact alone negates its effectiveness in reliably delivering a specified mass flow rate in certain circumstances. [4]

Capillary-tube flow meters incorporate the basic functioning of a U-tube manometer and are also related to Beckett's pulsing gas meter. In both of these cases however, the goal is simply to meter the flow rates through a physical mechanism without the capability to actually control the mass flow rate. Furthermore, the means by which the metering occurs actually causes a disruption to the flow that is neither useful nor predictable in terms of flow control. The mechanism by which the flow is metered involves the measurement of the displacement of a liquid that is held internally in a seal that breaks under specific operating pressures. The method through which this fluid is collected however, would

only function at standard gravitational conditions, and thus would not be applicable in spacecraft propulsion applications. [5]

One of the most basic versions of the obstruction flow meter involves the orifice feature which consists of a hole in a flat plate, or baffle feature that can either be a simple through hole or have variations to the chamfer or smoothing of the edges. This is often one of the most simplistic to manufacture and occupies minimal space within the piping length. Some of the drawbacks of this design however involve the production of swirl and eddy flow structures that introduce head and pressure losses that may not be recovered downstream of the orifice. [2] Other variations of this design include an array of holes through a baffle plate of greater depth, such as in the slotted orifice flow meter. This configuration essentially strives to incorporate channel structures into the obstruction plate meant to reduce the size of the swirl structures or flow field disturbances, but they rarely eliminate them without negating the compactness advantages. [6] This could be achieved though, by a nozzle meter. As implied by its name, it replaces the orifice with a nozzle placed within the flow stream, dramatically reducing the vena contracta size and likewise lowering the head losses. [2] In many cases, a nozzle flow meter is perfectly suited for most spacecraft liquid propellant flow control and metering needs, but more improvements could be made as discussed in the following section.

Cavitating vs. Non-Cavitating Venturi Flow meters

First invented by Clemens Herschel and named after a researcher in conical shaped flow sections, the Venturi meter is regarded as the most accurate of the obstruction flow meters. Despite its increased cost due to manufacturing complexity, it is a generally more preferred method of flow control and flow rate measurement because of its geometric features. In contrast to the abrupt contraction and/or expansion of the orifice and nozzle shapes, the venturi both contracts and expands the flow in a more gradual manner. The fluid passing through is thus prevented by the geometry from swirling. Flow separation is likewise prevented, meaning that only frictional losses are experienced from the fluid interaction with the inner walls. For this reason, Venturi meters are often used for applications in which large pressure drops must be prevented, as the head losses are extremely minimal. This means that the net effect of Venturi meters on a flow system results in the lowest minor loss (expressed as a coefficient)

of all the previously mentioned obstruction flow meters. [2] In situations where more control over the pressure drop was desired, but could not be achieved due to limitations imposed by machining tolerances, it was shown that the production and size control (through inlet temperature and pressure control) of cavitation bubbles could be employed for this purpose. In simplistic terms, the difference in control sensitivity of a Venturi meter and a cavitating venturi flow meter can be likened in scale to the difference between a standard, manually operated ball valve and a needle valve.

Cavitation is a physical phenomenon that is characterized by liquid rupture due to pressure drops in the fluid domain when the fluid temperature is constant, and is characterized by the formation of bubbles. These bubbles grow from cavitation nuclei, which are microscopic vacancies within a liquid. These nuclei are already present within the liquid as a result of the entrained gases and/or thermal responses to molecular interactions, but grow into bubbles when there is a reduction in pressure to the point where it falls below the saturation pressure corresponding to the temperature of the liquid. To be more specific, the literature mentions that the vacancies that become cavitation nuclei are created through the entrainment of gases into the fluid flow of pure substances. They can also occur in pure substances as a result of the thermal interactions of the molecules. In the case of this investigation, both sources of cavitation nuclei should be considered as there is likely some degree of the cryogen boil-off mixed in with the liquid in addition to the entrained air from the facility water source during the filling process. Furthermore, it is unclear if the gaseous helium used to pressurize the liquid methane tank or the gaseous nitrogen used to pressurize the water tank are likewise being diffused. So in this study it is unclear if the test fluids are in fact pure substances. [2, 7] In cavitating venturis, the pressure reduction falls below the saturation pressure on the inlet side, just upstream of the throat region because of the increase in fluid velocity. The bubbles will then collapse when they reach the point in the flow where the pressure exceeds the vapor pressure. [7] So, in a cavitating venturi, the goal is to control and meter the mass flow rate of the liquid propellant by controlling the growth of the cavitation nuclei. This is achieved through the manipulation of the inlet conditions, specifically the pressure and temperature. Since the propellant feed lines are not temperature controlled beyond the use of insulation, it is through the variation of the upstream pressure that the cavitation is controlled.

The previous section has gone into a fair amount of detail describing the improvements in accuracy of flow metering, flow stabilization and control, and reduction in power consumption and instrumentation that make using a cavitating venturi more advantageous than other passive and active flow control features. However, one of the most persuasive arguments for utilizing a cavitating venturi over other forms of passive flow control measures is that its ability to reliably supply constant flow rates is not influenced or dependent upon the effects of pressure changes within the rocket engine. This is true so long as the inlet pressures remain constant and the downstream pressure falls below approximately 85-90% of the upstream pressure. [1] Both cavitating and non-cavitating venturis have seen a great deal of use in liquid rocket engine propellant delivery systems for over five decades. However, the change in propellants and their respective physical properties, particularly with the use of more cryogens, makes it essential that the performance of cavitating venturis be revisited. Cryogenic propellant behavior is highly volatile, particularly near the critical region, and more work must be done to better characterize venturi performance with these propellant conditions.

1.1.2 Complications in flow control feature performance analysis with cryogenic propellants

Observations of cavitation and its influence on flow behavior through flow control devices such as cavitating venturis can be made using a number of techniques, many of which simply are not viable options when utilizing cryogens as the working fluids. One such method actually involves the production of an optically accessible venturi. However, in the instance described in Jean-Pierre Franc's investigation of cavitation behavior [8], a "central body" feature is incorporated into the downstream expansion region of the venturi as part of a widely accepted method of determining water quality and observing cavitation nuclei growth. This is done by starting with an inlet water velocity that is below a value that creates cavitation and incrementally increasing the velocity through the first instance of cavitation well into the cavitation nuclei growth. [8] While the study of cavitation growth would be important to the understanding of its mechanism as an enhancing flow control technique, a downstream obstruction such as the one described in the aforementioned work was not incorporated into the work detailed in this paper. This was primarily due to the fact that the working fluid choices involved cryogens as well as room temperature water. For this reason, plastics could not be used as their

toughness and thermal behavior were not compatible with cryogenic applications. This is especially true with Liquid Oxygen (LOx) as the combination of LOx and polymers react together to form hypergolic propellants that would most certainly combust with simple contact. Furthermore, as detailed with the obstruction flow meters, the downstream flow feature utilized by Franc would have created undesired losses while presenting manufacturing challenges that make its implementation unpractical for our purposes.

Another issue that complicates the process of analyzing the flow control performance of a cavitating venturi with cryogens is a general lack of experimentally obtained data detailing the relationship of temperature and pressure to phase near the critical region, as expressed in phase diagrams. Previous work done at the Center for Space Exploration Technology Research studied the heat transfer capabilities of liquid methane as coolant in regenerative cooling rocket systems. [9] As part of this work, a fairly intensive literature review was performed that revealed vast gaps in knowledge regarding liquid methane fluid phases near the critical region. It also showed that there was significant effort being invested in finding more accurate equations of state to use for predictive purposes in more clearly defining the critical region. The resulting conclusions drawn from this literature review state that one of the most computationally viable and acceptably accurate equation of state used for the prediction of cryogenic propellant behavior near the critical region (even below the triple point) was the Soave-Redlich-Kwong model. [9] The most computationally accurate however, was the Schmidt-Wagner equation of state with a 0.2% accuracy just below the critical point until the triple point on the phase diagram. Later, Setzmann and Wagner further expanded the pressure and temperature range for which this equation is valid to well above 600 K and 1000 MPa. The specific methodology utilized in this work for the prediction of the cavitation ranges for the produced cavitating venturi will be further detailed later on in this report, along with the solvers implemented in the CFD models. [9]

In Chapter 2, the design methodology employed for the development of the cSETR's cavitating venturi will be described; including the use of a NIST developed software called REFPROP, which was used in part, to determine the theoretical operating range. A simple "flow and catch" method, formally known as static weigh flow calibration, can be used to determine the correlation between observed mass

flow rate, pressure ratios, and discharge coefficient values. [10] For confirmation, these readings can also be compared to the readout of a turbine flow meter, which may be used as a master meter due to its established measurement accuracy. However, other methods are also desired to confirm the presence of cavitation and observe its functionality as a flow control mechanism. So, in the spirit of utilizing the computational tools and experimental data available, this study will also utilize CFD modeling techniques and combustion test observations made while the cavitating venturi was placed in situ within the Pencil Thruster propellant feed system. Doing so will likely provide more information to better assess the performance of the cavitating venturi, as both a flow control and metering device. Sections 1.2 and 1.3 will provide greater insight into these options.

1.2 Discussion of CFD Analysis Techniques

In a study performed at the Middle East Technical University in 2006 [11], a numerical model was produced to observe the cavitation behavior of fluids passing through a cavitating venturi. Before the models were used to compare with actual flow data from the cavitating venturi though, a validation analysis was performed that involved the modeling of another cavitating orifice for which sufficient experimental data had been produced for a point of comparison. First, it must be noted that the ANSYS FLUENT Mixture model was preferred for use of the volume of fluid (VOF) model because the VOF cannot account for the development of a second fluid phase during the solution process. Furthermore, the mixture model utilizes the idea of slip velocities to account for the different phases moving at varying velocities while interpenetration occurs between them. The specifics of the continuity, momentum, energy, and volume fraction equations solved in the Mixture model are detailed in the literature. [11, 12]

The validation model was developed in ANSYS FLUENT and was intended to detail the cavitation behavior of water flowing through a sharp-edged orifice. Test cases were run for inlet pressures that ranged from vacuum to well over 5000 psia with roughly ambient exit pressures. The case was run under the 2D axisymmetric, turbulent solver, with the standard k-epsilon turbulence model. The mass flow rate was then computed using this model and divided by the theoretical mass flow rate to obtain a discharge coefficient which was then compared with experimentally obtained data. The percent

difference between the numerically calculated discharge coefficient and the experimental data ranged from 1.28% for the coarsest mesh to 0.00% for the finest mesh size, despite the fact that this was a Reynolds Averaged Navier-Stokes (RANS) model. RANS models take averages of the various flow contours so it is extremely difficult, if not impossible to capture transient response. For short pulse widths, it may not be sufficient to show transient changes, which in terms of RCS thrusters, can cause major inhibitions to the thruster reaching its maximum ISP. But RANS models can provide an overall point of comparison when looking at the averages of the various characteristic flow contours and profiles, including the discharge coefficient, which itself is an average value. [11] So although the pressure and velocity contours produced by this model do not provide accurate enough resolution to visually discern cavitation nuclei growth, it can at least confirm changes in discharge coefficient values that would indicate cavitation.

1.3 Discussion of Combustion Performance Analysis

The Middle East Technical University study also detailed a method for verifying the cavitating venturi performance through a test where the engine is fired. In this experimentation, the pressure is measured at the exit of the venturi and in the combustion chamber of the engine. The main advantage of using a cavitating venturi is that the mass flow rate should remain constant regardless of the flow conditions downstream of it. To verify that this is occurred, the researchers observed the exit pressure of the venturi to ensure that it remained nearly constant even as the pressure wave resulting from ignition propagated back through the feed lines. [11] This is a reasonable method of analysis based on solid theoretical background, provided that the injection method of the propellants into the combustion chamber is a simple inlet. In the case of the Pencil Thruster used in the present work however, this is not the case. There is a propellant injection manifold that directs the propellants into the combustion chamber through small holes that could themselves provide pressure and head losses. The combustion characteristics of the thruster could therefore also be influenced by the losses due to the injection holes as well as the steep inclination of the propellant feed line as it enters the confinement for the RCS test article, thus skewing the results of a combustion related analysis. For this reason, a combustion analysis was not included in this work.

Chapter 2: Research Question and Design Methodology

This chapter will outline the research question addressed in this work and the methodology that was applied to answer it. These were developed utilizing the information provided in the background sections and literature review. The system requirements detailed in the following chapter also played a role in forming the research question and goals. The experimental setup of the Pencil thruster system likewise served as a strong driving force not only in the cavitating venturi testing process, but also in its design phase as well.

2.1 Research Question

There are several research questions that the work detailed here within endeavors to answer. The first of these is whether or not a cavitating venturi can effectively be utilized in cryogenic liquid propellant feed lines to control the flow rate of the propellants in a reliable and repeatable manner. In this instance, reliability would be defined as maintaining a desired flow rate for a constant set of given inlet conditions regardless of the conditions downstream of the venturi. If this is so, it is desired to determine the operating range of pressure ratios (downstream to upstream) for which the flow control can be enhanced through cavitation. Furthermore, it will be discerned whether or not the cavitating venturi, when instrumented with upstream and downstream pressure transducers and thermocouples, can be used as a flow metering device comparable in accuracy to its active control counterparts such as a turbine flow meter.

2.2 Success Criteria

Successful design, development, and implementation of the cavitating venturi as both a flow control and metering device would include strong agreement between the discharge coefficient determined through water testing and that which was predicted through theoretical calculations as well as in literature. Furthermore, agreement in flow rate data obtained experimentally (via the instrumentation for the venturi) with those calculated theoretically, as well as with the flow rates measured using the turbine flow meter during the testing. Further success would be achieved if the discharge coefficient and mass flow rate results of a CFD analysis are in agreement with the experimental results, as this would validate the CFD model. Although the CFD models utilized simply

do not have the resolution to accurately capture the growth progression of the cavitation nuclei, an overall observation of the pressure and velocity contours should clearly show the development of the vena contracta region, with values falling in the expected ranges. It is important to note that during the design process of the cavitating venturi, the surface roughness was not specified in the machining schematic. At the time, it was believed that adhering to tight machining tolerances on the geometric figures played a bigger role in the performance of the flow meter than the surface roughness. So, the decision was made to choose a manufacturing technique based on its capability to produce the geometric features. No post-production surface treatments were applied to smooth the surface finish, so the surface roughness could have been anything within a fairly wide breadth of values as detailed in Chapter 5. For this reason, the accuracy of the CFD model would be improved by inputting an internal surface roughness obtained through scanning electron microscope (SEM) analysis of the cavitating venturi cross section. Although there are numerous other factors involved in the propellant state and combustion process of the propellants with consideration to the Pencil Thruster performance testing, the other validations would shed light on the cavitating venturi's overall influence on the RCS engine combustion. This would provide future researchers with information for system optimizations that span from necessary propellant conditioning, injection hole and film cooling geometry design, to even the shape and elevation of the propellant feed lines. More detailed information is included in the subsections below.

2.3 Cavitating Venturi Design and Characterization Process

Before the cavitating venturi can be used as a flow metering device, the coefficient of discharge, C_d, must be determined so that the associated inlet pressure data collected during the testing process can be converted to a mass flow rate. These results can then be compared to the measurements taken by the turbine flow meter. The following section will describe the process of obtaining the C_d from the actual cavitating venturi design phase through the water testing phase.

2.3.1 Venturi Design (Requirements and Geometry Selection)

The cavitating venturi was intended to be used for both liquid oxygen (LOx) and liquid methane (LCH_4). The boiling temperature for LOx is significantly lower than for LCH_4 so for the sake of making

it applicable to both propellants, the venturi was actually designed to specifically modulate the LOx mass flow rate. To avoid designing another cavitating venturi specifically for LCH_4, the inlet pressure is manipulated to likewise ensure cavitation.

The first of the critical dimensions determined during the design process was the throat diameter. For this to be calculated, the Bernoulli equation for the mass flow rate, as expressed in Equation 1, was rearranged to solve for the throat diameter, Equation 2.

$$\dot{m} = C_d A_{th} \sqrt{2\rho(P_1 - P_{th})} \tag{1}$$

In the equation above, A_{th} is the area of the throat and is the term from which the throat diameter will be extracted in Equation 2. P_{th} is the throat pressure term, which in cavitating venturis, must be set as the saturation vapor pressure associated with the inlet conditions. P_1 is the inlet pressure term, which is typically determined by the tank conditions for the LOx, and the gaseous pressurant for the LCH_4. The ρ is the density of the fluid in the throat region at liquid state. In this case, the throat density is assumed to be equivalent to the inlet density, which, despite the cryogenic application, is considered to be a safe assumption because of the efforts made to maintain the liquid state of the cryogens throughout the testing process. [13] Finally, the C_d is the discharge coefficient and for design purposes was assumed to be a value of 1 since it is desired to design to maximum ideal performance and is close to the generally accepted value range of 0.95-0.99 for venturis. [2] Below is Equation 2, for the throat diameter, d_{th}. All of the nomenclature is the same as in Equation 1.

$$d_{th} = \left[\frac{4\dot{m}}{C_d \pi \sqrt{2\rho(P - P_{th})}}\right]^{1/2} \tag{2}$$

It is important to note that the LOx is supplied in the RCS experimental setup by a commercial dewar and as a cryogen, it is impossible to fully control and maintain the temperature and pressure of the fluid as it is released. Anything from the temperature of the regulator and supply lines to the tank pressure and quality of the LOx within the dewar can influence the exit temperature of the LOx as it is released. However, from observations made during previous tests, it was shown that a reasonable estimate of exit temperature from the dewar is within the range of 100-123 K. For the inlet temperature

of the venturi, a conservative estimate was taken to be 123 K (-238 ˚F). Due to the pressure rating limitations on certain pieces of hardware and instrumentation an inlet pressure range of 1.25-1.4 MPa (~181-203 psi) was selected. Given this information in addition to a required mass flow rate of 0.0075 kg/s, a series of possible throat diameters was determined. A throat diameter of 1.02 mm (0.040 in) was selected because it was feasible to machine this diameter and provided leeway for a wider breadth of maximum inlet pressures to be used. The thermal effects on the venturi material during operation caused by an approximate 200 K decrease in temperature were computed, taking into account the linear thermal expansion/contraction coefficient. They were shown to exert less than 1% diametral change. For this reason any diametral variation caused by thermal stresses exerted on the throat were considered negligible. Now that the throat diameter was fixed, it was calculated that for an operating temperature of 100 K, a minimum inlet pressure of 0.3 MPa could produce the cavitation conditions conducive to maintaining the desired mass flow rate. Note that an inlet temperature of 100 K was selected because it was at the lower end of the temperature ranges typically seen for the outlet flow temperatures of LOx dewars.

2.3.2 Pressure Recovery Geometric Features and the Estimation of P ratio Operation Range

While important, the throat diameter was only one of a myriad of dimensions that needed to be specified. The vena contracta is a fluid structure that forms as a result of the viscosity as a flow passes through an obstruction and into a relatively open space. It is characterized as the minimum cross sectional area of the flow stream and is located slightly downstream of the obstruction. In addition to being the region through which the fluid velocity increases, it is likewise the region of fluid under the lowest pressure. [7] So controlling how far the vena contracta region extends beyond the throat controls how quickly the liquid state recovers and the extent of the cavitation region along the inner wall of the venturi. This is accomplished through modification of the obstruction geometry. Furthermore, the angles as which the nozzle section converges and the diffuser diverges must be made as gradual as is practical in the effort to minimize losses and prevent hydraulic flip, which is defined as a complete fluid detachment from the inner walls. Mirroring the literature that was consulted during the design process, a 15° angle was chosen for the convergent side and a 7° angle was used on the divergent end. The

pressure recovery coefficient (C_p) that was likewise cited in this literature was given a value of 0.8. [13] The following equation will demonstrate how the critical pressure ratio relates to the C_p and other dimensions.

$$P_{cr} = \frac{C_p {C_d}^2}{1 - (\beta)^4} \tag{3}$$

The critical pressure ratio serves as the maximum value in range of pressure ratios, defined as downstream to upstream pressure, for which cavitation will occur in the venturi. Surpassing the critical pressure ratio will not only result in the cavitation processes ceasing, but the downstream pressure will also exert influence on the flow rate. As previously mentioned, the C_d is the discharge coefficient and the β is the ratio of throat to inlet diameter. The throat diameter was determined previously in computation and the inlet and outlet diameters would be related to the supply line diameter. Although much of the characterization testing was not performed in situ with the actual Pencil Thruster test setup, the venturi was designed with its future implementation in mind. For this reason, a 9.65 mm (0.38 in) inlet and exit diameters were machined, matching the inner dimension of the propellant feed lines. These dimensions, in combination with the convergence and divergence angles would determine the length of their respective sections. [9] Figure 2.1 below details the cavitating venturi geometry. It should be noted that a total of three cavitating venturis were produced of this design. This work primarily details the testing of the benchmark test article. The other two will be briefly discussed as only water testing was done to determine their discharge coefficients and critical pressure ratios. As will be discussed in Chapter 5, differences in machining tolerance between each of the cavitating venturis lead to significant variations in the aforementioned characteristic values. Aside from the altered throat dimension, the only other difference between the last two venturis and the benchmark test article venturi was the end fitting, which was a size 8 AN end fitting (SAE ¾”-16 threading) versus the ½” NPT.

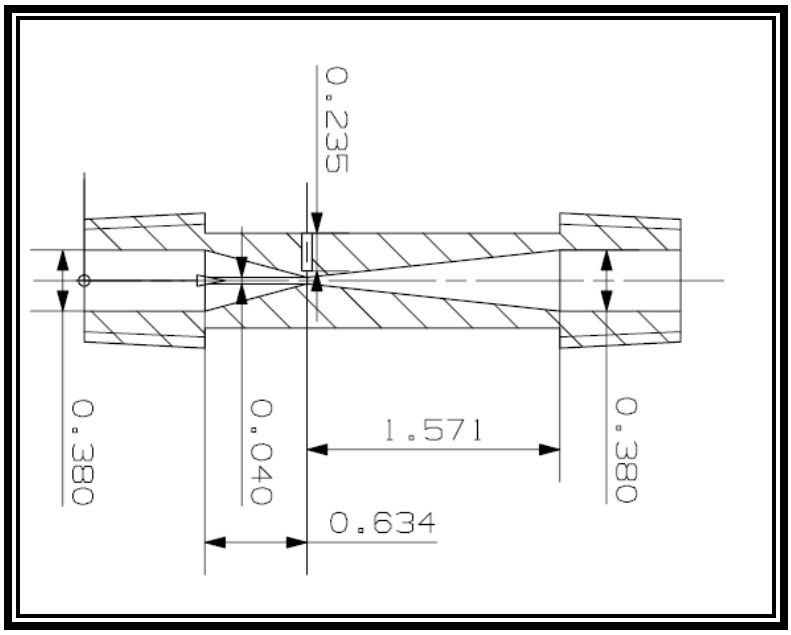

Figure 2.1: Cross sectional view of the Cavitating Venturi. *Flow runs from left to right, all inner geometries are uniform in design, and the dimensions are in inches.*

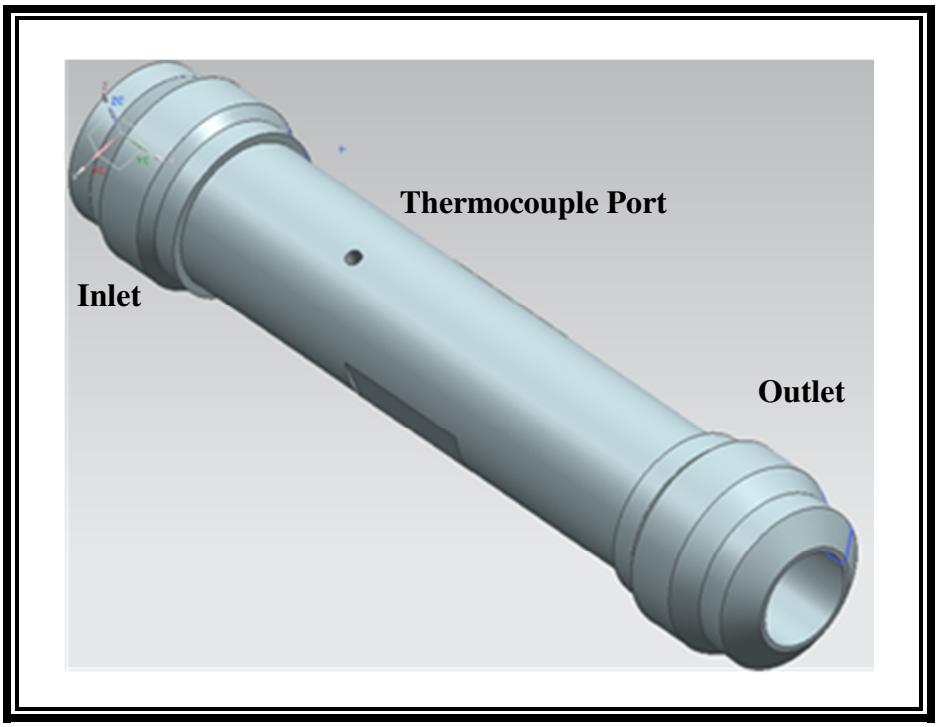

Figure 2.2: Cavitating Venturi overall view. *Flow runs from left to right.*

Now that all of the associated dimensions were defined, a regime of cavitation sustaining pressure ratios that extended up to the critical pressure ratio could be determined. Given the previously defined diametral dimensions, the calculated β and the suggested C_p from literature were substituted into Equation 3. The C_d value of 0.95 was used, which was on the conservative end of the widely accepted values. This decision was made because it is widely accepted by manufacturers of obstruction devices, and provides the lowest critical pressure ratio of the other options. This C_d value is conservative when compared to other accepted C_d values for obstruction flow meters. This means that above this C_d value, cavitation may or may not continue to occur even within the given range of accepted values spanning from 0.95-0.99, but beneath this value, cavitation would certainly occur. In terms of the testing to determine the actual discharge coefficient of the benchmark cavitating venturi flow meter, the pressure ratio, defined as P_2/P_1, is the testing parameter that can be modified by manipulating the hand valves to achieve the desired pressures. So, naturally, the flow regime in which cavitation would be expected should be described in terms of parameters that can be modified, specifically the upstream and downstream pressures. The critical pressure ratio therefore, serves as a limiting value comprised of readily controllable experimental readings to describe the limit in the range of the cavitating flow regime. The process through which the critical pressure ratio is defined begins with the computation of the measured mass flow rates from the venturi, comparing it with the average flow rate from the turbine flow meter and the catch flow test and calculating the discharge coefficient. The outlet pressure is modified, changing the overall pressure ratio and the test is repeated. The critical pressure ratio is then experimentally determined when the C_d values produced at the specified pressure ratios drastically decreases. Using this rationale, the theoretical critical pressure ratio was computed to be 0.72, and as shown in subsequent sections, was experimentally tested for verification purposes. [9] The coefficient of discharge experimental determination and validation process will be further described in Chapter 4, but essentially consists of a simple catch and measure methodology using water as the working fluid. This value was considered sufficiently applicable to use in the determination of the mass flow rates for the cryogens tested, as they were considered incompressible. This assumption will be likewise validated in the work presented in later chapters.

Chapter 3: Experimental Parameters

The experimental parameters were determined from the constraints imposed by four systems, namely, the propellant feed system, the data acquisition system (DAQ), the thrust measurement device and the actual Pencil Thruster. Each of the sections in this chapter will describe the influences that determined these specific requirements. Specifying these requirements will likewise further define the measures of success to which the cavitating venturi performance data will be compared. First, tables of the defined requirements will be listed and their contents explained in the following sections.

Table 3.1: DAQ System

Parameters	**Card Specs**
Type	NI PCI-6220
Accessories/Attachments	SCB-68 Connector Block
Analog Inputs/ Resolution (bits)	16/16
Digital I/O	24
Correlated (clocked) DIO	8- 1MHz
Max Acquisition Rate	1.5 kHz

Table 3.2: Propellant Feed System

	Water	**LCH_4**	**LOx**
Line Pressure	0.83 MPa	0.83 MPa	0.3-1.25-1.40 MPa
Line Temperature	298 K	123 K	100-123 K
Line Valve Response	4-20 ms	4-20 ms	4-20 ms
Line TC Rating	73-1523 K	73 – 1173 K	73- 1173 K
Flow meter Range (Temperature) (Flow rate)	5.4 – 505 K 0.25 – 4.5 gpm	5.4 – 505 K 0.25 – 4.5 gpm	5.4 – 505 K 0.25 – 4.5 gpm
Venturi Critical P Ratio	<0.69	<0.69	<0.69

Table 3.3: Torsional Thrust Balance Specifications

Functionality	**Specs**
Thrust range	8.9-35.6 N
Total stiffness	30.08 in-lbf/deg
Thrust measurement	Laser Interferometry (Micro-Epsilon OPTO-NCDT ILD 1402-100)

Table 3.4: Pencil Thruster Engine

Thrust	8.9 N – 35.6 N (2 lbf – 8 lbf)
ISP	> 150s
Mixture Ratio	1.5 – 2.7
Mass flow rate	0.0075 kg/s
Propellant State	Two-phase and liquid (LCH_4, LOx)
Burn Time	2 min at 50% duty cycle
Altitude 1	Phase 1: at ambient
Altitude 2	Phase 2: 11.3 psi (White Sands Test Facility +1km)

It is important to note that the driving factors behind determining the inlet condition requirements and the desired mass flow rate for the Pencil Thruster, was ultimately to specify the amount of thrust (and ISP) that the Reaction Control Thruster was theoretically capable of delivering. The specifications of the instrumentation will be detailed in Chapter 4 for their respective test setup applications.

3.1 Mass Flow Rate and Mixture Ratio Requirements

The mass flow rate and mixture ratio requirements were specified in the previous work to develop the Pencil Thruster. Meeting these specifications however, meant that the line pressures, and by extension the flow rate of both the oxidizer and the fuel needed to be carefully manipulated to maintain pressures and temperatures. The goal was to maintain the liquid state of the propellants to the greatest degree possible while keeping the mass flow rates and therefore mixture ratios stable. In addition, the line pressures must fall below the ratings specified by both the pressure transducers and the valves. Furthermore, the check valves incorporated into the line also had a pressure rating that required consideration. The pressure ratings for the supply tanks were sufficiently high that they were not considered to be a limiting factor in this case. Thermocouples and temperature diodes were purchased that had a sufficiently large range that they could capture a gamut of temperatures that fell well beyond those seen by the propellants under the desired conditions. For this reason, they were also not considered a limiting factor for this case. For the purposes of clarity, it is important to note that the main difference between temperature diodes and thermocouples is their junction. The thermocouples used in the venturi setup and to instrument the actual RCS thruster and methane condensation tank are cold junction thermocouples (K and E type) from Omega. The temperature diodes used on the LOx line in the RCS setup use a PN junction and were produces by Lakeshore. These junctions are what determine the linearity of the temperature measurements. It should also be noted that temperature diodes can be incorporated into a thermocouple to provide a reference for the summing junction.

3.2 P ratio range (Required Inlet Pressure)

Aside from the computations detailed in Chapter 2 to determine the critical pressure ratio ensuring cavitation, the inlet pressures themselves for both the LOx and LCH_4 were selected based on the pressure and temperature values that would keep them in liquid form, while maintaining the proper mixture ratios and flow rates. Pressure ratings for the solenoid valves, check valves, and pressure transducers were likewise taken into consideration. The temperature ratings on all of the aforementioned devices were all for cryogenic fluids, so this was not considered an inhibitive factor to the pressure range selection.

3.3 Operating Temperature Range

The operating temperature range clearly must include temperatures for which the propellants remain liquid at their given operating pressures. Since liquid oxygen has the lowest boiling temperature of the possible working fluids, the temperature range was determined primarily with LOx in mind, but also includes the temperature ranges for which the methane would remain in liquid form. It is important to note that the only mechanism currently in place within the experimental setups to help maintain the temperature involves the insulation installed on the supply lines and methane condensation/supply tank. To some degree, the flow rate of the propellants (controlled by the tank pressure) also helps to regulate the line, and likewise the fluid temperature. However, due to the fact that the LOx is supplied from a commercially available dewar, its only mechanism for maintaining tank pressure throughout the span of a test is through the manipulation of a hand actuated pressure valve. This is significantly less effective than having a blow-down supply system consisting of a tank pressurized by a separate gas source.

3.4 Testing Duration

The testing duration for both the in-situ testing within the Pencil Thruster setup as well as the independent venturi setup involved 10 second, automated tests. The original intended "burn" duration was 2 minutes. However, because of film cooling issues relating to the Pencil Thruster design, the burns have only been a maximum of 10 seconds in duration. For this reason, the flow test durations for the cavitating venturi characterization testing have likewise been limited to 10 seconds. This was done with the intent to observe if fully developed flow could be reached through steady cavitation, despite the residence time it takes for the cavitation nuclei to grow sufficiently.

Chapter 4: Experimental Setup and Procedure

This chapter details the experimental setup and the modifications made to accommodate each of the different working fluids. The first section of this chapter details the water testing that was done to determine the critical pressure value and coefficient of discharge characteristic of the cavitating venturi, which was then utilized for the mass flow rate computations in the subsequent cryogen tests. Explanations and figures will be provided to highlight the necessity for these changes. It is important to note that the water testing was performed strictly for the purpose of determining the characteristic parameters of the cavitating venturi. For this reason, the results of the water testing will be included in this chapter, as they are utilized in the data processing of the subsequent working fluids to process the pressure and temperature data into mass flow measurements for the cavitating venturi flow meter. The steady-state cryogenic testing on the other hand, was performed to observe the deviations from this ideal performance caused by the behavior of the cryogens and to determine if they were significant enough to invalidate this flow control method for cryogenic use.

4.1 Venturi Test Setup

Many of the differences in the test setup involved downstream valve placement and the upstream source of the working fluid. However, we will begin by first discussing the instrumentation that is common to each of the testing configurations. All subsequent sections in this chapter will describe the specific differences.

4.1.1 Shared Instrumentation

In all of the setup configurations, the common components include the turbine flow meter, the pressure transducers, and the thermocouples. Below are three tables that enumerate the operating ranges with their associated measurement uncertainties. This information was obtained directly from the manufacturers in the user manuals. Please note that the row labeled ‘Implementation Location’ is making reference to the instrument’s placement within the test apparatus. Their locations will be more clearly denoted in the diagrams included in the subsequent sections of this chapter.

Table 4.1: Liquid Turbine Flow meter [14]

Make/Model	Hoffer Flow Control
Operating Flow Range	2.21×10^{-5} to 2.21×10^{-4} m^3/s (0.25-3.5 gpm)
Measurement Uncertainty	+/-0.1% for 1.58×10^{-5}-2.84×10^{-4} m^3/s (0.25-4.5 gpm)
Op Temperature Range	5.4-505 K (-450 to 450 °F)
Implementation Location	In parallel with cavitating venturi

Table 4.2: Cryogenic Pressure Transducers [15]

Make/Model	OMEGA thin-film, cryogenic
Operating Temp Range	77-422 K (-320 to 300 °F)
Measurement Uncertainty	Combined linearity, hysteresis, and repeatability accuracy +/- 0.25% of full scale output
Implementation Location	Upstream and downstream of venturi

Table 4.3: Thermocouples [15]

Make/Model	OMEGA, ungrounded, cryo rated, E-Type
Operating Temp Range	73-273 K (-328 to 32 °F)
Measurement Uncertainty	+/- 1% for 73-273 K (-328 to 32 °F)
Implementation Location	Upstream and downstream of venturi

4.1.2 Water Testing Setup and Operational Procedure

This section details the water testing setup and operational procedure used in this investigation to experimentally determine the discharge coefficient and actual critical pressure ratio. It was based on a previously detailed industry standard methodology for obstruction flow meter calibration. The description will contain both figures and a detailed operation for this process. Furthermore, the graphs of the data that were used to indicate the C_d and the P_{cr} are likewise contained in this section along with a physical interpretation of the data showing the need for specific design features included in the experimental apparatus.

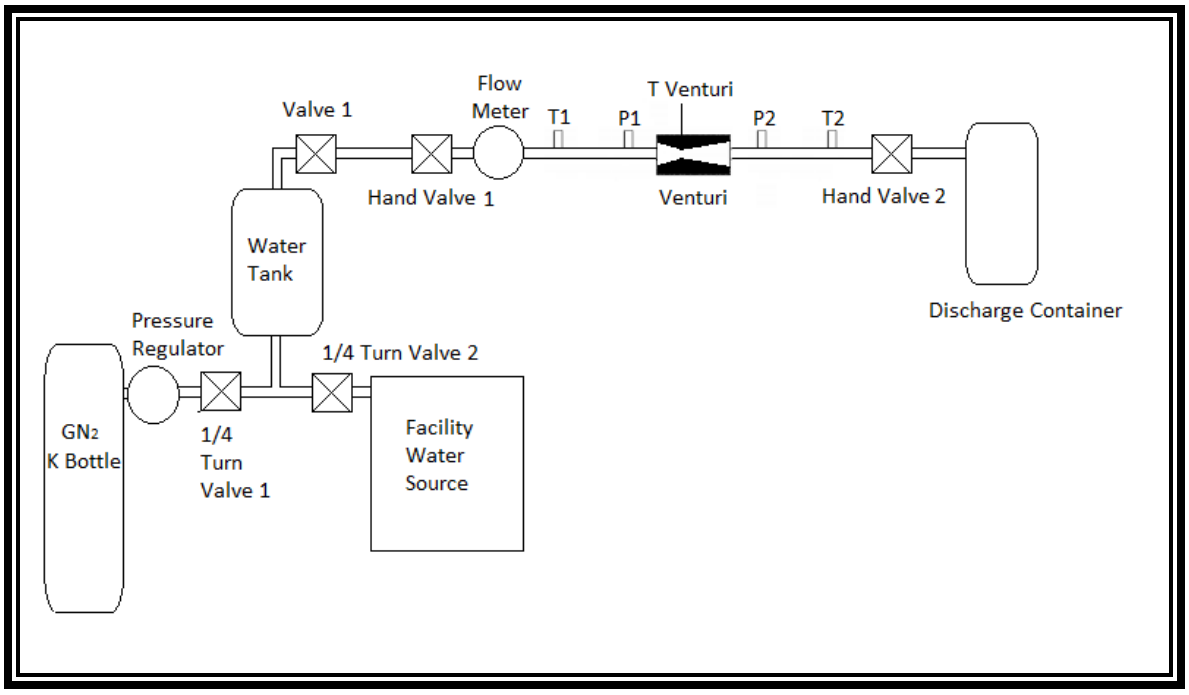

Figure 4.1: Water test setup (a) for Venturi. *Solenoid valve 1 is located upstream of the venturi. Figure is compliments of source [16].*

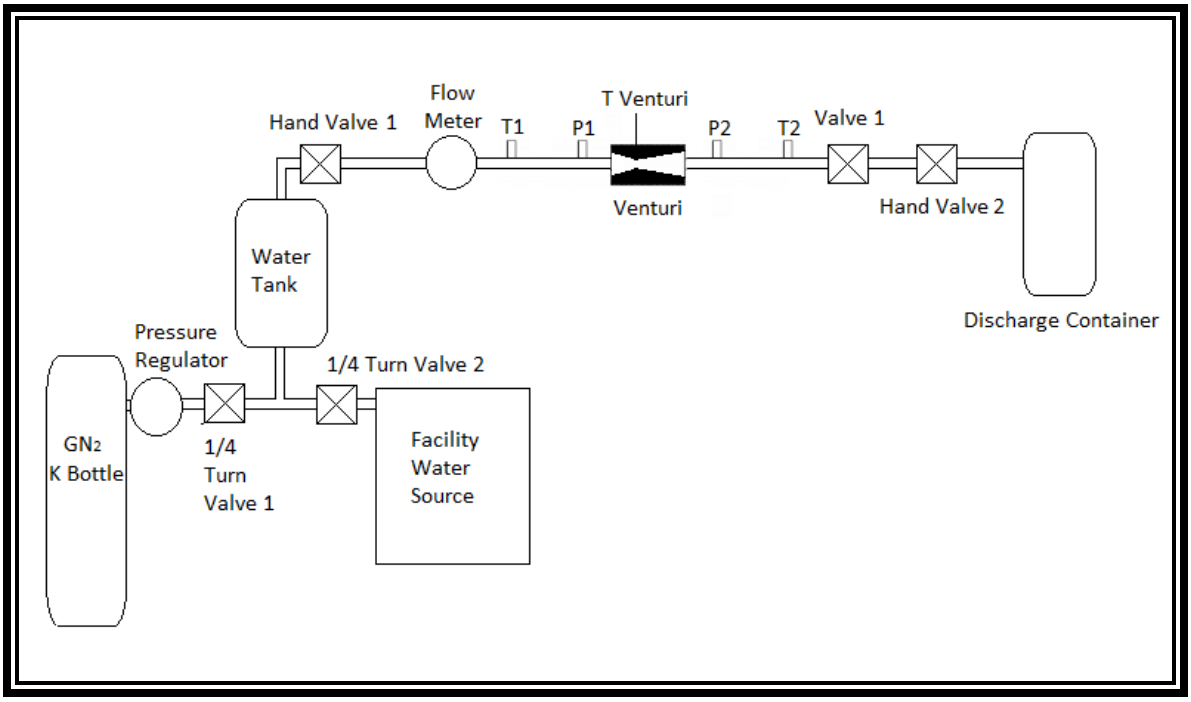

Figure 4.2: Water test setup (b) for Venturi. *Solenoid valve 1 is located downstream of the venturi. Figure is compliments of source [16].*

The figures above illustrate the test apparatus used to determine the discharge coefficient of the cavitating venturi flow meter. There are common features of both test setups but the main difference lies in the placement of the solenoid valve, labeled in the figure as Valve 1. Figure 4.2 defines the final placement of solenoid Valve 1 and the reasoning for this design change will become evident upon further discussion in this section. The following table is a matrix of testing conditions that governed the water validation testing.

Table 4.4: Liquid Water Cavitating Venturi Flow meter Testing Parameters

Working Fluid	Liquid Water
Operating Temperature	Room Temperature (295 K)
Inlet Pressure	0.83 MPa (120 psia)
Pressure Ratio (P_2/P_1) Range	0.2 – 0.85
Data Acquisition Rate	10 Hz
Test Duration/Pulse Width	10 seconds

The testing procedure beings with filling the water tank with water from the laboratory facility supply line via the ¼ turn valves as shown in the figures. This was done by first opening all of the valves, both hand actuated and solenoid, downstream of the tank to allow for the expulsion of the air in the tank. The turbine flow meter was protected from overspinning by limiting the flow out of hand valve 1 to an acceptable range, as was assessed by a LabVIEW boolean that read the turbine flow meter voltage output. The valve was manually operated so that the voltage reading was not allowed to exceed 4 volts, which was within the range of safe usage specified by Hoffer, the turbine flow meter manufacturer. Hand valve 1 was closed to allow for the water to accumulate in the supply tank as soon as a steady stream of water was observed flowing out of the line exit into the discharge container. Upon filling, the ¼ turn valve from the water supply to the tank was closed and the ¼ turn valve from the gaseous nitrogen (GN_2) was then opened to pressurize the tank to the desired upstream pressure.

Recalling the idea put forth in the literature review and design chapters, the development of cavitation allows the mass flow rate to be determined based on the upstream pressure only. So to ensure that cavitation actually occurs, a range of ratios of the downstream to upstream pressures (P_2/P_1) was implemented during the testing that spanned from 0.2-0.85 as indicated in the table above. It should be noted that this range extends from below to beyond the calculated critical pressure ratio of 0.72 because this value needed to be experimentally verified as well. The aforementioned pressure ratios were achieved by manually actuating the downstream hand valve 2 while hand valve 1 remained constant to provide the required upstream pressure of 120 psia.

The actuation of the solenoid Valve 1 was automated using a command sequence generated in LabVIEW. This facilitated a 10 second pulse width per test to be implemented. It was likewise through this LabVIEW GUI that the temperature, pressure, and turbine flow meter data was collected. The first two measurements allowed for the mass flow rate through the cavitating venturi to be calculated through the Bernoulli equation as detailed in Chapter 2. The turbine flow meter data provided a point of comparison to validate the average mass flow rate obtained by dividing the total mass of the water collected during the test by the 10 second flow duration.

Through analysis of the data, it became apparent that there was a spike in the turbine flow meter readings before the flow reached steady state. This transient overshoot condition was likely due to the buildup of ambient air in the line that formed during the filling and pressurization process after hand valve 1 was closed to allow for water accumulation in the tank. In an effort to minimize this initial phenomenon, the solenoid valve was placed downstream of the cavitating venturi as shown in Figure 4.2; thus allowing the facility to be primed prior to beginning the experiment. When compared with the mass flow rate data collected during the testing performed in the Figure 4.1 apparatus, the only significant difference noted was found in the transient overshoot readings. The resulting graphs from these comparisons are shown and explained below.

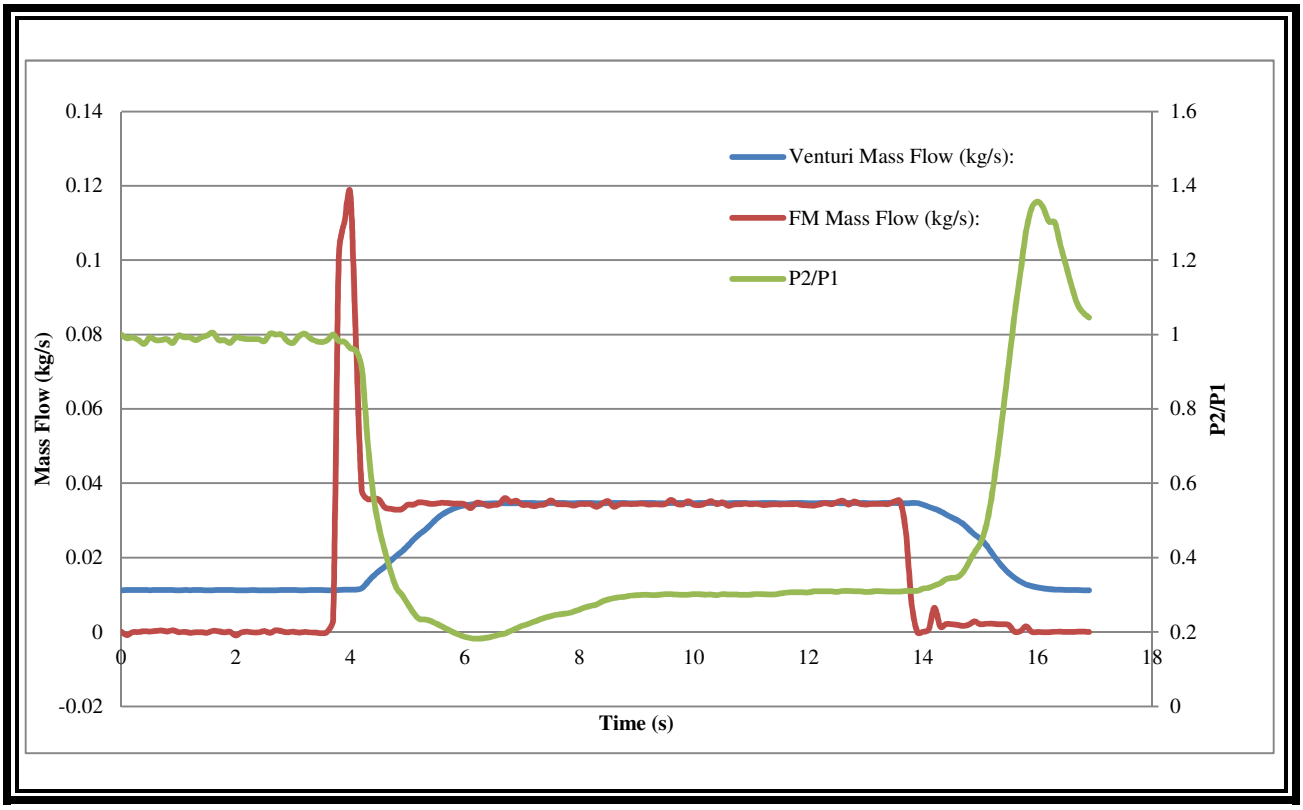

Figure 4.3: Water test ran at pressure ratio below the critical pressure ratio. *Mass flow rate versus time when solenoid valve 1 is upstream of the venturi. See figure 4.1. [16]*

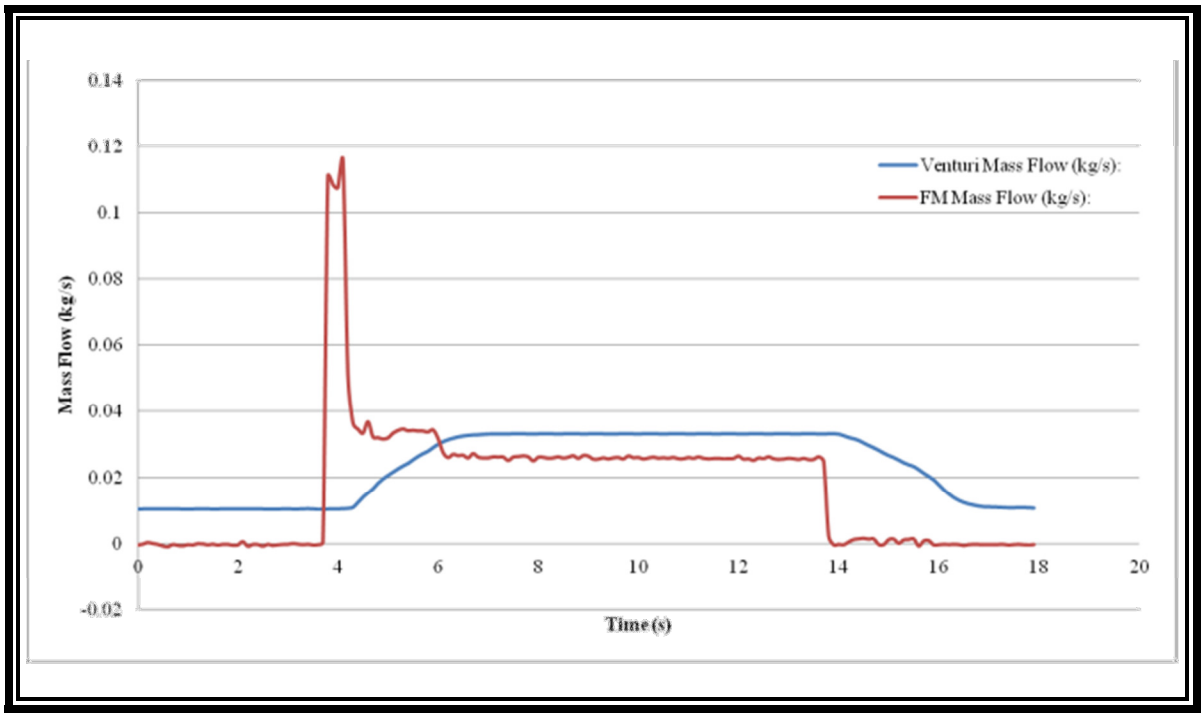

Figure 4.4: Water test ran at pressure ratio above the critical pressure ratio. *Mass flow rate versus time when solenoid valve 1 is upstream of the venturi. See figure 4.1. [16]*

The mass flow rates as measured with the cavitating venturi flow meter and the turbine flow meter over the timespan of the pulse is depicted in Figures 4.3-4.6. Figures 4.3 and 4.4 are both showing data from the first water testing configuration with solenoid valve 1 placed upstream of the cavitating venturi. The first test graphed in Figure 4.3 details the mass flow rates for a pressure ratio that falls below the critical value and the graph in Figure 4.4 is for a pressure ratio above the critical value. In both of these graphs, the transient overshoot behavior can be clearly observed. It should be further noted that in both of these graphs, it is shown that the cavitating venturi flow meter and the turbine flow meter both experience a rise in mass flow rate and decline in mass flow rate at the beginning and the end of the test period respectively. The rise for the cavitating venturi mass flow meter is much more gradual than that of the turbine flow meter. This is by virtue of the kinds of measurement sensors that each employs to measure the mass flow rate. The piezoelectric sensor within the turbine flow meter is activated by the momentum of the moving fluid and is not meant to obstruct/control the fluid flow so its response time is nearly instantaneous. In the cavitating venturi flow meter, the response is much slower as the pressure transducers obviously are operating in response to a change in pressure.

The flow obstruction of this flow meter delays the relief/changes of the pressure within the supply line, likewise affecting the response time of the cavitating venturi flow meter overall. This response delay between the pressure transducers and the turbine flow meter can be observed in Figure 4.3 where you would expect the pressure ratio to respond in tandem with the mass flow rate to the valve actuations. The more gradual nature of the pressurization and depressurization regions contrast the more instantaneous behavior of the turbine actuation of the turbine flow meter.

The most notable deduction that can be made from the graphs in Figures 4.3 and 4.4 though is that the mass flow rates measured with the turbine flow meter and the cavitating venturi flow meter are in agreement when operating with a pressure ratio below the P_{cr} value. As expected, this is not the case for pressure ratios that exceed the critical value. To be specific, the data from the turbine flow meter depicts a significantly lower mass flow rate than what is predicted through the mass flow rates obtained from the cavitating venturi flow meter section of the testing apparatus. This is likely due to the lack of cavitation, as predicted through the equations in Chapter 2, in the flow regime exceeding the critical pressure ratio.

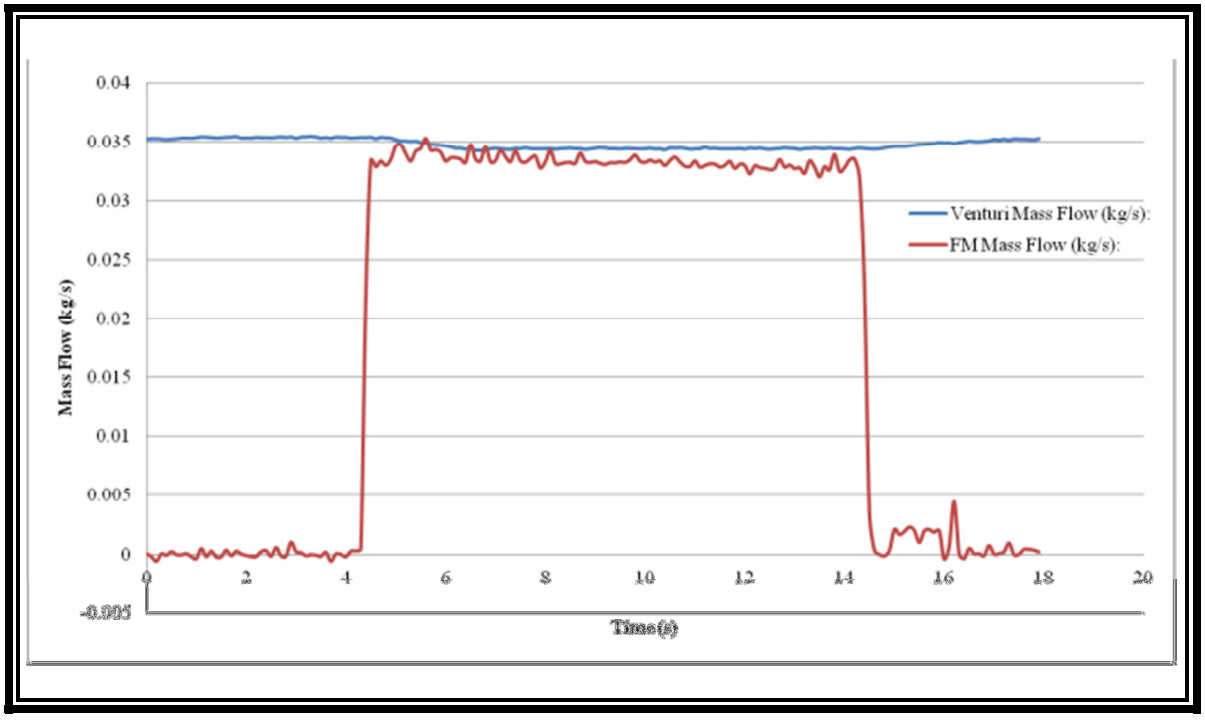

Figure 4.5: Water test ran at pressure ratio below the critical pressure ratio. *Mass flow rate versus time when solenoid valve 1 is downstream of the venturi. See figure 4.2.*

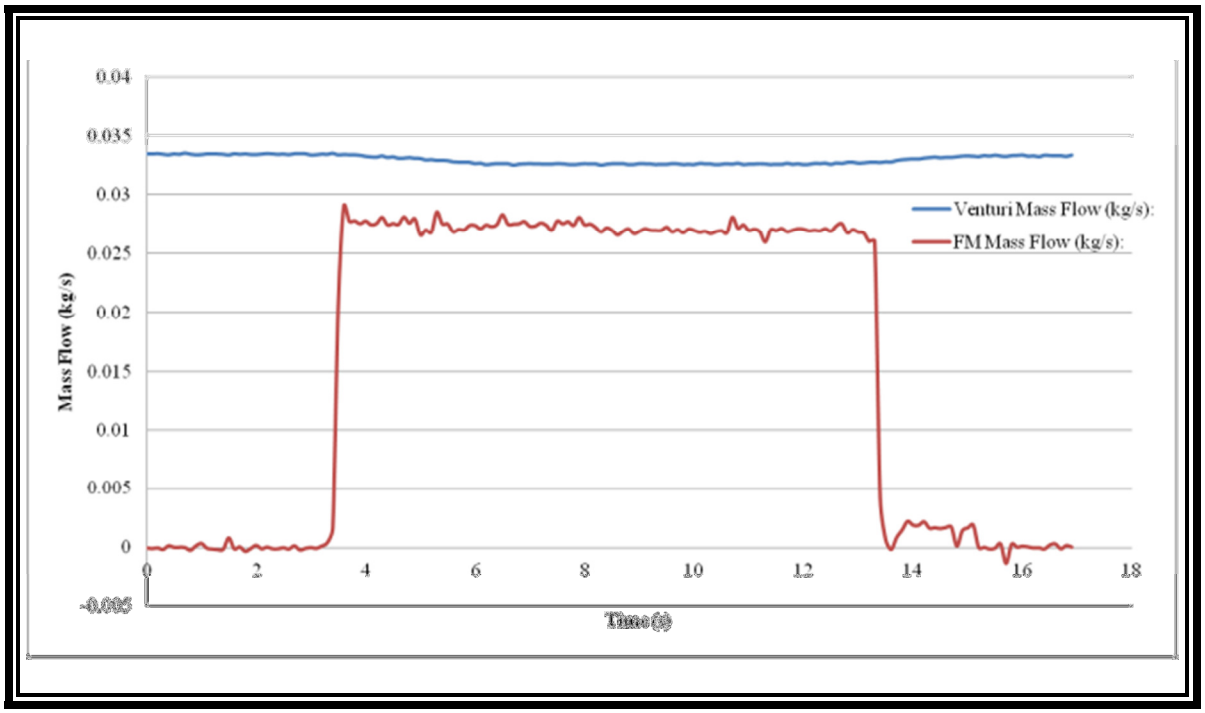

Figure 4.6: Water test ran at pressure ratio above the critical pressure ratio. *Mass flow rate versus time when solenoid valve 1 is downstream of the venturi. See figure 4.2.*

Figures 4.5 and 4.6 represent a repetition of the water testing, using the apparatus configuration described in Figure 4.2, where solenoid valve 1 is placed downstream of the cavitating venturi flow meter. Both of these graphs show a decrease, nearing a complete elimination of the transient overshoot phenomenon experienced by the turbine flow meter in the testing done with the previous solenoid valve configuration. Another notable difference between the data obtained with this apparatus configuration as opposed to the previous is the seeming lack of a transient mass flow rate conditions experienced by the cavitating venturi flow meter at the beginning and end of the testing. This is directly a result of the placement of solenoid valve 1 downstream of the cavitating venturi flow meter, allowing the sections of the line before and after the flow obstruction to be pre-filled and thus eliminated in the pressure variations at each pressure transducer location.

The results obtained from the secondary water test apparatus are congruent with those of the previous apparatus in that for pressure ratios below the critical, the turbine flow meter data is consistent with the mass flow rates obtained from the cavitating venturi flow meter. When compared with the subcritical pressure ratio results from the first test (Figure 4.3) there was less than a 2% deviation in the

data obtained from the second subcritical test (Figure 4.5), when disregarding the transient region. Furthermore, for pressure ratios exceeding the theoretically computed critical value, the mass flow rates obtained from the cavitating venturi flow meter were likewise higher than those obtained from the turbine flow meter. When comparing the data obtained from the two different apparatus configurations in the supercritical pressure ratio range, the mass flow rate values were comparable (in Figures 4.4 and 4.6) and likewise only possessed significant deviations from each other in the transient flow regions of the graph. The experimentally confirmed critical pressure ratio was deduced from the following graphs relating variations in the coefficient of discharge to a range of pressure ratio flow settings. It should be noted that the criterion used for ascertaining the critical pressure ratio was a sharp drop in the coefficient of discharge value, which would indicate that the cavitation has ceased to choke the fluid flow at the throat. When this occurs, the pressure downstream of the cavitating venturi flow meter begins to affect the upstream flow behavior.

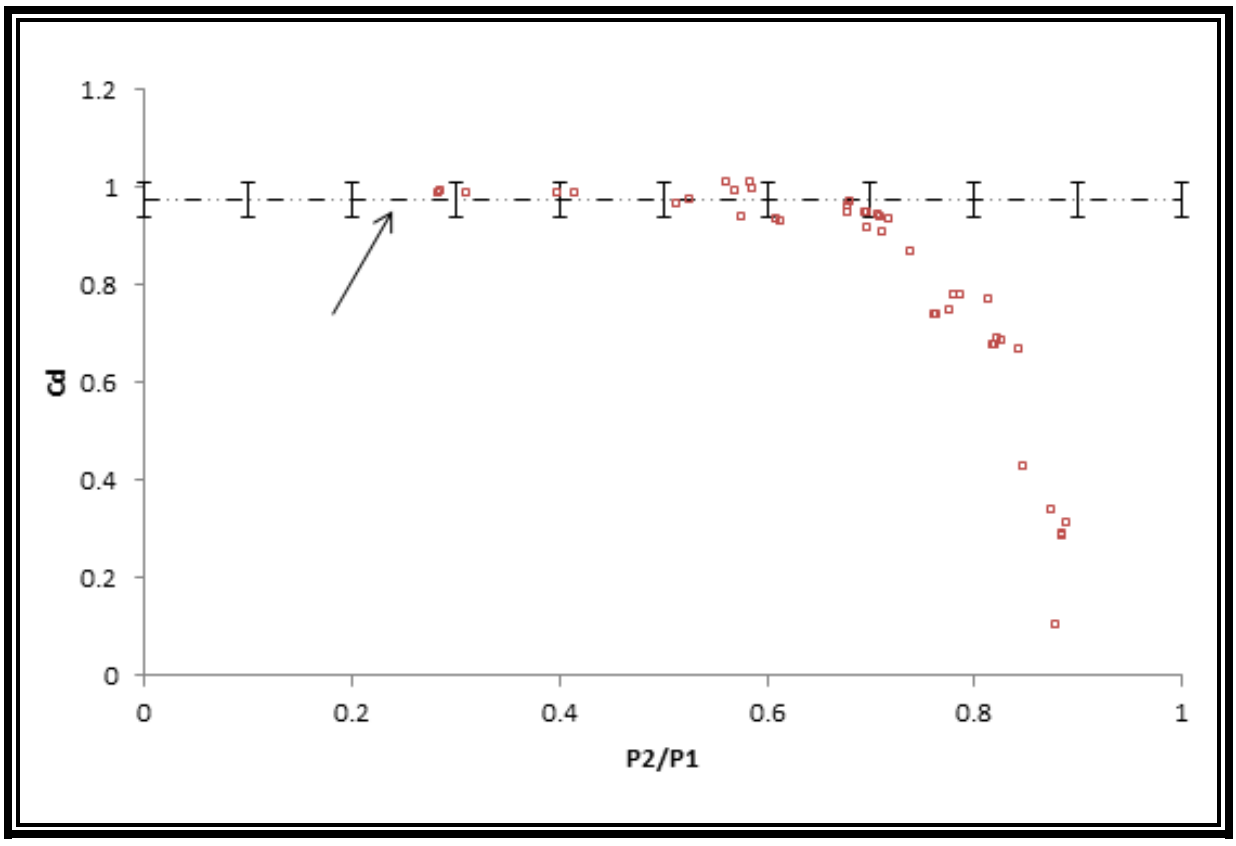

Figure 4.7: Discharge coefficient vs. Pressure Ratio. *Liquid Water at standard inlet conditions. [16]*

In the graph shown above, the average discharge coefficient within the cavitating region of the flow regime is denoted with a dashed line with error bars indicating the associated uncertainty. As can be seen, the minimum of 0.94 with the average C_d value of 0.977 is observed while cavitation is occurring, possessing an uncertainty of ±0.0357 with a 90% confidence interval that accounts for both precision and biasing errors. It should be noted that the precision error is considered the more predominant component of the total error. The high level of accuracy in the machining at the venturi throat along with the inlet pressure measurement renders the bias error in the mass flow rate (as computed by the Bernoulli Equation) negligible when compared to the precision error. As shown in Figure 4.7, the regime of useful cavitation flow control extends up to a pressure ratio nearing 0.69, which slightly deviates from the theoretically predicted value of 0.72. The experimentally obtained Cd value of 0.69 could then be used to calculate the actual mass flow rate being metered by the cavitating venturi flow meter through implementation into Equation 1. The results involving the liquid methane will be detailed in Chapter 5.

4.1.2 Liquid Methane Testing Setup and Operational Procedure

The liquid methane ($LCH_{4)}$ test apparatus for the cavitating venturi flow meter verification testing was a modification of the water test setup. The main alterations were made to accommodate a LCH_4 condensation unit and a liquid nitrogen (LN_2) coolant system. The LN_2 was supplied by a commercially available dewar. Due to the safety concerns associated with storing large, commercially available amounts of LCH_4, it was liquefied in the required amounts on site from high purity gaseous methane using a condensation unit that was previously developed in the Center for Space Exploration Technology Research. An image detailing the condensation unit is shown in the figure below.

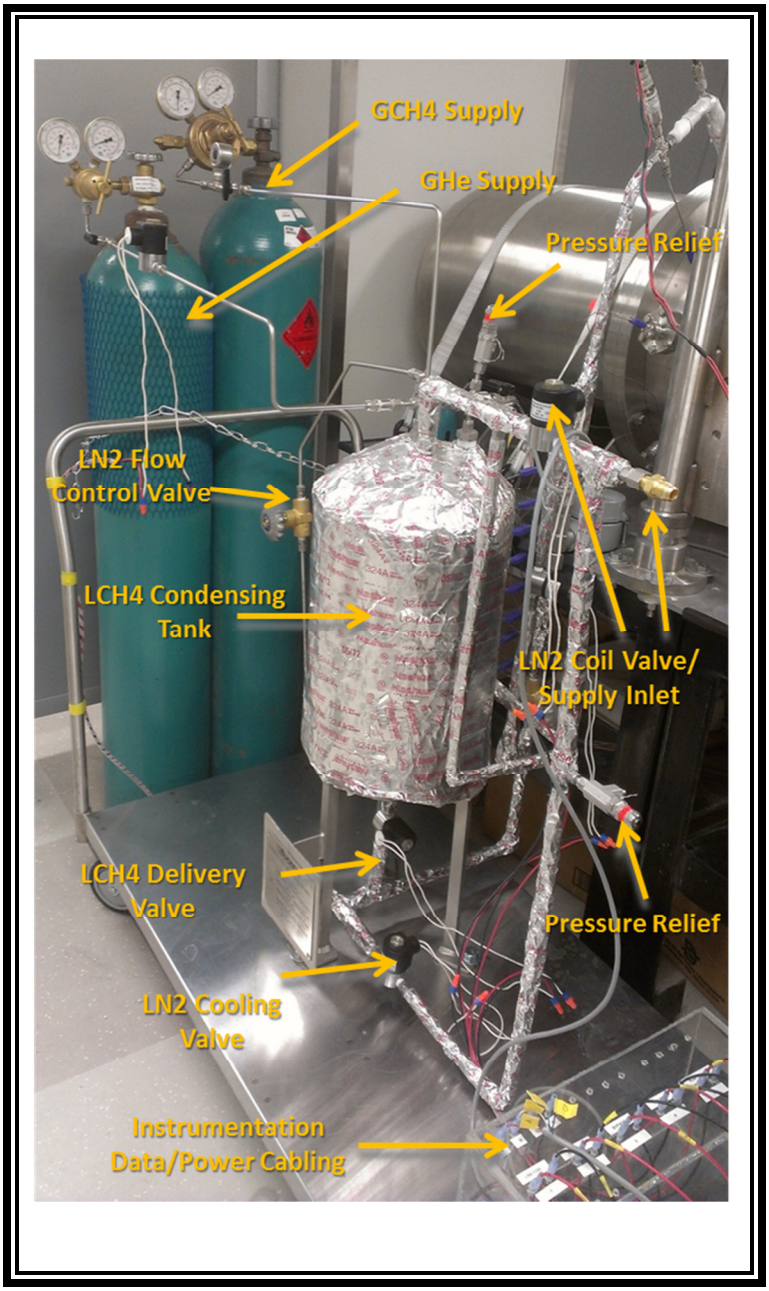

Figure 4.8: Liquid Methane Condensation Unit. *Photo was taken by Manuel Galvan.*

The LN_2 coolant system shown in Figure 4.9 was incorporated to chill the entire testing apparatus prior to flow testing with the LCH_4 in an effort to mitigate erroneous results caused by the boiling of LCH_4 coming in contact with warm lines. It encompasses the addition of a coolant relief line and discharge catch-dewar that intersects the supply line between hand valve 1 and the turbine flow meter. The relief line begins with a secondary solenoid valve (Valve 2) that both serves as an outlet for the LN_2 during the cooling process and prevents the release of LCH_4 through the coolant discharge line

during the actual LCH_4 flow test. Intricately choreographed actuations of hand and solenoid valves take place during the cooling process that balance the need to protect the delicate inner workings of the turbine flow meter from overspinning while relieving the LN_2 boil-off from the supply tank before the actual liquid state LN_2 can flow through the line. This is achieved by opening solenoid valve 2 completely while keeping hand valve 1 partially closed during the initial phase of the cooling process. It is the regulation of hand valve 1 that prevents the piezoelectric sensor components of the turbine flow meter to spin beyond their 4 volt output limit while the LN_2 boil-off is released. Upon the discharge of actual liquid state nitrogen, hand valve 1 is opened further and the solenoid valves are actuated to produce flow cycling until a target line temperature of approximately 123 K is reached. The entire feed line and apparatus was insulated with two layers of Cryogel® insulation adhered to the line with standard aluminum ducting tape. The insulation in conjunction with periodic cooling sequences between each test was used to simulate as closely as possible, isothermal conditions within the feed lines and the cavitating venturi.

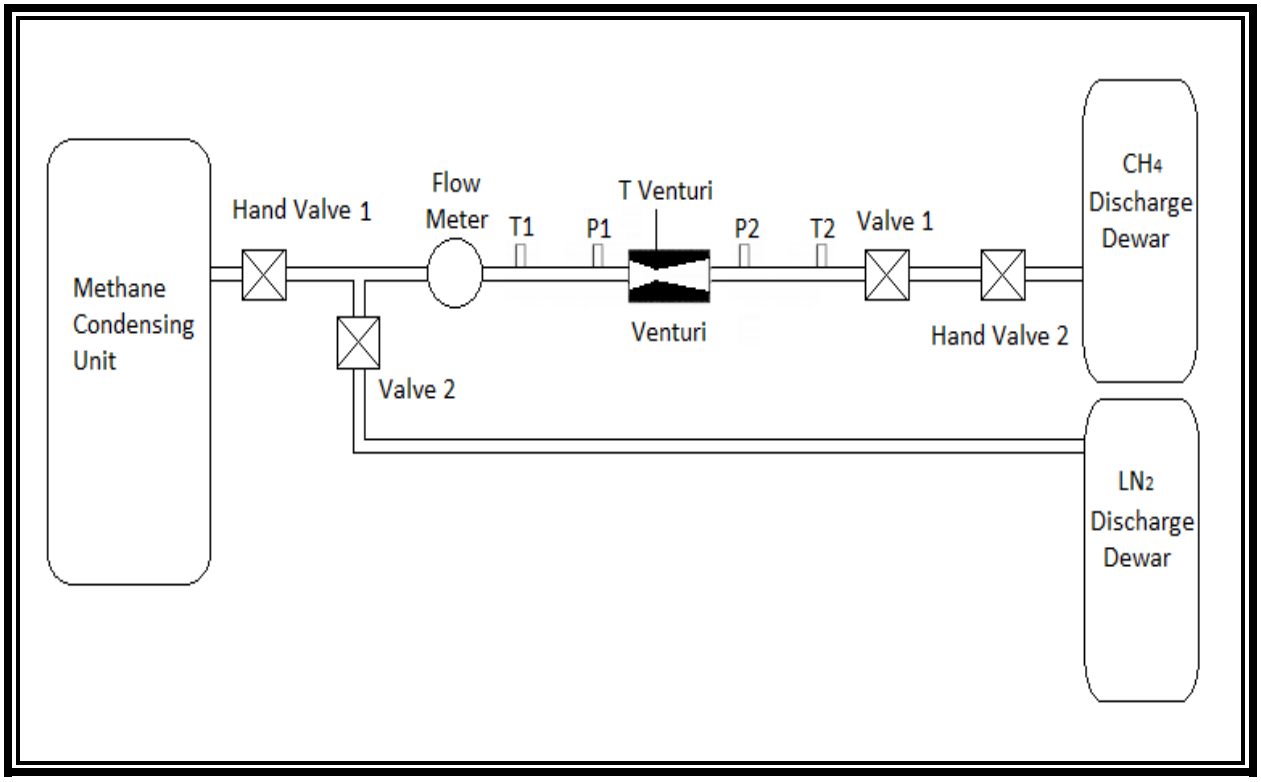

Figure 4.9: Venturi setup for liquid methane tests. *Figure is compliments of source [15].*

The liquid methane (LCH_4) testing procedure consists of three general phases. The first phase is the methane condensation process which is detailed in the cited Galvan work [17], followed by the cooling sequence described in the previous paragraphs. Upon completion of the cooling sequence, the flow testing could commence. Similar in structure to the water testing, the LCH_4 procedure differs only in two key aspects. First, the methane tank is pressurized by a gaseous helium source which is incorporated into the methane condensation unit. Furthermore, the LCH_4 collected in the discharge dewar is not measured and used to provide an average mass flow rate as in the water tests because it boils off during the span of the testing and would not provide a reliable point of comparison. So, in this testing only the turbine flow meter data serves as a point of comparison for the cavitating venturi flow meter validation. The testing parameters, which closely mirror the liquid water tests, are detailed in the table below. Please note that the data acquisition rate applies to the collection of the pressure, temperature, and turbine flow meter flow rate data through the entire duration of the test.

Table 4.5: Liquid Methane Cavitating Venturi Flow meter Testing Parameters

Working Fluid	Liquid Methane (Liquid Nitrogen coolant)
Operating Temperature	123 K
Inlet Pressure	0.83 MPa (120 psia)
Pressure Ratio (P_2/P_1) Range	0.2 – 0.95
Data Acquisition Rate	10 Hz
Test Duration/Pulse Width	10 seconds

After the conclusion of the testing cycle, some data processing is required to obtain the correct mass flow rates from both the cavitating venturi flow meter (with its associated instrumentation) and the turbine flow meter. In the previous section, it was discussed that the mass flow rate through the cavitating venturi flow meter could be obtained simply through the substitution of the experimentally

obtained C_d value into the Bernoulli equation as expressed in Equation 1. The turbine flow meter measurements could then be applied directly as the comparison value for calculation of the C_d as it is specifically calibrated for use with water at standard conditions. Liquid methane however, is less viscous than water and is expected to have a higher discharge coefficient. With this consideration in mind, it is logical to assume then that the Cd for the liquid methane should fall somewhere between the average value for liquid water, which is 0.977 and 1.0. Given that a C_d value of 1.0 implies no losses through the flow obstruction feature and the calculated total error of 0.0357 is likewise applied to the liquid methane C_d, it is a sound assumption that the variation between the water flow C_d and the liquid methane C_d would fall within the uncertainty bounds. For this reason the C_d applied for the determination of the mass flow rate of water through the cavitating venturi flow meter, is likewise considered applicable when determining the mass flow rate of the liquid methane. The processed data will be presented in the following chapter.

Chapter 5: Experimental Results

This chapter details the experimental results obtained through flow testing performed on the cavitating venturi flow meter. Please note that the results from the water testing performed with the benchmark cavitating venturi flow meter were included in the previous chapter for the purposed of defining how the liquid methane tests were conducted. However, a section is again included in this chapter relating to the water testing. This is simply because two other venturis were manufactured and underwent the same testing regiment, with somewhat differing results. The details and explanations for this will likewise be discussed before moving on to the results of the liquid methane testing in the subsequent section.

5.1 Water Testing, determination of the steady cavitation flow regime C_d and $P_{critical}$

In response to requests made by counterparts from NASA Johnson Space Center working on the Pencil Thruster project, two additional cavitating venturi flow meters were produced with the same internal flow geometry as the benchmark test article. In an effort to provide characteristic values such as the coefficient of discharge and critical pressure ratio, water flow tests were likewise performed on the venturis given the part number of VFM-001 and VFM-002. As previously mentioned there were some dimensional differences between all three of the cavitating venturi flow meters. Tolerances were given for each of the dimensions as detailed in the following table that references the specific dimensions shown in the associated figure. The most notable variations however, were in the throat region and exceeded the allowable tolerances. The benchmark cavitating venturi flow meter was well within the allowable tolerance and was sized at exactly 0.040 in throat diameter with a caliper sensitivity in the +/- 0.001 inch range. VFM-001 and VFM-002 however possessed throat diameters of 0.041 and 0.043 inches respectively. [18]

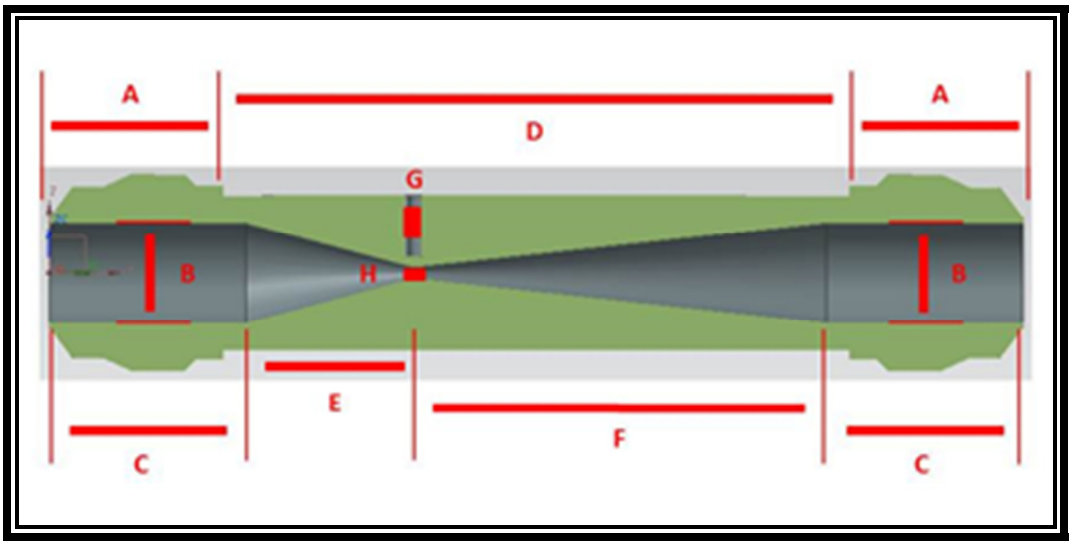

Figure 5.1: Cavitating Venturi Reference Geometry. *See table below for reference identifiers.*

Table 5.1: Venturi Dimensions

Identifier	Size (in)	Tolerance (in)	Surface Finish (micro in)
A	0.660	+/-0.01	32-250
B	0.380	+/-0.005	32-250
C	0.75	+/-0.01	32-250
D	2.384	+/-0.005	32-250
E	0.634	+/-0.005	32-250
F	1.571	+/-0.005	32-250
G	0.063	+/-0.005	32-250
H	0.040	+/-0.005	32-250

The resulting coefficients of discharge and critical pressure ratios associated with each of the cavitating venturi flow meters likewise changed and their averages are detailed in the tables below along with the corresponding confidence values. These variations could best be explained by the significant variations in the throat diameter sizes. [18]

Table 5.2: Cavitating Venturi Discharge Coefficients

P_2/P_1 Range (+/-0.05)	**Benchmark VFM (0.977 +/- 0.036)**	**VFM-001 (0.917 +/- 0.037)**	**VFM-002 (0.973 +/- 0.028)**
0.20	0.95	0.94	0.98
0.30	0.95	0.94	0.98
0.40	0.94	0.93	0.98
0.50	0.94	0.90	0.98
0.60	0.99	0.86	0.96
0.70	0.86	0.73	0.93
0.80	0.71	0.62	0.74
0.90	0.43	Not Tested	0.60

The graphs below are visual representations of the data from which the coefficient of discharge values were obtained. The dashed line depicts the average coefficient of discharge experimentally obtained at particular pressure ratios within the cavitation inducing testing regime. The error bars shown in the graphs depict the uncertainty of the coefficient of discharge values and are ±0.037 and ±0.028 for VFM-001 and VFM-002 respectively with a 97.5% confidence interval. [18]

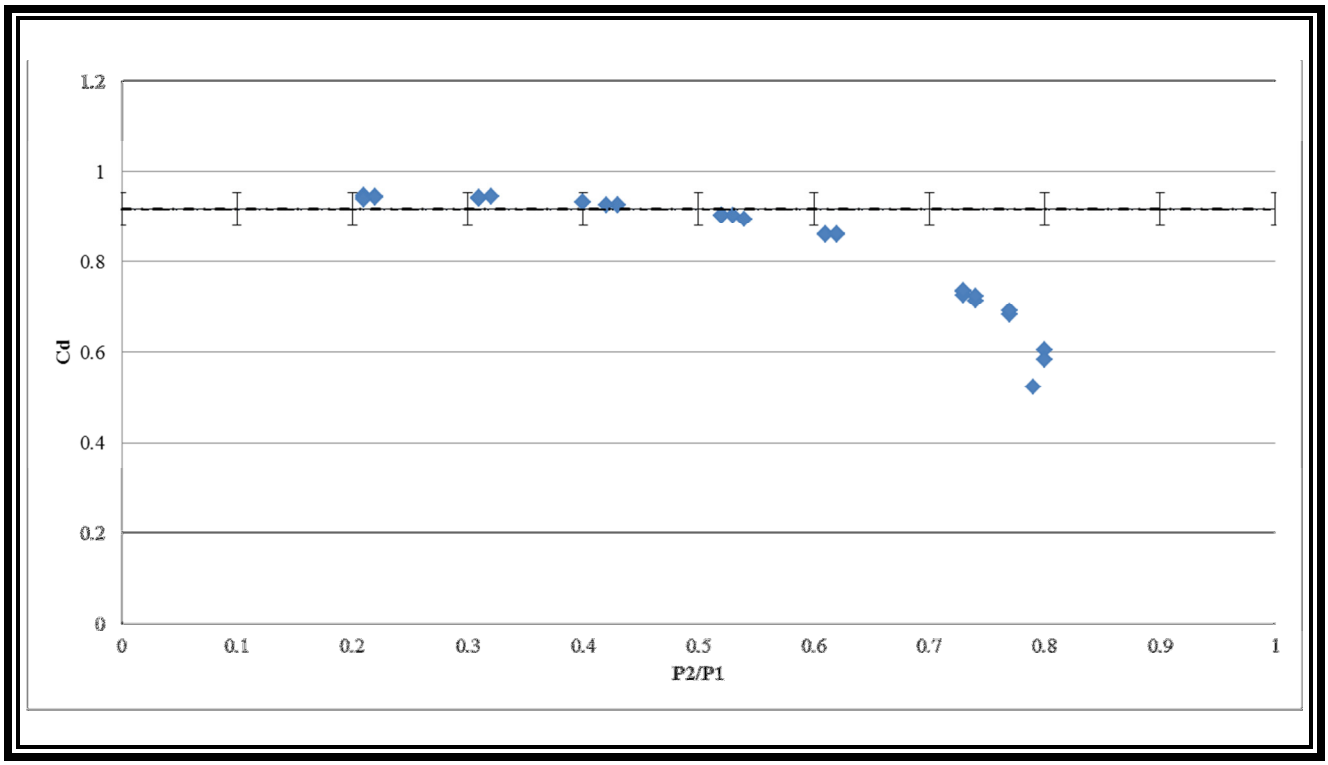

Figure 5.2: VFM-001 Discharge Coefficient vs. Pressure Ratio. [18]

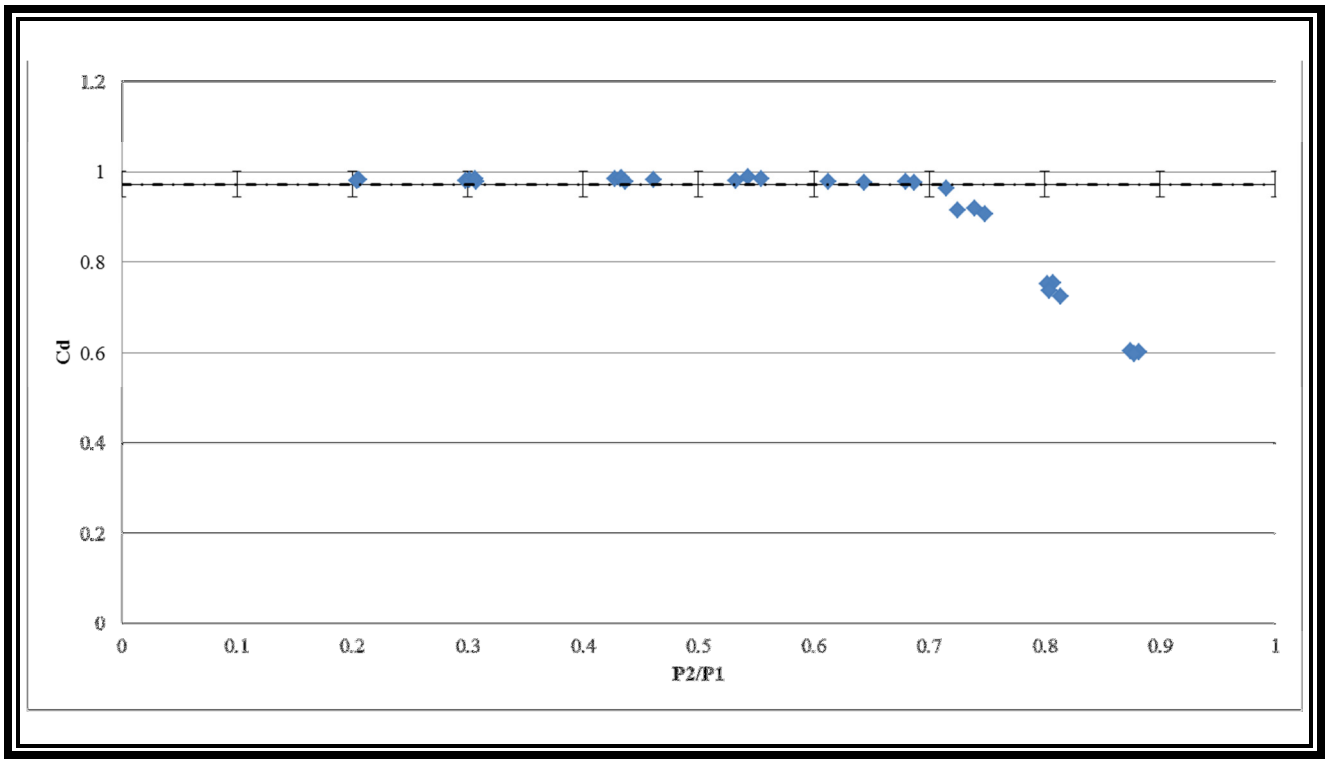

Figure 5.3: VFM-002 Discharge Coefficient vs. Pressure Ratio. [18]

The test procedure previously described was repeated for the two new test articles, VFM-001 and VFM-002. After having performed water flow tests at pressure ratios spanning from 0.2 to 0.85 with a constant inlet pressure of 0.83 MPa (120 psia), it was shown that the critical pressure ratios were 0.58 and 0.71 for VFM-001 and VFM-002 respectively. As with the previous water tests performed on the benchmark cavitating venturi flow meter test article, the venturi data was compared with the turbine flow meter data, revealing a 2% deviation in the venturi data. [18]

5.2 Cavitation Transience and Pressure Dependency

The work done during the aforementioned water testing was the basis for developing the discharge coefficient used in the mass flow calculations for the methane flow tests through the cavitating venturi flow meter. To demonstrate the need for empirically determining the discharge coefficient and critical pressure ratio, the graph found in Figure 5.4 depicts the mass flow rates for both the turbine flow meter and the cavitating venturi flow meter at different pressure ratios. The vertical axis on the left hand side of the graph is the mass flow rate obtained without the incorporation of the empirically determined discharge coefficient. The vertical axis on the right hand side of the graph shows the varying pressure ratios at which the testing was conducted. It can be clearly seen in this graph that the C_d was not incorporated because the cavitating venturi flow meter maintains the maximum flow rate reading even when the pressure ratio is beyond its critical value. At this point however, the turbine flow meter readings drop, as is consistent with expected behavior.

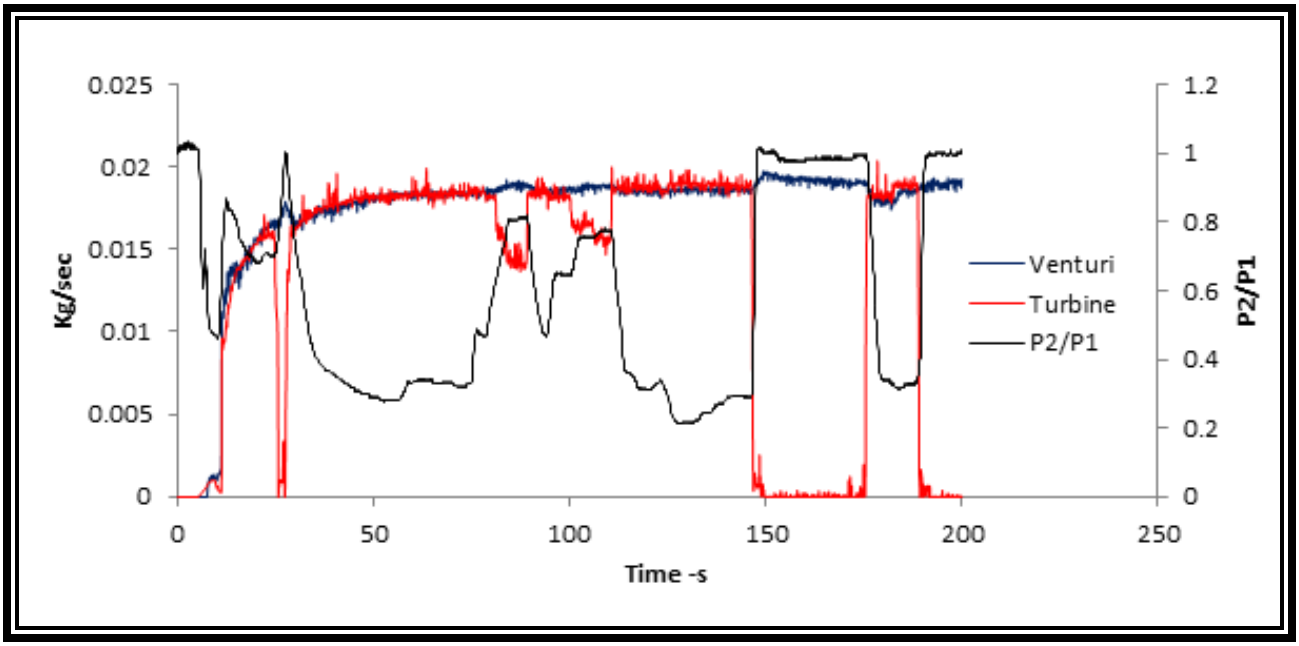

Figure 5.4: Cavitating Venturi and turbine flow meter mass flow readings at varying pressure ratios. ***The C_d was not applied to the cavitating venturi mass flow rate readings.*** [16]

The cavitating venturi flow meter was designed with the intent to use it within the propellant feed system of actual, flight-grade hardware. During initial firing and throttling operations of a rocket engine, it is probable that the cavitating venturi will be subjected to pressure ratios that fall outside the breadth of the cavitating flow regime. Curve fitting the pressure ratio versus coefficient of discharge data expressed in Figure 4.7 produces a calibration parameter to better estimate the mass flow rate in these flow conditions. This is achieved by subsequently applying the obtained pressure dependent discharge coefficient (calibration parameter) in Equation 1 for the pressure ranges that lie outside the cavitating flow regime. From this, the modified mass flow rates are obtained, as shown in the following figure. As can be seen in the graph, application of the calibration parameter improves the agreement of the cavitating venturi flow meter flow rate readings with that of the turbine flow meter across the entirety of the pressure ratio range. [16]

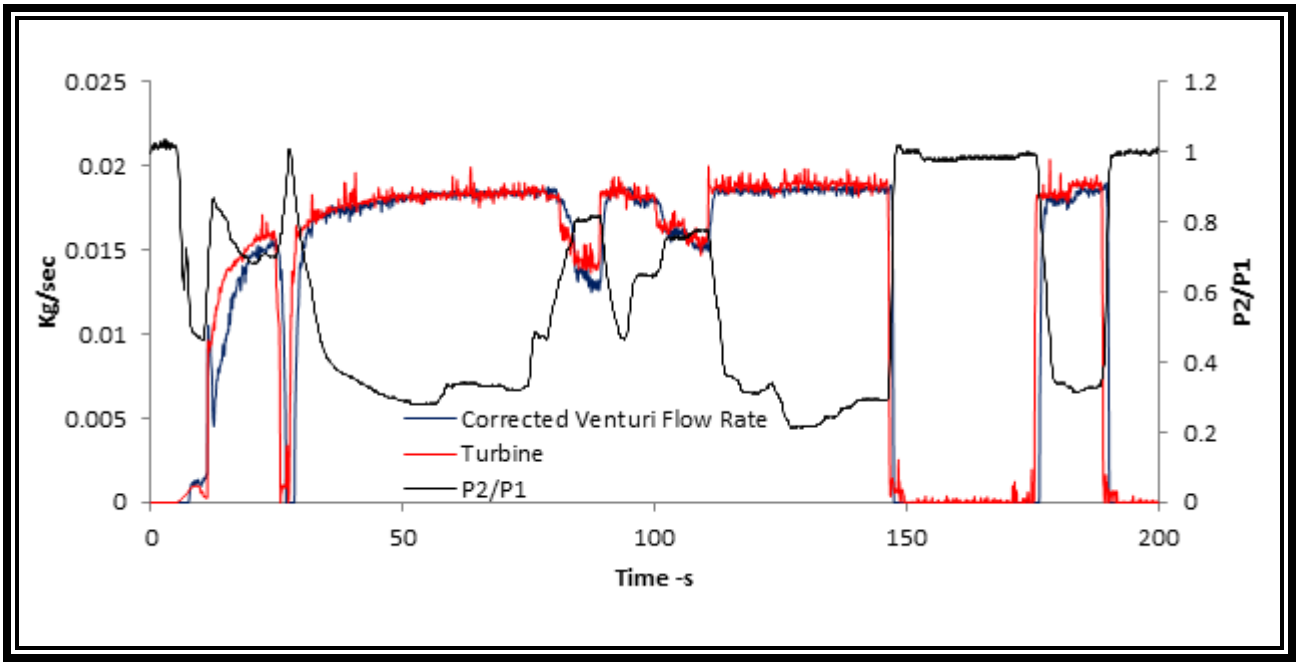

Figure 5.5: Cavitating Venturi and turbine flow meter mass flow readings at varying pressure ratios. ***The curve fitted C_d was applied to the cavitating venturi mass flow rate readings. [16]***

The discharge coefficient, as obtained from the ratio of the turbine flow meter flow rate data to the cavitating venturi flow meter data, is transient in its behavior. The graphs shown in Figure 5.6 detail this transient nature of the discharge coefficient along with the pressure ratios. The graph for liquid methane can be found at the top of Figure 5.6. The graph for water is found right beneath it in the same figure. There are three clearly defined regions within the operating regime depending upon the pressure ratio applied in the flow; namely, the stable cavitation regime, the quasi-stable cavitation regime, and a regime with no cavitation. For both the water and liquid methane graphs, it can be seen that stable cavitation is induced when the pressure ratio is significantly lower than the critical pressure ratio value. Quasi-stable cavitation regimes seem to exist near the critical pressure ratio and are characterized by a lower discharge coefficient than in the stable cavitation regime. Yet the C_d in this region is not dependent upon the pressure ratio which is indicative of the presence of cavitation. One possible explanation for this behavior is that the viscous effects are more predominant in the quasi-stable regime than they are in the stable cavitation regime.

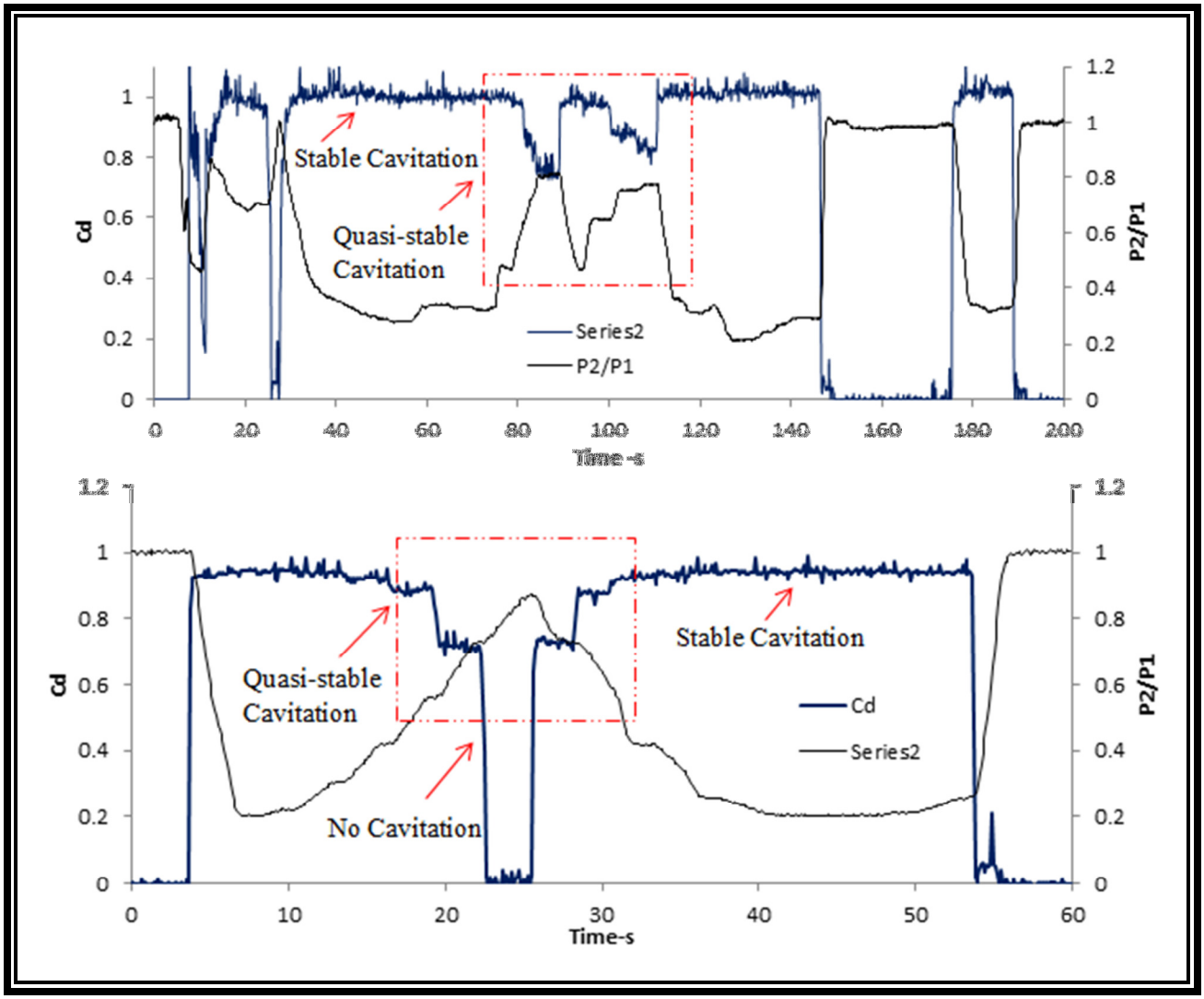

Figure 5.6: Transient data for liquid methane (above) and water (below). [16]

Figure 5.7 is a graph detailing the relationship between the radius of the cavitation bubble within the stable regime and the ambient pressure. This correlation between bubble radius and ambient pressure was discerned through the analysis of the force balance between the forces within the bubble and the external forces acting on the outside of the bubble. The mathematical expression of the aforementioned force balance is detailed in Equation 4.

$$P_0 + \frac{2\gamma}{r} = P_g + P_{vap} \tag{4}$$

The ambient pressure is denoted with P_0, the force exerted on the bubble by the liquid surface tension is expressed as $2\gamma/r$, the pressure of the dissolved gases that have been evolved inside the bubble is P_g, and the vapor pressure of the liquid vapor is P_{vap}. On the graph shown in the Figure 5.7, the vapor pressure of the liquid, water, is located where the x and y axis cross.

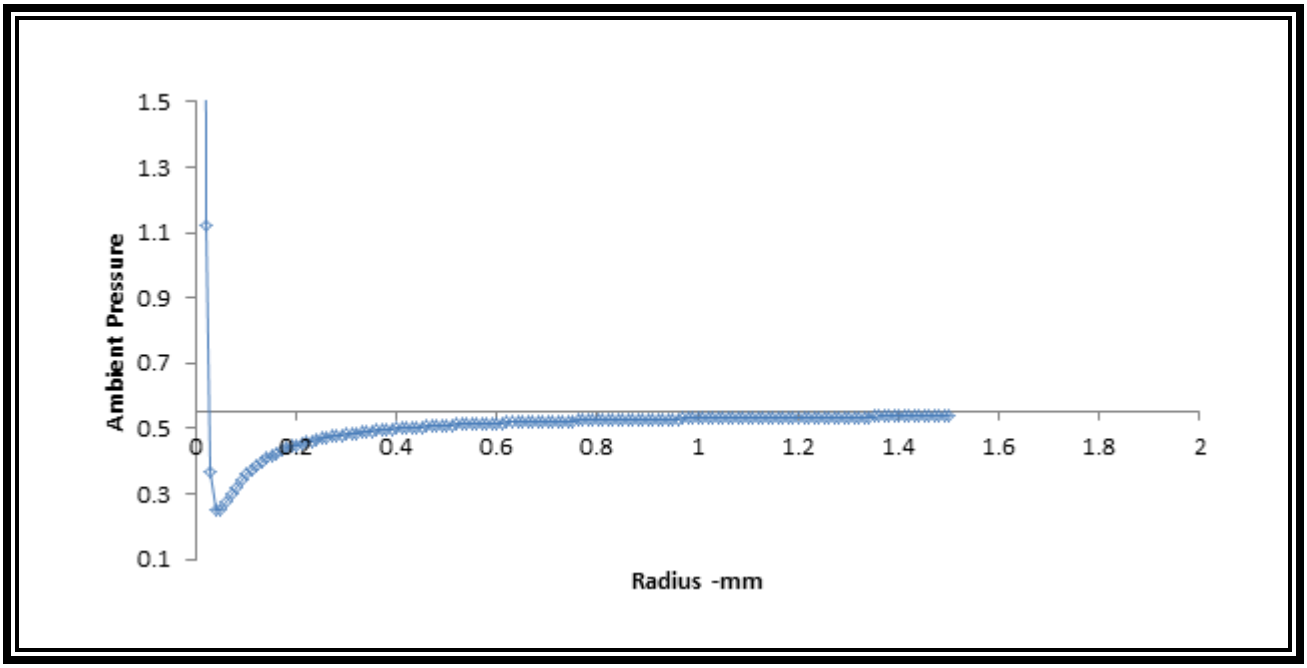

Figure 5.7: Bubble radius versus ambient pressure for a cavitating water bubble. [16]

It can be seen in the figure above, that even as the pressure is lowered, the cavitation bubble will remain small until the pressure is reduced below the liquid vapor pressure by a finite amount. The growth of the cavitation bubble is unstable at the point of inflection and the ambient total pressure nears the vapor pressure. This can be predicted through force balancing Equation 4. As the ratio of the surface area to volume decreases, the surface forces exerted externally on the bubble is relatively minute in comparison to the internal forces exerted on the bubble as expressed by the left hand side of the equation above. Simply put, as the radius of the bubble decreases, the effect of the surface tension becomes larger and more dominating since it is proportional to 1/radius. It should be noted that the interior forces are a function of the temperature and volume of the gas encapsulated within the bubble. So, by extension this means that at sufficiently low ambient pressures, the bubble growth is unstable and

significantly reduces the volume fraction of the liquid in the throat region, where the cavitation occurs. The total viscosity can be described as the summation of the gas volume fraction multiplied by the gas viscosity and the products of the liquid volume fraction and the liquid viscosity. So, when the liquid volume fraction is decreased, the total viscosity likewise decreases because the viscous gas is largely dominant of the sum. In summary, it is believed that that although cavitation occurs within the quasi-stable cavitating regime, the smaller sized bubbles cause an increase in the liquid volume fraction. Thus, the viscosity increases while the discharge coefficient decreases.

Chapter 6: Surface Roughness Analysis and Determination

6.1 Scanning Electron Microscope Technology (SEM) and Sample Preparation Process

Three imaging technologies available at the University of Texas at El Paso were considered when trying to optically observe the surface roughness of the cavitating venturi flow meter. When selecting the best of these options several things needed to be considered. First, the cavitating venturi itself was produced out of 316 Stainless Steel using electrical discharge machining (EDM) technology which carries a standard surface finish of 32-500 micro inches with the most common range spanning from 63-225 micro inches. [19] In comparison to other manufacturing techniques, EDM is on the lower range in terms of surface roughness due to manufacturing. [19] Furthermore, the surface that needs to be analyzed is a curved, interior, machined, optically reflective surface. These characteristics make standard imaging techniques extremely difficult to utilize.

Figure 6.1: Cavitating Venturi Sectioning for SEM Analysis. ***The yellow arrows indicate along which diametral sections the venturi was prepared for analysis.***

For the most accurate assessment of surface roughness, grain diameters, the distance between peaks, and the troughs of the surface features must be accurately measured. Profilometer instrumented, micron-scaled digital microscopes can often achieve this with a relative degree of accuracy when dealing with samples possessing a flat surface of a matte or highly corroded surface. With samples such as the cavitating venturi flow meter, these conditions do not exist in the regions of interest. The university does not have a profilometer but does have a DinoLite brand digital microscope. The figure below demonstrates that simply modifying the direction and intensity of the light source can drastically alter the refraction of light by the surface features, causing erroneous grain diameter measurements. This limitation is amplified by the fact that this is a 2-D analysis of the 3-D sample characteristics and therefore, cannot observe the trough depth without destroying the sample.

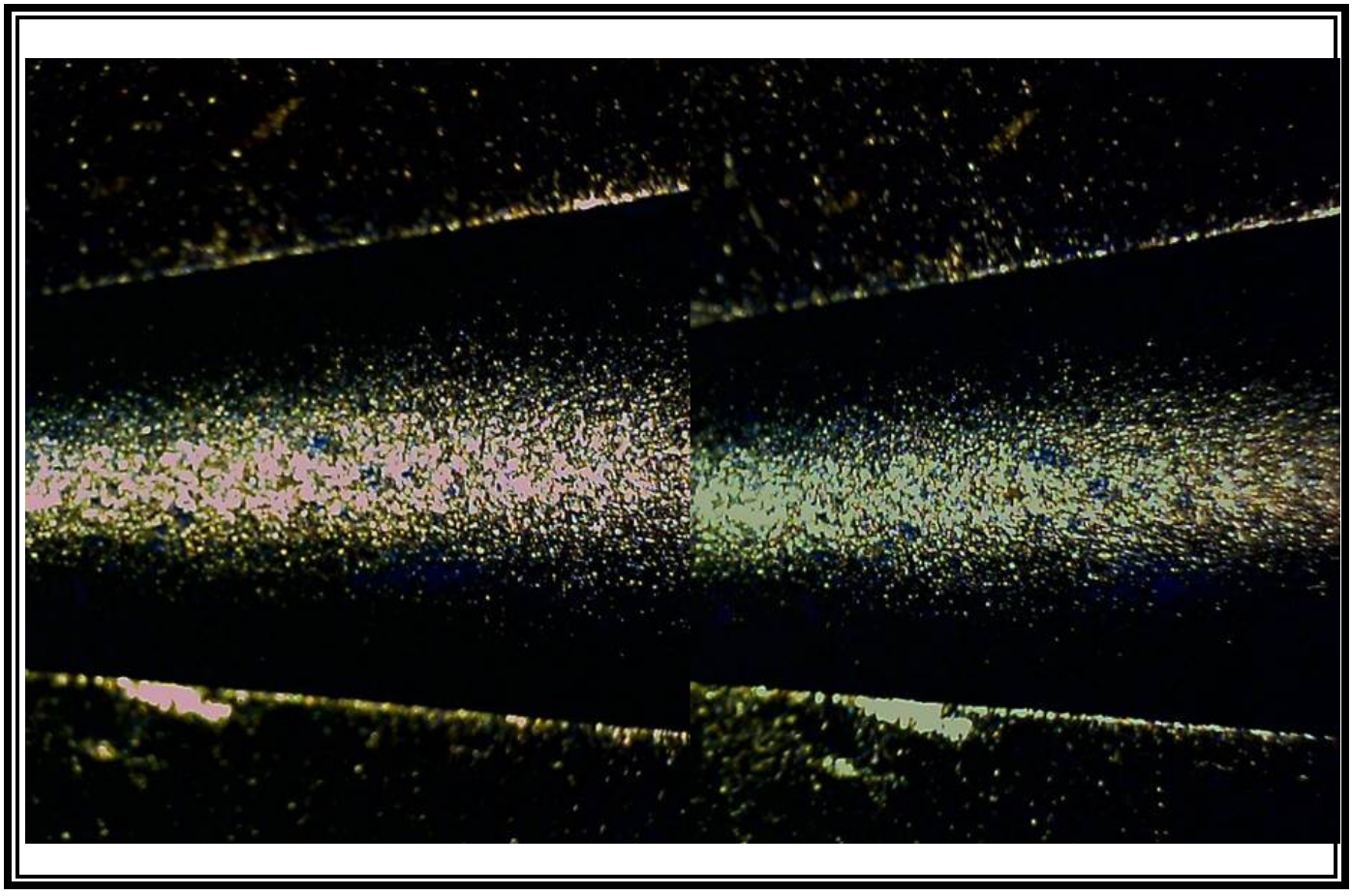

Figure 6.2: Light Refraction Example. *Cavitating Venturi converging section, digital DinoLite microscope, 55x magnification with overhead lighting (left) and side light (right).*

One method of analysis that encompasses the need for measuring the diameter and trough depth of surface roughness features is the 3-D laser microscope. The University of Texas at El Paso possesses a Keyence 3-D laser microscope that functions as both a microscope to measure the surface feature dimensions on a 2-D plane and doubles as a surface profilometer to measure trough depth between the roughness features. The main drawback of using this technology is that the surface roughness is assessed using interferometric microscopy, which is also highly susceptible to erroneous readings resulting from the highly refractive nature of minutely rough metallic surfaces, such as those of EDM machined metals. Furthermore, this technology would work best in regions where the surface being analyzed is level, meaning that for the inlet and outlet sections that are not conical, this technology may be sufficient for analyzing surface roughness tracing a thin line along the depth of the sample. However, in the sections for which surface roughness analysis is most critical because they are the cavitating regions, this analysis is likely to involve a greater degree of error. This is true because the changes in depth due to the conical geometry could be misread by the microscope as a more drastic trough depression than is actually present on the surface due to the changes in the light refraction and diffusion. For this reason an alternative methodology for analyzing surface roughness was selected.

Scanning Electron Microscopy (SEM) analysis is effectively a 2-D imaging technique employed to measure surface textures and grain features on the submicron scale of magnitude. Specimens analyzed with this technique require careful preparation in terms of sectioning, mounting, and polishing for best results. When considering a lengthwise sectioning technique where multiple samples are taken along the length of the half sectioned venturi as shown in the top cut in Figure 6.1, this technology would be seemingly ineffective in analyzing surface roughness due to machining as the samples would need to be polished to a flat surface, thus eliminating the machining effects. Instead, the samples were cut along the diameter of the venturi at various locations along the length of the venturi as specified in the bottom cut venturi shown in Figure 6.1. This reveals the trough profiles of the surface defects caused by the machining at various locations. Samples were taken in the inlet region, the converging nozzle, and the throat region, as shown in the figure below.

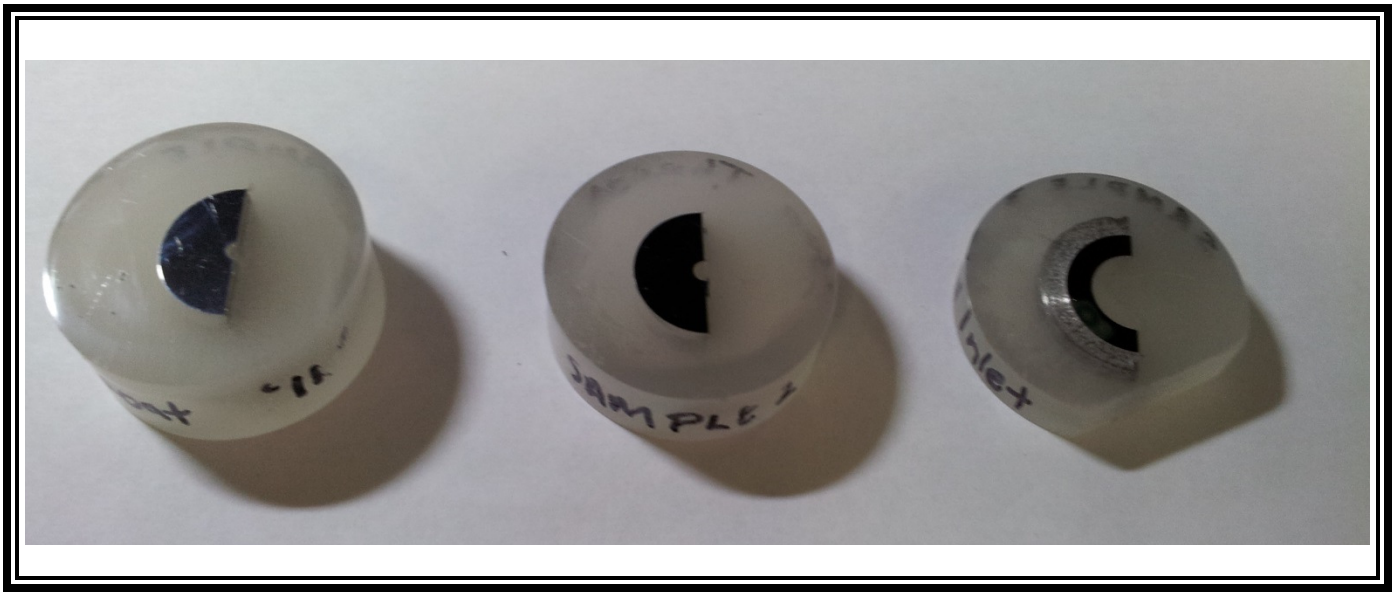

Figure 6.3: Cavitating Venturi Sectioning for SEM Analysis. ***Samples 1-3 are shown from left to right respectively starting with the near throat sample, the converging cross-section and the inlet.***

For the most accurate assessments of surface roughness, the trough depth alone though cannot simply be used for surface roughness determination. Atomic Force Microscope (AFM) instruments are widely considered to be among the best-suited instruments for this endeavor as it has the capability of producing 3-D imaging of the surface roughness features and morphology. Unfortunately, the university is not in possession of one of these instruments so techniques involving the SEM were explored in its absence.

One of the most common expressions to describe surface contours is the roughness average, R_a, which is defined as the arithmetic average of the height deviations above the mean line of the topography along the length of the sample. [20, 21] While manufactures often express roughness in these terms, it can be a somewhat misleading representation of the actual surface profile because the computational methods employed make it quite possible that surfaces with significantly different profiles will still possess the same R_a. [20] Related to this value is the roughness parameter, R_q, which is the root mean square (RMS) value. The roughness parameter ultimately is the geometric average elevation of the roughness topographic features over the span of the sample. By virtue of its formulation, the R_q is generally more sensitive to sporadic occurrences of unusually high or low features

with respect to the mean line. [20, 21] A visualization of the differences between the R_a and R_q values can be seen in the Figure 6.4. [20] It should be noted that the equations in the picture are just an approximation, whereas the actual equations are listed below. The Y_i term is the height deviation from the mean line and n is the number of peaks/dips.

$$R_a = \frac{1}{n}\sum_{i=1}^{n}|Y_i| \tag{4}$$

$$R_q = \sqrt{\frac{Y_1^2 + Y_2^2 + Y_3^2 + \cdots + Y_n^2}{n}} \tag{5}$$

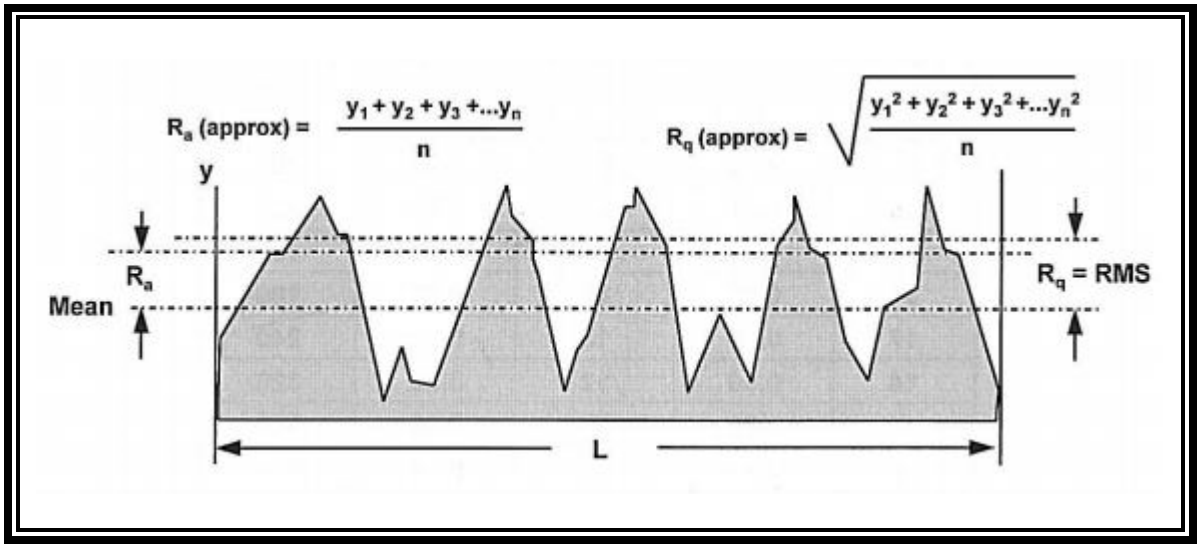

Figure 6.4: Surface Roughness Measurement Techniques. *Figure courtesy of source [20].*

With the understanding that a topographic profile like that shown in Figure 6.3 above could only be attained through SEM analysis by preparing samples of the cavitating venturi cross-section, three analysis sections were selected in the inlet and converging region. These locations were chosen as it was presumed that the surface roughness in these regions would be most influential on the fluid pressure profile before it reaches the throat. As previously discussed, it is the pressure behavior in this region that heavily governs the cavitation process. A band saw was used to cut the samples down to the proper size for analysis in the SEM and the samples were then potted in the mounting material before polishing

down the top of the sample to a mirror finish. Initial analysis of the samples produced fairly ambiguous images with undesirable artifacts due to a phenomenon known as charging. [22] In many cases this can be alleviated with the use of copper tape that touches the metallic surface of the sample on one end and the microscope stage on the other end to better control the discharge of the electrons built up in the sample. This was not an effective technique for these samples, so a gold coating was instead applied with greatly improved results. The following figure depicts the drastic difference in image quality.

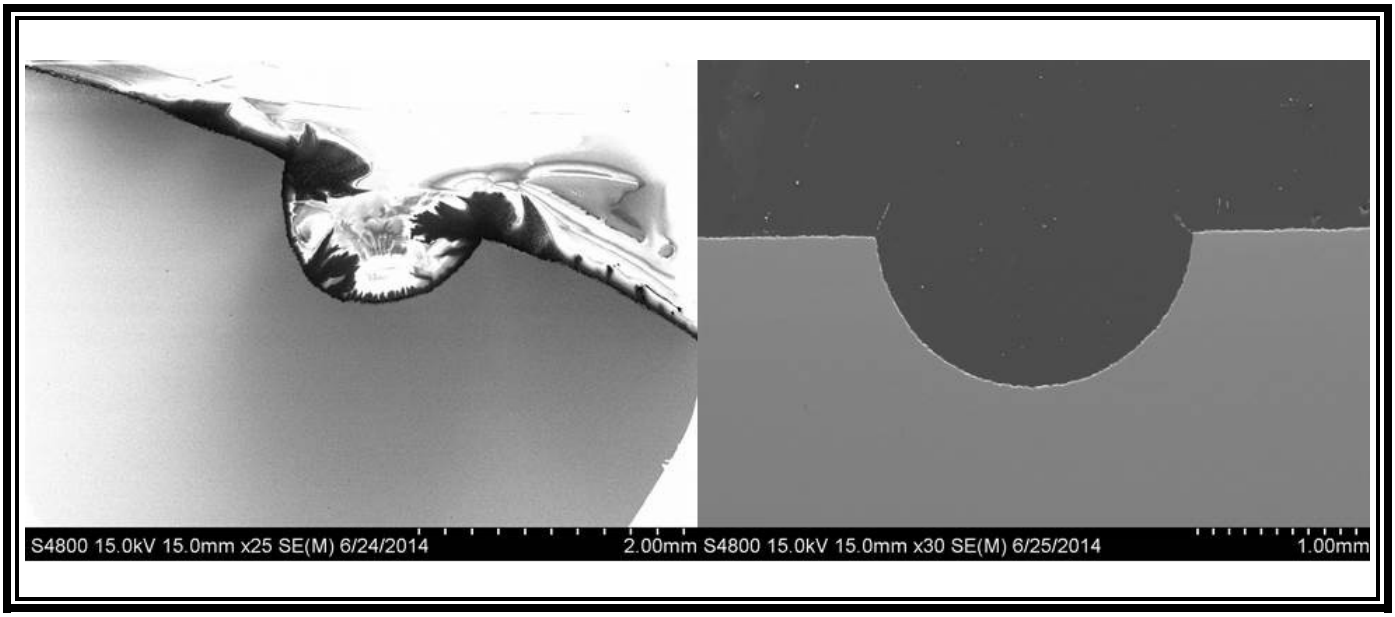

Figure 6.5: Sample Charging. *Image on the left is with copper tape and image on the right is of the same cross-section with gold coating.*

The SEM images were then used to measure the mean height of the roughness features, the trough depth of the surface defect, and the sampling length. Several defects were analyzed per sample and a roughness average along with a roughness parameter was calculated from the trough measurements taken for each of the representative cross-sections. The averages obtained through this process are detailed in the following table with the estimated precision error being calculated for each of the sample areas. These roughness factors were not specified in the CFD modeling software for this work because of the high degree of error (due to the small sample size). Furthermore, the values were close to those already implemented automatically under the steel material settings in ANSYS FLUENT. However, it is possible to do so as detailed in the following chapter.

Table 6.1: Roughness Variation Chart

Sample # /Region	Cross Section Average (μm)		
	R_a	R_q	Student t-dist. 90%
1: Throat	5.97	6.03	5.87
2: Convergent	6.30	6.52	12.21
3: Inlet	4.21	4.74	5.84

There are significant differences between the average roughness and roughness RMS parameter at each section; however the large uncertainty factor indicates that these values are no more valid in terms of application in the CFD model than the default values. In order for this technique to be valid for application in both CFD models and life cycle studies, it is recommended that the full circumference of the cavitating venturi cross section be evaluated at more sampling locations.

6.2 Image Processing and Surface Roughness Determination

The SEM images were post-processed using ImageJ, a program developed specifically for the processing of images taken with various types of microscopes. By entering a measured pixel value correlated to known a length measurement into the software, the pixels can be calibrated into a specific unit. This methodology proved difficult to ensure the proper placement of the mean line from which the measurements were taken so an alternative method was employed. A best fit curve was produced along the curve of the venturi wall that bounded the roughness features below the troughs. Another curvature was produced touching the tallest of the peaks while maintaining equidistance from the lower curvature at all points. A median curvature was then produced that was equidistant from the two previously produced curves. The height/depth of the surface features was then measured at tangent intersections with the median curve. The SEM provided measurement gradient in the bottom right hand side of the pictures served this purpose. Using the Equations 4 and 5, the roughness parameters were computed in terms of micrometers, an industry standard. In the pictures produced by the SEM, the units of

measurement were not in the standard micrometer form so they were converted during the averaging calculations performed in Microsoft Excel. For each cross section, three patches of surface features were closely analyzed to take at least a total of eighteen roughness features into account per cross section. For consistency, patches were analyzed along the left hand side of the view field, the center of the concavity, and the right hand side of the view field. The error analysis done in this section, as in the previous chapters was based on the student t-distribution scheme.

It should be noted that in the SEM images, there appears to be a darker ring that outlines the surface profile of the metallic sample. This is simply the void space between the cavitating venturi sample and the polymer mounting material. A quick setting polymer mount was used in this application because of its ease of use and faster preparation time, but in the process resistance to shrinkage during the curing process was sacrificed. These voids could have been prevented by using other mounting techniques such as hot mounting with a slow-cure polymer material or cold mounting the sample with a slower curing material. These options were not available at the time of sample preparation so the quick set mount material was used. From the SEM images, it does not appear that any adverse effects were experienced as a result beyond the formation of the aforementioned voids. Furthermore it does not appear that the voids caused edge damage/buckling to occur during polishing that would influence the trough measurements taken at the inner sample edge.

Chapter 7: CFD Analysis

7.1 Description of CFD Model and Software Selection

The modeling methodology was based primarily on two resources, one of which was mentioned previously in Chapter 1 and the other was simply a cavitation tutorial produced by ANSYS FLUENT. In both example situations however, flow through a flat-faced orifice flow obstruction was evaluated. [11, 23] Although the bulk of the case setup was similar, the fact that the pressure downstream played a factor in the upstream flow behavior necessitated that some variations from their methodology be made for application in this work. Furthermore, their models operated under the assumption of steady state cavitation conditions. [11, 23] As was shown in the experimental work, there is transient behavior that needs to be accounted for not just in the experimental phase of development but with the idea that the cavitating venturi flow meter will also be put into service. [16] The goal of this analysis therefore is to create a model that produces sufficiently similar flow results to the experiment so as to provide confidence in the more detailed internal flow results such as phase conditions that cannot be experimentally observed with accuracy.

7.2 Model Case Development

7.2.1 Geometry and Meshing

The geometry of the fluid domain was drawn using the geometry module in the ANSYS Workbench software. It was drawn in inches to keep with the units used in the actual production of the test article. It is important to note that by referring to the geometry in this section, it is the geometry of the fluid domain that is being described. For clarity, the full cavitating venturi will be called a “part” in this section to differentiate it from the fluid domain geometry. This is important to note as the geometry of the fluid domain consists only of a 2-D axisymmetric cross section of the cavitating venturi. In terms of computational efficiency, for axisymmetric parts such as the one described in this work can be effectively modeled in 2-D with results highly congruous with those obtained through 3-D characterization simply by specifying the axis of symmetry; reducing computational complexity and time while maintaining the integrity of the model.

Upon completion of the geometry formation, the geometry file was imported into a mesh development tool in ANSYS that allows for mesh refinement beyond that of the auto-generation methodology. In this simulation, a structured two dimensional quadratic mesh element was used. Meshing involves a fairly delicate balancing of discretization refinement, continuity between different sized/spaced cell zones, and computational efficiency. The goal of the mesh refinement process is to achieve a solution result that is mesh-independent. Mesh independency is evaluated by creating different meshes and running the same case file for each of the different meshes. Mesh independency is neared when two different sized meshes produce a similar result within a desired error range. A third mesh is then produced in between the two other mesh sizes. If a sufficiently similar result is likewise produced, the median size of the aforementioned meshes is selected for use with the remaining cases. [24] It should be mentioned that in the mesh independence analysis several other factors are considered such as whether or not the solution converges for the case when that mesh is used, along with the orthogonal mesh quality. In general meshes with orthogonal mesh qualities nearest to 1 are selected, however mesh maximum and minimum cell refinement does not always illicit the best mesh qualities as this is also influenced by the cell paving pattern and how well that promotes continuity between the cells of different sections in the geometry. But in short, it is important to check the mesh quality before proceeding to the next phases of the case file development. The mesh of the fluid domain geometry as well as the cell sizing settings of the discretization that passed the mesh independence test are detailed in the following figure.

Table 7.1: Orthogonal Mesh Quality vs. Mesh Discretization Size

Mesh Size	**Minimum Orthogonal Quality**	**Maximum Aspect Ratio**
2.50e-002 in	9.45704e-01	3.08046e+00
2.52e-002 in	9.41012e-01	3.09319e+00
2.55e-002 in	9.71868e-01	2.93295e+00
2.60e-002 in	8.92687e-01	2.97449e+00

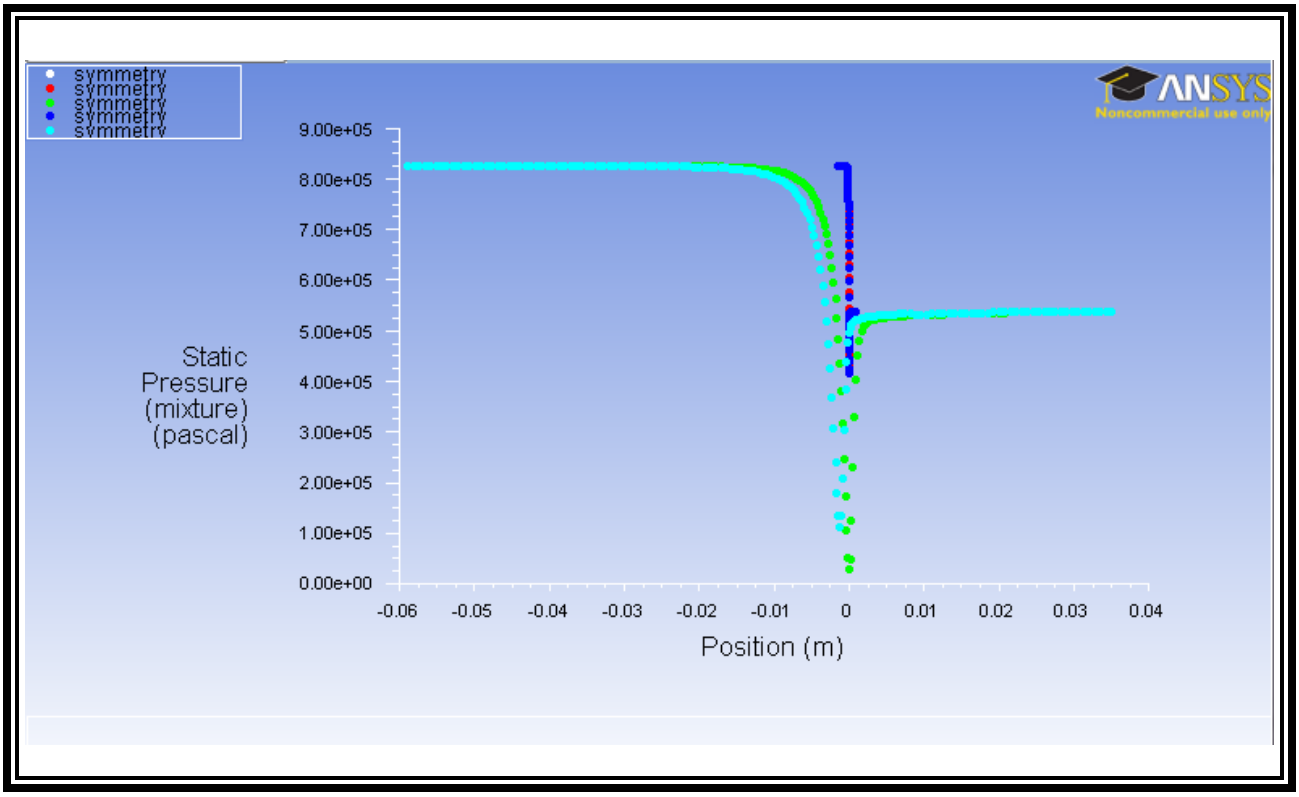

Figure 7.1: Mesh independence test with static pressure along the symmetry line. *Mesh independence achieved in range of 2.52-2.6 e-002 inch discretization sizing.*

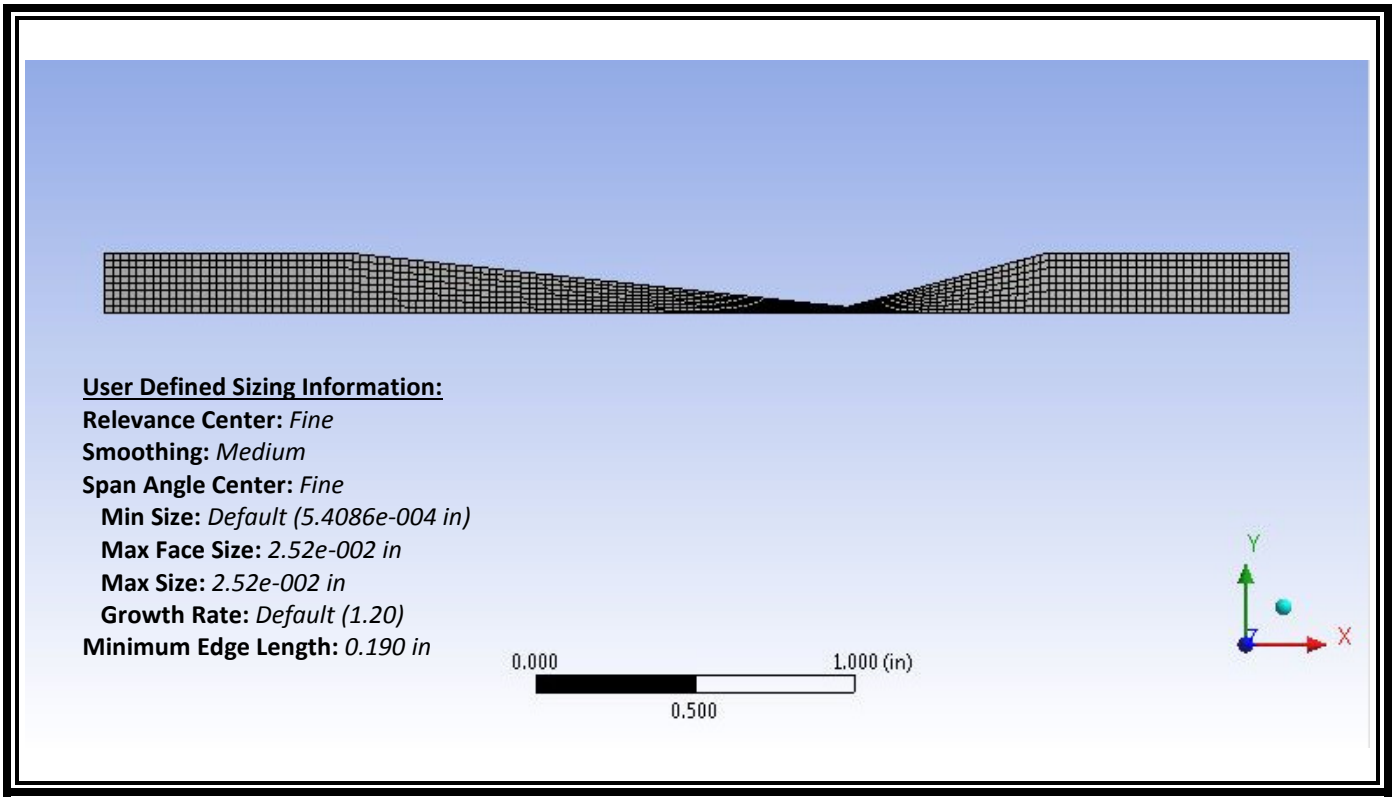

Figure 7.2: Mesh of the fluid domain. *Discretization sizing is detailed in inches.*

7.2.2 Case Setup

Solver and General Problem Establishment

Upon entering the ANSYS FLUENT GUI, the double precision solver was selected as is recommended for multiphase flow simulations. Another characteristic of multiphase flow simulations is the use of a pressure-based solver with an absolute velocity formulation in an axisymmetric 2-D space. Although there is transient response expected during the time steps where the cavitation nuclei are growing and immediately following their collapse, the steady time setting was selected as an average output value for mass flow rate is desired to calculate the discharge coefficient of the model.

Model Selection

Aside from the geometric influences, the flow behavior of the working fluids will likewise be defined by the quality of the fluid and the viscous effects that the fluid phases exert on the flow profiles. In cavitation models, analysis of the fluid phases will reveal the location, intensity, and stability of the cavitation nuclei/bubbles. Since the viscous interactions between the fluid region of the flow and the

cavitation bubbles are one of the predominating flow control influences on the fluid flow profiles, it is important to enable the multiphase model. The mixture multiphase model was selected with two Eulerian phases specified. As mentioned, the viscous effects are important as they are part of the flow control mechanisms. A realizable k-epsilon with standard wall function treatment was selected for the viscous model, leaving the default model constants in place. This model produces results in agreement with the standard physics of turbulent flows through the mathematical constraints it applies on the Reynolds stresses. Furthermore, the realizable k-epsilon model differs from the standard model in the turbulent viscosity formulation and the derivation of the dissipation rate transport equation is rooted in the exact mean-square vorticity fluctuation transport equation. The advantage of using the realizable k-epsilon model lies in its ability to predict the spreading rates of both round and planar jets with greater accuracy. Furthermore, in comparison to other models, it better captures the characteristics of flow profiles involving rotational behavior, and boundary layers that encompass adversely strong pressure gradients, recirculation, and flow separation. [25]

Materials and Phases

Given that the target operation of the cavitating venturi is to control the flow rate through the production of cavitation at the obstruction feature, it is expected that there will be at least two phases of fluid interacting with the solid features. For this model four fluid materials were created in addition to the pre-existing air. Liquid and vapor water materials were created using the pre-existing materials in the ANSYS FLUENT database. These materials were applied solely in the cases modeling the water flow. For the methane flow model, a separate liquid and vapor methane profiles were likewise created. However, for these two fluids, a base fluid that was listed in the ANSYS FLUENT database needed to be modified and subsequently renamed to create them as they were not previously part of the ANSYS FLUENT stock materials. Given the observed operating conditions of the liquid methane during the experimentation process, the required material properties were computed using REFPROP, software developed by the National Institute of Standards and Technology, which computes the material properties from well-established equations of states and extensive databases of empirical results when given two user defined input parameters. The Helmholtz Energy Equation of State as detailed in

literature by Setzmann and Wagner, circa 1991, was utilized for the viscosity and melting line liquid methane property formulations obtained in this study which was among one of the investigated equations of state mentioned in the literature section of this work. The inlet temperature was below the set range specified in the empirically obtained data applied by REFPROP for property formulation. For this was the reason the Helmholtz energy equation of state was employed the formulation of the material properties. As previously mentioned, empirical data collected from several other resources was used in the formulation of the other specific material properties employed in the model to define the boundaries of the liquid and vapor regions. The solver information for the material properties was provided directly by REFPROP in the printout of the materials properties.

The solid material comprising the body/walls of the flow field geometry is also specified in this stage of the case development process. As with the fluid properties, ANSYS FLUENT has an available database from which body materials can be selected and modified. Steel was selected as the working body material, in agreement with the benchmark experimental test article. Steel is a very general classification however, so it is possible to modify many of the material properties to fit the unique characteristics of each steel alloy. In this case however, the values already in the database were within the range of values obtained from other resources so the default values were maintained at this juncture in the case development process.

Two fluid phases were specified for each of the water and methane cases. For both the water and the methane cases, the primary phase was selected to be the liquid phase. There was one mass transfer phase interaction specified for the primary phase, and it included the transition from phase 1 (the liquid) to phase 2 (the vapor) via cavitation.

Cell Zone and Boundary Conditions

The Cell Zone Conditions are used to specify the bulk of the fluid domain. The cell zone in this model was defined as the body surface. The phase of this zone was specified as a fluid with a mixture of phases and standard atmospheric pressure was specified under the operation conditions.

The Boundary Conditions are also specified by zones. These zones however are generally planes for 3-D models or lines for 2-D models, that were created during the geometry drawing and meshing

phases. Due to the fact that this is an axisymmetric model the lines will not only define the body and fluid domain boundaries, but also the specific line of symmetry. In this section of the case generation, the inlet was specified as a pressure-inlet with a mixture phase. It should be noted that this does not necessarily mean that there will be a mixed phase fluid at the inlet. It simply provides the proper boundary conditions to allow for the possibility of phase variations between a mixture of gas and liquid to a mixture ratio that is sufficiently close to saturated liquid to model its behavior with reasonable results. The momentum aspects of the zone were specified with an absolute reference frame, the desired gauge total pressure and accompanying supersonic/initial gauge pressure, and the direction specified as normal to the boundary. The turbulence aspect of the model was specified by the intensity and hydraulic diameter with a 2% turbulent intensity and a hydraulic diameter matching the straight length inlet diameter of the cavitating venturi. The outlet boundary condition was set to a gauge pressure of the desired ratio of the inlet and possessed the same turbulent model settings as the inlet. The backflow direction was likewise set to a position normal to the boundary. Standard atmospheric pressure was also set for the operating conditions. The defaults were maintained for the dynamic mesh and reference values.

The only other zone for which the boundary condition was altered from the default was the wall surface. Here, again the defaults were left with the exception of the wall roughness. For the current study, the default setting for the wall zone remained and the roughness height and roughness constants were not included in the formulation of the wall boundary conditions as it was noted that the sample analyzed had only been put into a brief period of service before it was discovered that it was not built to specification and could not be utilized. For this reason, the surface roughness is near the values of a newly machined component. It is common knowledge that cavitation damages surfaces. Given the thermal stresses induced by the fluctuation between room temperature and cryogenic fluid operating conditions, the pitting effect normally caused by cavitation will likely be exacerbated and influence the overall coefficient of discharge unique to the venturi flow meter. The surface roughness analysis detailed in this work however, could be used in future models to predict how the increase in roughness

over time due to surface degradation in service could affect the cavitating flow regime. More details about this methodology will be detailed in Chapter 9, regarding future work.

Solution Formulation

The solution formulation process consists of selecting the solution methods, controls, monitors, and initialization features. A PISO (Pressure Implicit with Splitting of Operators) pressure-velocity coupling scheme was selected as it was the recommended algorithm for transient flow calculations in ANSYS FLUENT user literature. This algorithm was originally intended to compute unsteady compressible flows in a non-iterative fashion [26], as would fit the characteristics of the mixed-phase cryogenic flow conditions present in this study. Furthermore, it has also been adapted for iteratively solved steady state problems with the incorporation of a predictor and two corrector steps involving the discretized momentum equations Such additions make the PISO algorithm applicable to steady state problems as would be expected of incompressible fluids such as standard condition water. [27]

The calculation activities and run durations are also specified. Although, distortion of the mesh was minor, the default 1, under-relaxation factors were maintained for the skewness and neighbor correction factors as no estimate of these correction factors was available to help pinpoint a viable first guess. The Skewness-Neighbor Coupling was left enabled to increase the speed of the computation at the cost of a minor loss in the variation robustness of the PISO scheme. [28]

The spatial discretization selected possessed a least squares cell based gradient, with standard pressure, second order upwind momentum, quadratic upwind differencing scheme (QUICK) volume fraction, second order upwind TKE and second order upwind turbulent dissipation rate. The least squares cell-based gradient was selected because of its comparability to the node-based gradient and superiority to the cell-based gradient. In addition to this reasoning, its reduced cost when compared to that of the node-based gradient is frankly less expensive. So it is actually the gradient solution method used as the default methodology in the ANSYS FLUENT solver. [29] None of the transient formulations were enabled as they were unavailable.

The under-relaxation factors in the solution controls tab serve as a method for managing the computed variable updates within each of the iterations of the solution process such as those involved in

pressure-based solvers with even the inclusion of the non-coupled equations computed with solvers based on density relations. While the defaults in this section may fit many of the commonly modeled flow conditions, for situations such as various kinds of natural convection or turbulent flow simulations, the under-relaxation factors may need to be reduced initially if the residuals continue to increase under the default settings after 5 or so iterations. [30] In this case, the only under-relaxation factors that were reduced involved the reduction of the pressure and momentum terms to 0.3 and 0.5 respectively. The remaining categories were left at their default settings.

Several surface monitors were set for each of the cases files that were run. These surface monitors involved the pressure, density, velocity, and phase field variables of the working fluids under the integral reporting type. Depending upon the location of the surfaces and their position with respect to predicted flow feathers to be analyzed, either a mixture, liquids, or vapor phase was selected. The plots were set to include the desired output information at a modifiable data acquisition/recording rate. The solution was initialized using the hybrid method. The calculation and auto-save rates were set, the case file was checked for errors and the case file was run, producing the results shown in the following subsection.

7.2.3 Profile and Contour Generation and Visualization

As mentioned at the beginning of this chapter, there were several aspects of the model solutions that were of particular interest. First, the validity of the model needed to be confirmed through the production of results in agreement with the experimental data obtained with a theoretically supported model. A sufficient level of agreement between the model and the experimental data was established through the analysis of the average water discharge coefficient as calculated through the comparison of the average mass flow rate from the outlet plane to the flow rate measured by the turbine flow meter. These results are detailed in the figure below and provided a sufficient level of confidence in the model to continue its application with only minor alterations to the case file to account for the switch from water to liquid methane as the working fluid.

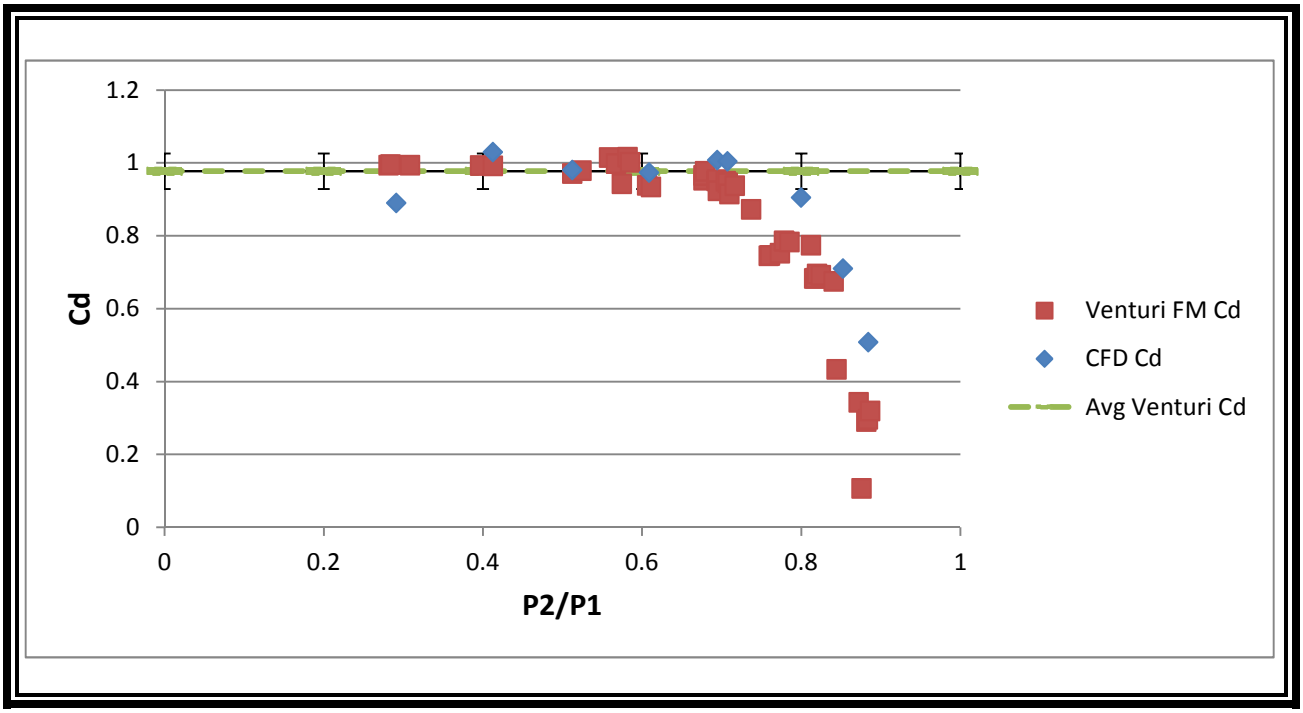

Figure 7.3: Discharge coefficient comparison. *All three of the water Cd values are within the 3.57% range of agreement.*

The following figures are representative pressure, velocity, and phase profiles generated by the CFD model for both liquid water and liquid methane. The pressure ratio at which these profiles were generated is denoted in the caption for each image. It should be noted that through the experimental water testing, the critical pressure ratio was determined to be 0.69 and the profiles taken at this segment of the flow regime represent, for all effective purposes, the critical values representing the maximum cavitation region.

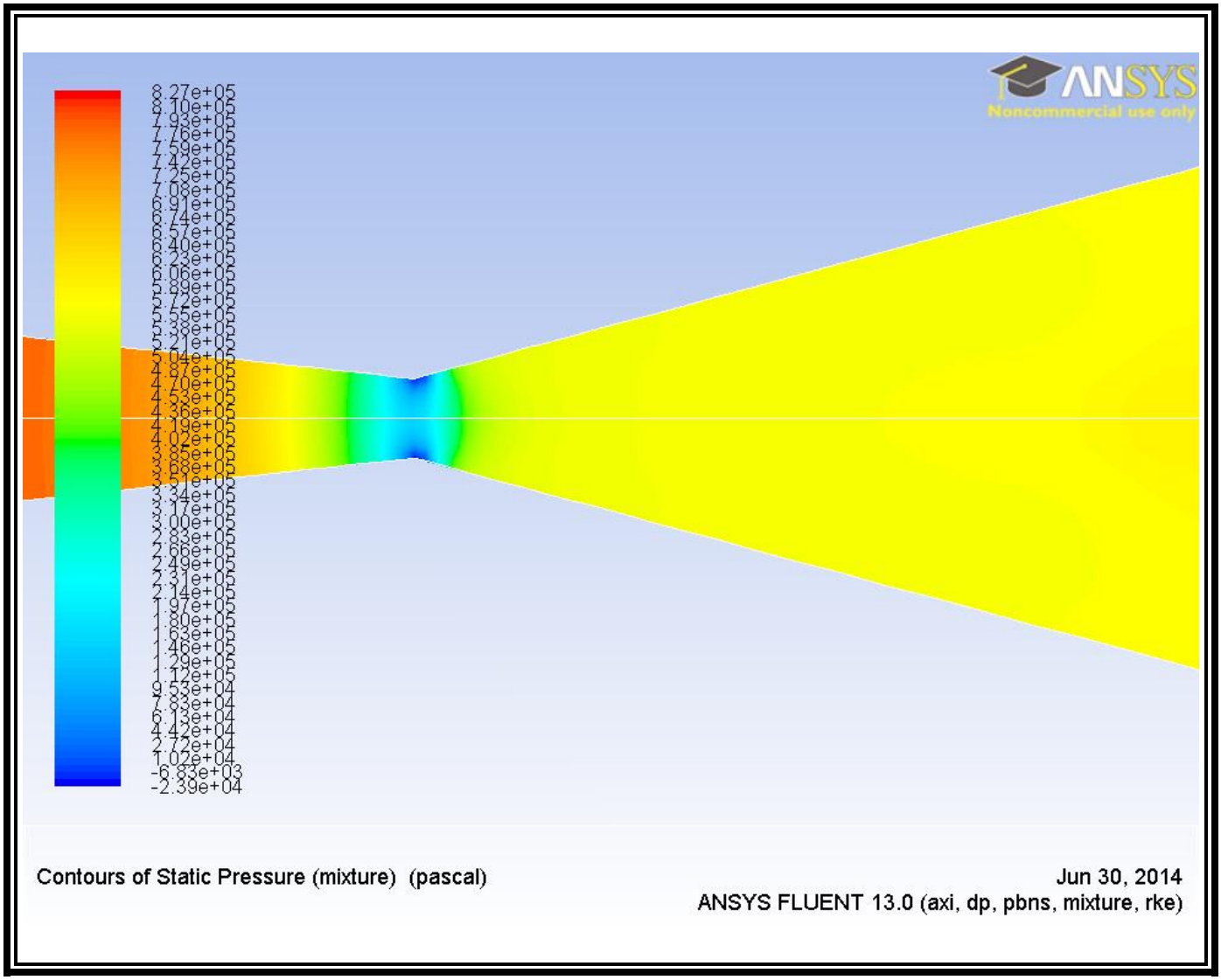

Figure 7.4: Static Pressure Profile of Water at P2/P1=0.69. *Contour of Static Pressure (mixture) in Pa, produced in ANSYS FLUENT.*

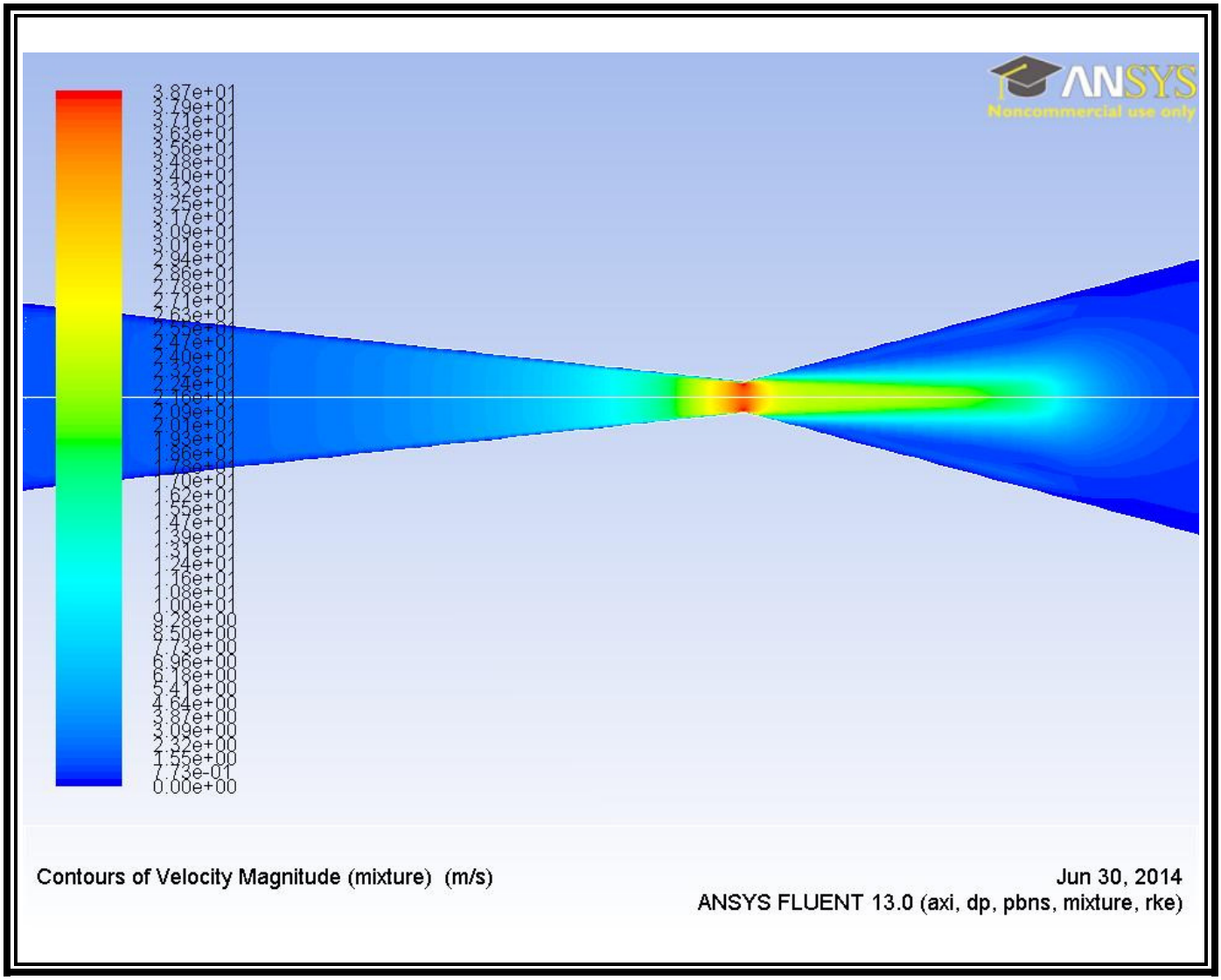

Figure 7.5: Velocity Magnitude Profile of Water at P2/P1=0.69. *Contour of Velocity Magnitude (mixture) in (m/s), produced in ANSYS FLUENT.*

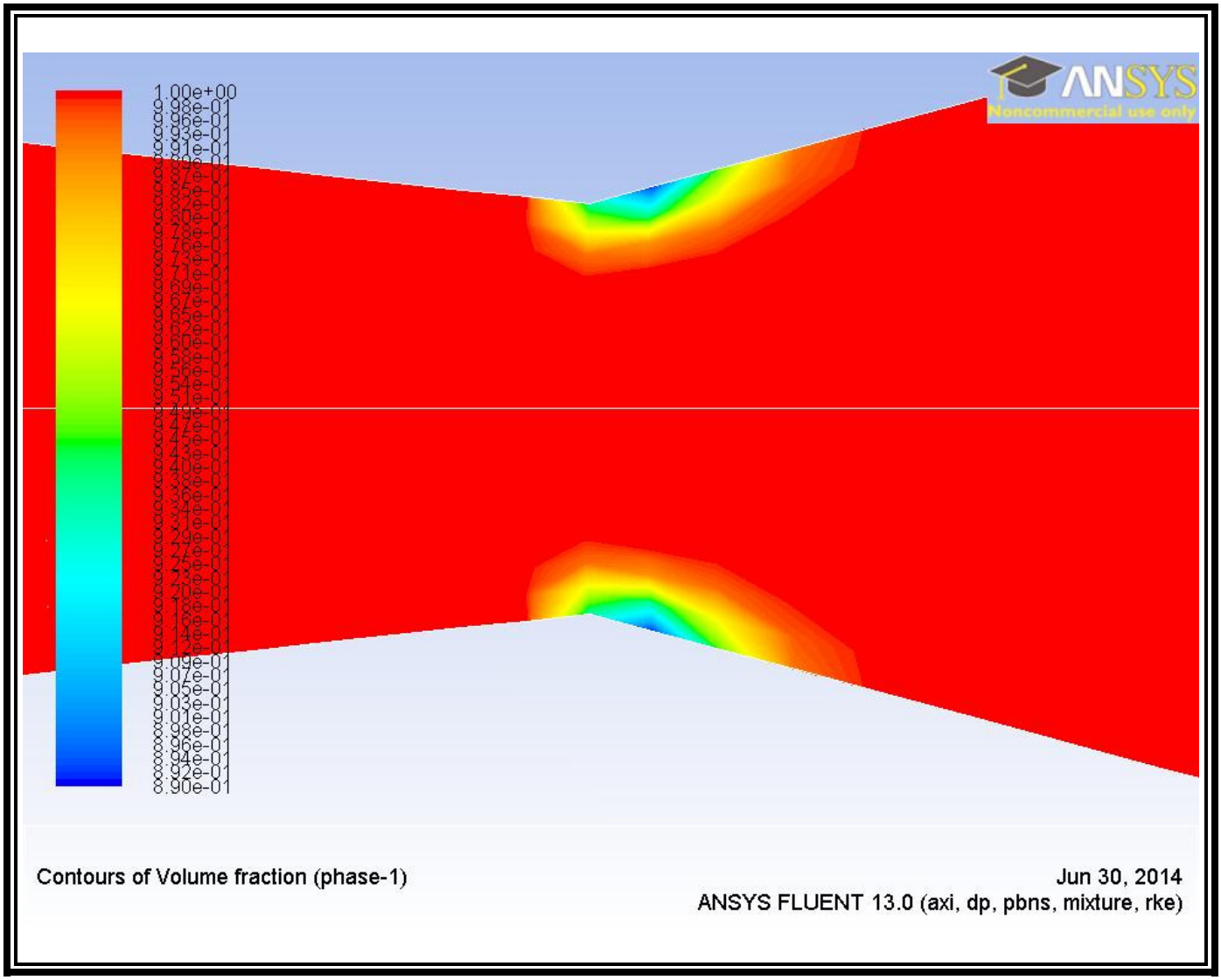

Figure 7.6: Liquid Phase Profile of Water at P2/P1=0.69. *Contour of Liquid Volume Fraction, produced in ANSYS FLUENT.*

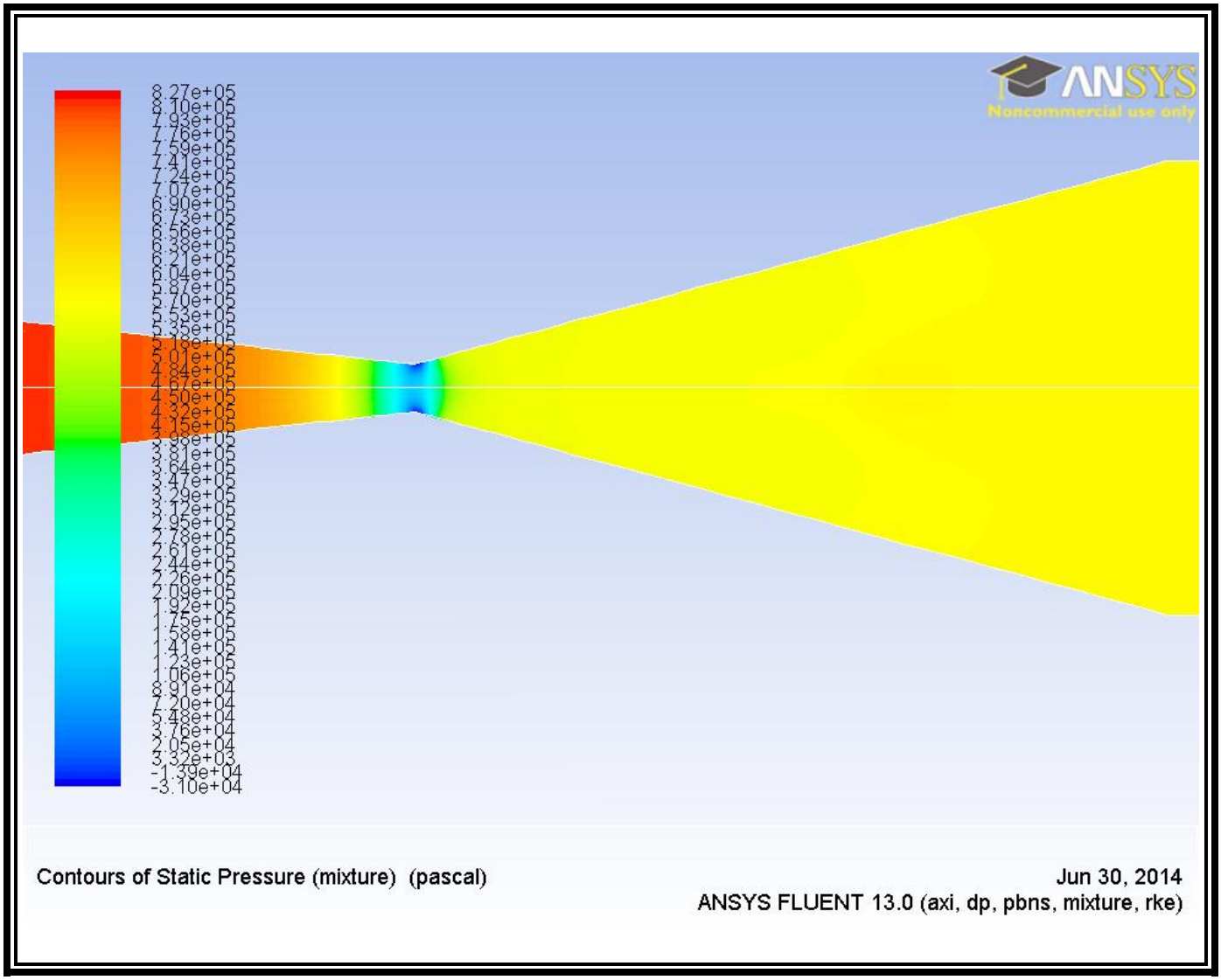

Figure 7.7: Static Pressure Profile of Liquid Methane at P2/P1=0.69. *Contour of Static Pressure (mixture) in Pa, produced in ANSYS FLUENT.*

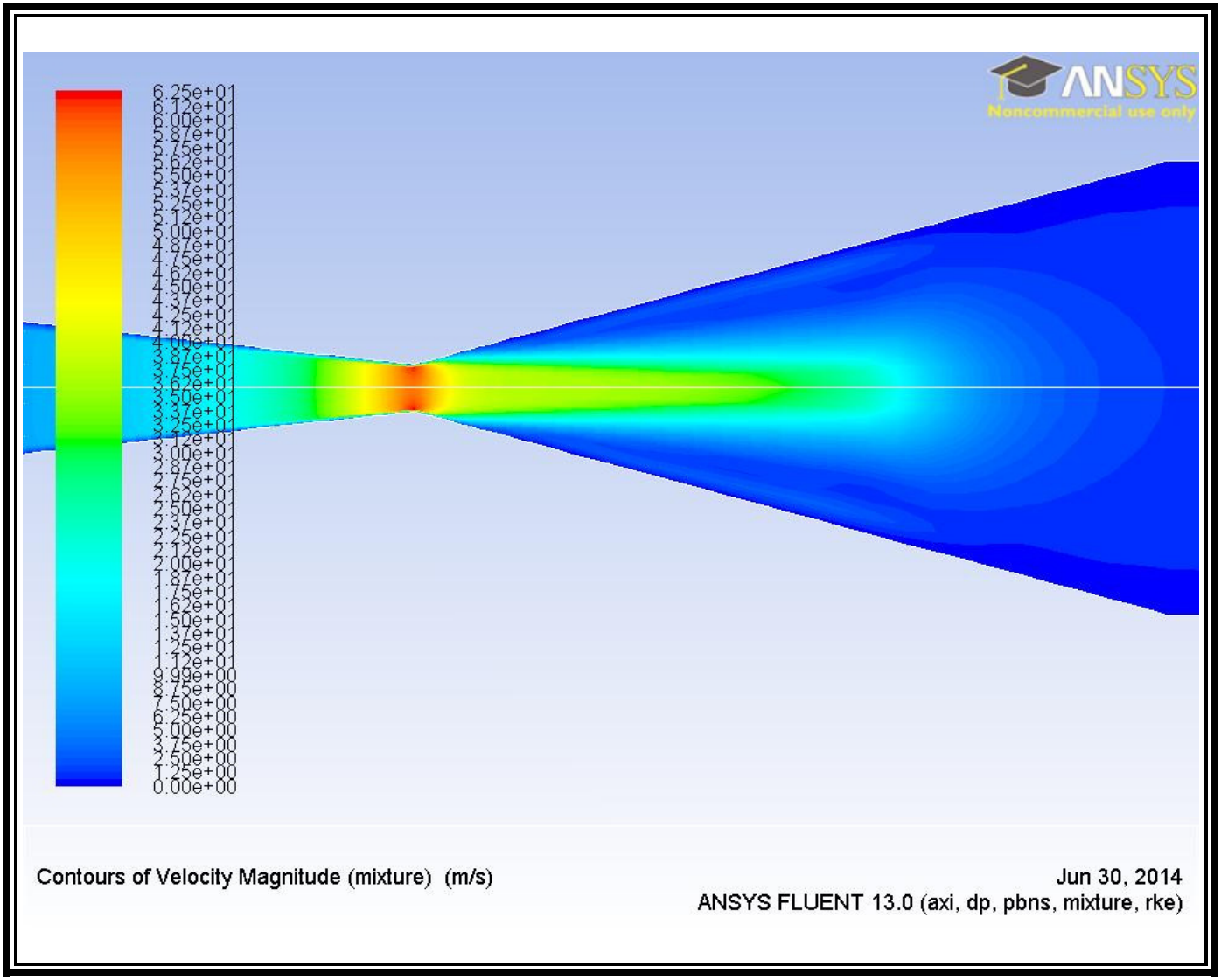

Figure 7.8: Velocity Profile of Liquid Methane at P2/P1=0.69. *Contour of Velocity Magnitude (mixture) in (m/s), produced in ANSYS FLUENT.*

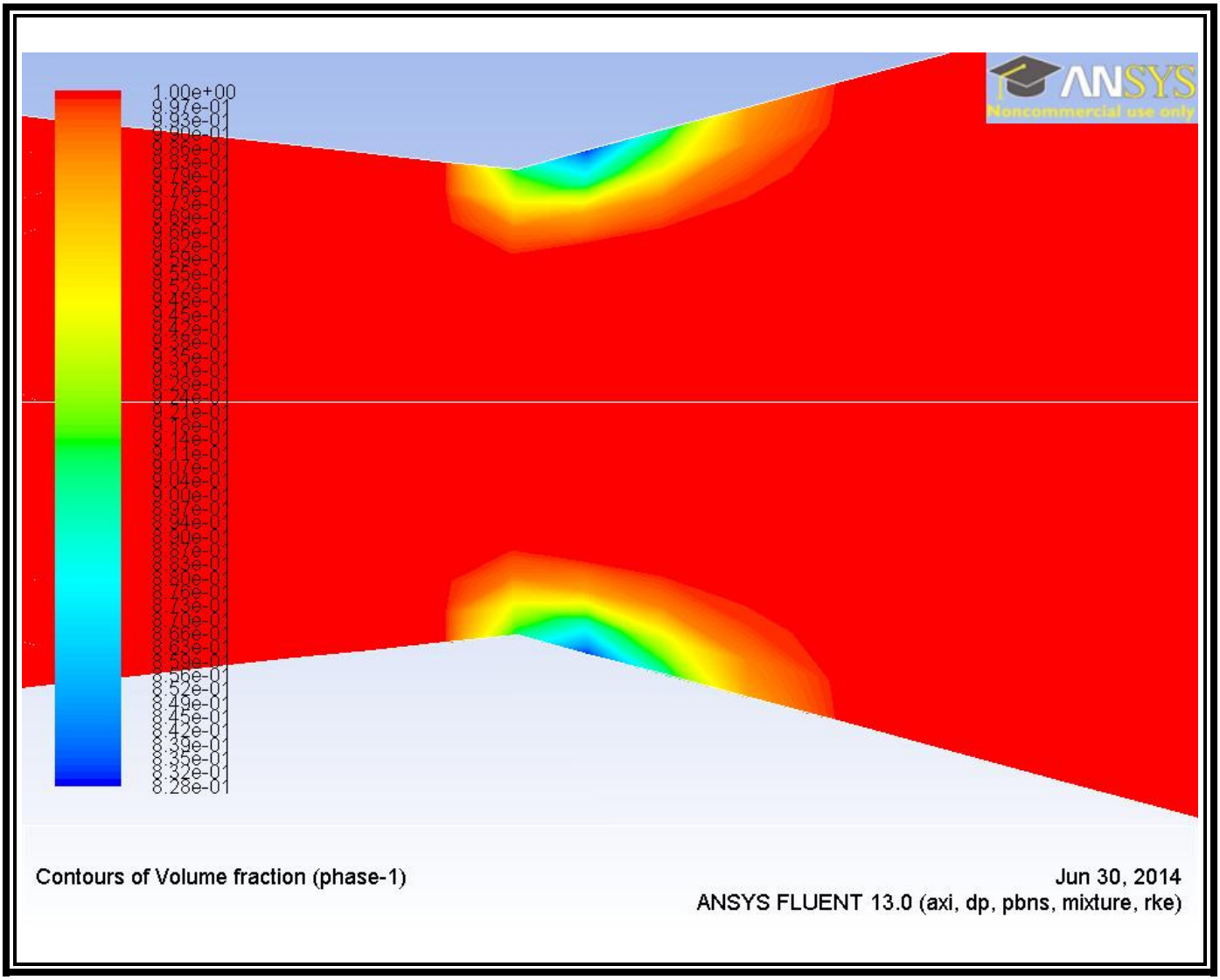

Figure 7.9: Liquid Phase Profile of Liquid Methane at P2/P1=0.69. *Contour of Liquid Volume Fraction, produced in ANSYS FLUENT.*

7.3 Results and Analysis

Figures 7.4-7.9 all display behavior that is expected in the cavitating fluid flow regime. Figures 7.4 and 7.7 both have similarly shaped pressure gradient behavior, most particularly in the near throat region where the pressure is expected to drop dramatically to the saturation value to produce cavitation. The velocity magnitude contours shown in Figures 7.5 and 7.8 clearly display the vena contracta region of the fluid flow domain with thinly defined eddy/energy dissipation regions shown in lightly varying gradients of blue near the throat along the outer boundaries of the vena contracta. This is precisely the

same location where the pressure drops and accompanying phase changes are expected, indicating the presence of cavitation nuclei growth and bubble formation. This is shown in Figures 7.6 and 7.9 that detail the liquid volume fraction contours for both water and liquid methane respectively. Please note that the blue regions in Figures 7.6 and 7.9 indicate the presence of a saturated vapor region surrounded by mixed phases of varying quality layered above.

It should be noted that a comparison similar to the one shown in Figure 7.3 was performed with the liquid methane data, with fairly poor agreement between the experimental readings and the CFD obtained mass flow rate data. This is likely a result of the average mass flow rate from the CFD model being taken over a much longer time period than took place during the experimental testing. The duration of the experimental testing is believed to be within the span of the transient time period before the flow settles into its long-term flow pattern so the average mass flow rate would naturally differ.

Another highly probable source of deviation from the experimental data is the application of different equations of state to predict the fluid properties at various phases and transition points. ANSYS FLUENT does not have a liquid or saturated vapor methane profile within the material database so new fluid profiles needed to be created. REFPROP was utilized to obtain the input fluid parameters at one point for each of the liquid and vapor phases to define the materials in ANSYS FLUENT. From there, ANSYS FLUENT relies solely on its embedded equation of state to predict the fluid properties as it transitions from one phase to another. As shown in the previously referenced equations of state study for liquid methane, there are significant variances in the results produced by each equation of state. For this reason, REFPROP relies primarily on a large database of experimental values to develop most of the fluid properties and relies only on the Helmholtz energy equation of state for its characterization of a limited number of the liquid methane fluid properties. This implies that there is a greater degree of error introduced in the CFD formulations for liquid methane than for a well-characterized fluid such as water, which is also immensely less sensitive than liquid methane to the effects of equation of state prediction variances. Further CFD and experimental studies should be performed to further investigate these possibilities.

Chapter 8: Conclusions

8.1 Coefficient of Discharge

To generally state the findings of this work, the performance of the benchmark cavitating venturi flow meter as a flow control and metering device was validated. This validation is specifically for use with liquid water and liquid methane when operated under steady-state conditions below the critical pressure ratio (0.69 for the benchmark venturi). Furthermore, a C_d with pressure dependency factored in was determined, allowing for more accurate prediction of flow rates throughout the expanse of the pressure ratio range, including the transient response regions.

8.2 Experimental vs. CFD Results

A CFD cavitating flow model was developed showing a strong correlation with the experimental data obtained in the water flow testing. This strong agreement between the model and experimental data for water validates the model parameters and overall solution methodology that could be applied towards the accurate modeling of cavitating liquid methane and liquid oxygen flow behavior. Analysis was done to observe any agreement between the liquid methane flow test data and those modeled in ANSYS FLUENT. The agreement between the mass flow and C_d graphs was poor for the liquid methane and is believed to have resulted from differences in the way the fluid properties are determined through the equation of state applied in ANSYS FLUENT. Furthermore, the mass flow rate values produced in the CFD model and compared with the turbine flow meter data were averaged values that included a transient flow regime that could have caused a skew in the average when combined with the more stable flow achieved after a longer time step. Preliminary observation indicates that the duration of the transient flow observed in the CFD model exceeds, the experimental testing duration, although testing would be needed to verify this presumption. Although liquid oxygen data was gathered during in-situ Pencil Thruster testing, it was not included in this work because of the insufficient number of pressure ratios tested spanning an equivalent flow regime to the other working fluids. Furthermore, only two in-situ tests were performed with the turbine flow meter implemented into the supply line, meaning, the results would have been statistically insignificant.

The region in the CFD liquid methane models right after the seeming transient region show steady, periodic oscillations in the flow pattern. Upon recollection, it was also noted that during firings of the Pencil Thruster associated with this project, periodic throttling behavior could be observed in the combustion. During these occurrences, the benchmark cavitating venturi flow meter was implemented in the liquid oxygen supply line upstream of the propellant injector interface. The duration of the flow pulse is longer in the thruster tests as the propellant must travel a longer distance to the combustion chamber before the 3 to 10 second burn tests even commence. It is possible that the periodic throttling behavior noted in the thruster combustion behavior is related to periodic flow variations through the venturi. As there are a number of other factors such as a lack of size optimization in the injector holes that could contribute to this behavior, it is too early to determine if the CFD results can be validated through experimentation.

8.3 SEM Roughness Analysis

An SEM analysis of a venturi cross-section manufactured with the same technology as the benchmark cavitating venturi test article was performed. This resulted in the determination of a roughness average and roughness parameter (RMS) at 3 different locations along the length of the venturi cross section. Although this value was not implemented into the CFD models detailed in this work, it serves to narrow down the fairly wide breadth of typical values exhibited for 316 stainless steel machined using EDM technology. Furthermore, a technique for surface roughness analysis was determined for the cavitating venturi, despite the presence of a curved surface without a uniform finish across its length in the flow direction or a flat length from which to measure a mean line or peak deviations from said mean line.

Although liquid oxygen data was gathered during in-situ Pencil Thruster testing, it was not included in this work because of the insufficient number of pressure ratios tested spanning an equivalent flow regime to the other working fluids. Furthermore, only two in-situ tests were performed with the turbine flow meter implemented into the supply line, meaning, the results would have been statistically insignificant.

Chapter 9: Proposed Legacy Work

This chapter details the work of future graduate students taking on the mantle of responsibility for furthering the understanding and optimization of cavitating venturi flow meters for use in hardware for the Center for Space Exploration Technology Research and its affiliated research and industry entities. Continuation of this work is vital to the determination of life/duty cycle determinations for these devices along with their optimization to meet very specific mission requirements.

9.1 Continued Repeatability Tests and Pulse-width Modifications

To date, the collection of data obtained through experimentation is limited to liquid methane and water at standard conditions. Realistically, the need for cavitating venturi flow meters will extend to a myriad of other liquid propellants as the research focus of the center expands. As discussed previously, there were some variations between the liquid methane data obtained through long duration CFD models and it was unclear if this was a result of periodic fluctuations in the fluid behavior that occur over a period of time beyond what is currently being tested experimentally. For this reason, the current testing matrix must be repeated while also extending the test durations to provide an empirical source of comparison with the CFD models. This will either validate or show the need for revision of the CFD model for liquid methane and other cryogens. More testing should be done to determine and repeatedly confirm the length of the transient time period within various operating regimes. This information is vital to determining whether or not the cavitating venturi flow meter can be reliably used for operating conditions that span the gamut of short pulse-widths to extended, steady-state flows.

9.2 Increased inlet pressure testing

To date, the RCS system has only been tested at operating pressures that are approximately half of what the center's industry counterparts would like to implement. This was a result of safety concerns, hardware limitations, and propellant supply methods. Although the aforementioned impediments will likely remain for the short term, mitigating factors can be taken to achieve the increased inlet pressures such as the implementation of valves with higher pressure ratings and replacement of direct flow from a

commercially available liquid oxygen dewar with another storage tank that can maintain the needed pressure without actuating the pressure relief valve. An effort to study the entrainment and dissolution of pressurization gasses in the propellant could likely become a facet of the efforts to change the propellant feed system. This information would contribute to the efforts of those studying propellant cavitation in the venturi and those studying the performance of the RCS thruster too. Furthermore, the inlet pressure will be able to be safely increased when a test article engine is produced that is capable of structurally withstanding the combustion that is predicted at the higher operating pressures.

9.3 Life Cycle Studies

The specific long-term effects of the cavitation occurring in the venturi flow meter with this specific operating regimen are not well understood as they have not been previously explored. Cavitation of room temperature water alone can cause pitting and surface defects that influence the flow behavior and compromise the adherence of the article to its required dimensioning. If nearly instantaneous thermal fluctuation of the venturi is taken into account during cryogenic operation, the destructive nature of the cavitation collapse is likely amplified. This can best be explained by saying that the collapse of the cavitation bubbles exerts an extremely high pressure on a relatively small surface area of the venturi inner walls. For metals operating under conditions where the material retains its specified toughness, pitting does occur as a result of the cavitation collapse. The material degradation resulting from the cavitation is likely to be amplified as fairly drastic alterations to the thermal conditions can reduce the toughness of the material, especially on machined surfaces that may not have been treated to improve the surface roughness and toughness.

To assess the actual functional duty life of a cavitating venturi flow meter in service with cryogenic propellants, it will be necessary to perform flow testing at periodic points. For example, the initial water testing would be performed to determine the C_d characteristic of a particular venturi immediately after manufacturing it and before it is implemented into cryogen supply service. After six months of use with a particular cryogen, another water flow testing regiment would be conducted to see if there was an observable change in the characteristic C_d. This would again be repeated at other

subsequent time frames. With enough data, it may be possible to produce a relationship that correlates changes in the C_d value to hours of operation in strictly controlled operating conditions.

Another more invasive method for determining surface life would require a significantly greater time, human capital, and financial investment but could potentially reveal not only duty life but fluid behavior. Essentially this methodology would involve the production of a large quantity of cavitating venturi flow meters to be implemented and then analyzed using the flow testing and SEM roughness measurement methodologies detailed in this work. At the beginning, a group of uniformly manufactured (within the given tolerances) cavitating venturis would be produced and characterized through water flow tests. For a smaller number of venturis, SEM roughness analysis would be performed right after manufacturing to provide for a point of comparison for other samples that were actually in service. A large portion of the venturis would then be distributed for use to different teams within the laboratory using the same propellants at similar operating conditions. The details of their operation such as the propellant conditions, flow durations and characteristics (steady cavitation, transient, high velocity and pressure, etc.) would be carefully monitored and documented and then flow testing would again be performed to observe changes in the C_d value. For a certain percentage of the venturis that reach a pre-determined operation time, SEM roughness analysis would be performed to correlate the change in C_d to change in roughness. Of course, this would only be accomplished after a significant amount of data had been produced, but employing other projects in the endeavor would help increase the sampling size while contributing to the work and objectives of other research teams and drastically reducing the amount of time it would take to generate a substantial data collection.

9.5 Alternative Materials and Manufacturing Techniques

When the benchmark cavitating venturi was designed, there was no significant consideration of defining surface roughness requirements. The primary concern was whether or not the geometry could be machined with enough sensitivity to defined dimensional tolerances. So in terms of surface roughness, the machined roughness was accepted. No post-production surface finishing was performed in an effort to maintain the dimensioning and ensure that potentially reactive agents did not remain even after sonic bath cleaning. It is possible that the insights obtained from the previously mentioned

investigations could lead to the development of a cavitating venturi flow meter comprised of different materials or produced through alternative machining methodology. Additive manufacturing processes are improving and changing to meet a variety of fluid flow demands. Given that the University of Texas at El Paso houses the W. M. Keck Center for 3D Innovation, which is currently the largest additive manufacturing research laboratory in North America, provides for a unique opportunity to explore the various technologies within this classification of manufacturing.

9.6 Alternative CFD Techniques

There is clearly a great deal of room for improvement in the development of the liquid methane (and other cryogen) cavitation CFD models. With open source CFD software such as OpenFOAM, there is much more freedom in terms of solver specification and modification. Through the modification of the provided library samples, it is possible to revise the solver and model coding to incorporate controls to select, and if necessary, change solvers to those most accurate for a specific flow regime. Equations of state often have different levels of accuracy depending upon how close to the critical region they are implemented. This was a clear observation made when comparing various equations of state to be used for designing the methane condensation unit. It is equally clear that NIST recognizes this need as REFPROP likewise incorporates the functionality to modify the methodology to compute fluid properties using different data sources or equations of state best suited to characterize fluid in the user defined operating conditions. Even in commercially available software with well-defined GUI options, there is room for improvements to be made to the model detailed herein relating to transience modeling that can be made using the included tools.

References

[1] Ulas, A. Passive flow control in liquid-propellant rocket engines with cavitating venturi. *Flow Measurement and Instrumentation*, 93-97. Retrieved January 13, 2014, from http://www.sciencedirect.com/science/article/pii/S0955598605000968

[2] Çengel, Y. A., & Cimbala, J. M. (2010). *Fluid Mechanics Fundamentals and Applications* (2 ed.). New York, New York: McGraw-Hill Higher Education.

[3] Schmidt D. P. and Corradini M. L. [Online] = One-dimensional analysis of cavitating orifices. - Informally published manuscript, Engine Research Center, University of Wisconsin. - http://thehuwaldtfamily.org/jtrl/research/Hydrodynamics/1D Analysis of Cavitating Orifices.pdf.

[4] Graham, C., & Huang, P. (2010). Analysis of a Passive Flow Control Device via Flow Visualization Techniques. . Retrieved January 28, 2014, from http://digitalcommons.calpoly.edu/cgi/viewcontent.cgi?article=1012&context=aerosp

[5] Barr, G. (1934, August 22). Two Designs of Flow-meter, and a Method of Calibration. . Retrieved April 7, 2014, from http://iopscience.iop.org/0950-7671/11/10/305/pdf/0950-7671_11_10_305.pdf

[6] Hall, K. R., Morrison, G. L., & Holste, J. C. United States Patent and Trademark Office, (1995). *United States Patent: Slotted orifice flow meter* (US005461932A). Retrieved from The United States Government website: http://www.google.com/patents/US5461932

[7] Jones, J. B., & Dugan, R. E. (1996). *Engineering thermodynamics*. (pp. 407-411, 658-659, 682-686, 734). Englewood Cliffs, NJ: Prentice Hall, Inc.

[8] Franc, J.-P. (2006) Physics and Control of Cavitation. In Design and Analysis of High Speed Pumps (pp. 2-1 – 2-36). Educational Notes RTO-EN-AVT-143, Paper 2. Neuilly-sur-Seine, France: RTO. Available from: http://www.rto.nato.int/abstracts.asp.

[9] Choudhuri, A., Robinson, N., Garcia, C. P., Ingle, M. A., Gonzalez, A., & Acosta-Zamora, A. (2010).*Equations of state for methane: A comparative study*. Unpublished manuscript, Mechanical Engineering, The University of Texas at El Paso, El Paso, TX, Available from cSETR Knowledgetree. (EOS Final version5_21_10). Available from: http://www.csetr.utep.edu/knowledgetree.

[10] Shinder, I. I., & Marfenko, I. V. U.S. Department of Commerce, Technology Administration. (2006).*NIST measurement services: NIST calibration services for water flow meters water flow calibration facility* (NIST Special Publication 250). Retrieved from National Institute of Standards and Technology website: http://www.nist.gov/calibrations/upload/sp250_73.pdf

[11] Yazici, B. (2006). *Numerical and experimental investigation of flow through a cavitating venturi*. (Master's thesis), Available from Middle East Technical University. Retrieved from http://etd.lib.metu.edu.tr/upload/3/12607924/index.pdf

[12] Turns, S. R. (2006). *An introduction to combustion: Concepts and applications*. (2nd ed., pp. 256-263). Boston, MA: McGraw-Hill.

[13] Abdulaziz A. M. *Performance and image analysis of a cavitating process in a small type venturi* [Journal] // Experimental Thermal and Fluid Science. - [s.l.] : Elsevier, 2013. - 53. - pp. 40-48.

[14] Hoffer Flow [Online]. - http://www.hofferflow.com/datasheets/hogas.pdf. - Product Technical Specification Sheet.

[15] OMEGA Engineering [Online]. - http://www.omega.com/toc_asp/frameset.html?book=Temperature&file=tc_colorcodes; http://www.omega.com/pptst/PX1005.html. - Product Technical Specification Sheet.

[16] Mena, J.L., Ingle, M.A., Shirsat, V., Choudhuri, A.(2014).*An Investigation of a Cavitating Venturi Feature in a Cryogenic Propellant Delivery System*, AIAA Propulsion and Energy Forum and Exposition 2014: 50th AIAA/ASME/SAE/ASEE Joint Propulsion Conference, [Pending Publication]

[17] Galvan, M. (2014). *An experimental investigation on liquid methane heat transfer enhancement through the use of longitudinal fins in cooling channels*. (Master's thesis, University of Texas at El Paso).

[18] Ingle, M. A., & Mena, J. L. (2014). Cavitating venturi 4.0 v1.1.0 (2012-13) cSETR cavitating venturi flow feature-AN fitting technical specification sheet. Informally published manuscript, Department of Mechanical Engineering, University of Texas at El Paso, El Paso, TX, .

[19] Surface Finish Charts. (2013). L.J. Star, Inc. Retrieved June 3, 2014, from http://www.ljstar.com/design/surface_charts.aspx

[20] Surface Roughness Measurements. (2008). KEPCO, Inc. Retrieved June 3, 2014, from http://www.kepcoinc.com/downloads/Electro_Polishing/LC_surface-roughness-measurements.pdf

[21] Young, P. L., Brackbill, T. P., & Kandlikar, S. G. (2007, June). *Estimating roughness parameters resulting from various machining techniques for fluid flow applications*. Conference Paper Fifth international conference on nanochannels, microchannels, and minichannels, Puebla, Mexico. doi: ICNMM2007-30033

[22] Australian Microscopy & Microanalysis Research Facility. (2012). SEM troubleshooting: edge effect, charging, sample damage. In MyScope Training for Advanced Research. Sydney, Australia: Australian Government Office for Learning & Teaching. Retrieved from http://www.ammrf.org.au/myscope/sem/practice/principles/troubleshooting.php

[23] Fluent, Inc. (2006, August 30). Modeling cavitation. Retrieved from http://aerojet.engr.ucdavis.edu/fluenthelp/html/tg/node272.htm

[24] Leap Australia CFD Team. (2012, January 17). Tips & tricks: Convergence and mesh independence study [Online forum comment]. Retrieved from http://www.computationalfluiddynamics.com.au/convergence-and-mesh-independent-study/

[25] Fluent, Inc. (2006, September 20). 12.4.3 realizable k-epsilon model. Retrieved from http://aerojet.engr.ucdavis.edu/fluenthelp/html/ug/node480.htm

[26] Fluent, Inc. (2006, September 20). 25.9.1 Choosing the pressure-velocity coupling method. Retrieved from http://aerojet.engr.ucdavis.edu/fluenthelp/html/ug/node1021.htm

[27] Versteeg, H. K., & Malalasekera, W. (2007). An introduction to computational fluid dynamics: The finite volume method. (2nd ed., pp. 156-196). New York, NY: Pearson Education Limited.

[28] Fluent, Inc. (2006, September 20). 25.9. Pressure-Based Solver Settings: Choosing the Pressure-Velocity. Retrieved from http://aerojet.engr.ucdavis.edu/fluenthelp/html/ug/node1021.htm

[29] Fluent, Inc. (2012, October). Ansys fluent theory guide. Retrieved from http://www.mecheng.osu.edu/documentation/Fluent14.5/145/flu_th.pdf

[30] Fluent, Inc. (2006, September 20). 25.9. Pressure-Based Solver Settings: Setting Under-Relaxation Factors. Retrieved from http://aerojet.engr.ucdavis.edu/fluenthelp/html/ug/node1022.htm

Vita

Marjorie Adele Ingle is a Masters of Mechanical Engineering degree candidate at the University of Texas at El Paso. She completed her B.S. in Mechanical Engineering in 2012 at the University of Texas at El Paso and has been performing research for the university since 2007. Her areas of research experience range from additive manufacturing techniques, mechanical failure modes of biomedical implants, micro-propulsion testing and evaluation, and fluid modeling. To date, she has co-authored work published in four international publications relating to her materials work and micro-propulsion performance evaluation. In total, her published body of work includes upwards of nine publications during her tenure at UTEP. Ms. Ingle is a National Science Foundation Bridge to the Doctorate Research Fellow in the UT-System LS-AMP Alliance, an alumnus of the undergraduate UT-System LS-AMP Summer Research Academy, a NSF-XSEDE Student Engagement Summer Immersion Program participant, and a Texas Space Grant Consortium Graduate Fellowship Recipient.

Aside from her participation in research, Marjorie has been a member of the UTEP Women's Advisory Council to the President, the University Chorale, the Honorable Guard of St. Pat since 2007, Kalpulli Tlalteca/Danza Azteca Omecoatl since 2007, and a founding member of the Alpha Eta Chapter of Theta Nu Xi Multicultural Sorority, Inc. Her service to UTEP and the community also includes involvement in social advocacy work, educational outreach programs, volunteering for campus events, and participation in various non-voting campus policy advisory committees. Most recently she participated in the organization and operation process of the 2014 SAE Mini Baja Competition at UTEP, hosted in commemoration of UTEP's Centennial Celebration.

Upon graduation, Ms. Ingle will work in industry while earning her Doctorate Degree and pilot's license. She will likewise pursue her dream of becoming a NASA Mission Specialist/Commander in the Astronaut Corps.

Permanent address: 10333 Kinross

El Paso, Texas 79925

This thesis/dissertation was typed by Marjorie Adele Ingle